DAA/LANGLEY



# COLLEGE OF ENGINEERING

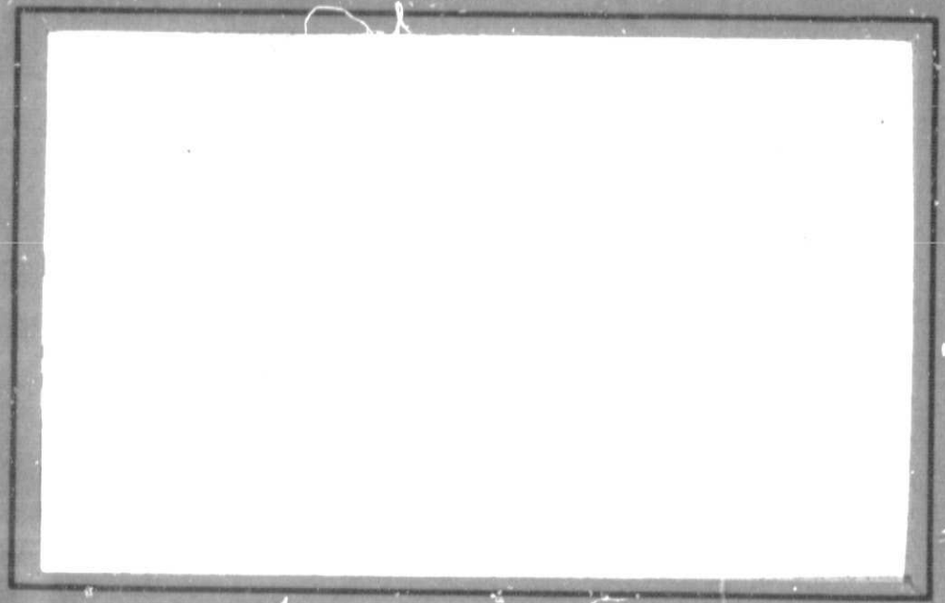

# VIRGINIA POLYTECHNIC INSTITUTE AND STATE UNIVERSITY

BLACKSBURG, VIRGINIA

# ENERGY MANAGEMENT OF THREE-DIMENSIONAL MINIMUM-TIME INTERCEPT

by

H.G. Visser, H.J. Kelley and E.M. Cliff

September 1985

Interim Report

NASA Grant 1-203

NASA Langley Research Center
Hampton, Virginia

Aerospace and Ocean Engineering Department
Virginia Polytechnic Institute and State University
Blacksburg, Virginia

## ABSTRACT

A real-time computer algorithm to control and optimize aircraft flight profiles is described and applied to a three-dimensional minimum-time intercept mission.

The proposed scheme has roots in two well-known techniques: singular perturbations and neighboring-optimal guidance. Use of singular-perturbation ideas is made in terms of the assumed trajectory-family structure. A heading/energy family of prestored point-mass model state-Euler solutions is used as the baseline in this scheme. The next step is to generate a near-optimal guidance law that will transfer the aircraft to the vicinity of this reference family. The control commands fed to the autopilot consist of the reference controls plus correction terms which are linear combinations of the altitude and path-angle deviations from reference values, weighted by a set of precalculated gains. In this respect the proposed scheme resembles neighboring-optimal guidance. However, in contrast to the neighboring-optimal guidance scheme, the reference control and state variables as well as the feedback gains are stored as functions of energy and heading in the present approach.

A detailed description of the feedback laws and of some of the mathematical tools used to construct the controller is presented. The construction of the feedback laws requires a substantial preflight computational effort,

but the computation times for on-board execution of the feedback laws are very modest. Other issues relating to practical implementation are addressed as well.

Numerical examples, comparing open-loop optimal and approximate feedback solutions for a sample high-performance fighter, illustrate the attractiveness of the guidance scheme. Optimal three-dimensional flight in the presence of a terrain limit is studied in some detail.

ACKNOWLEDGMENTS

This research was supported by NASA Langley Research Center under grant NAG-1-203. Dr. C. Gracey and Dr. D.B. Price of NASA Langley served as technical monitors. Thanks are due to Dr. K.H. Well of DFVLR, Oberpfaffenhofen, F.R.G., for kindly supplying the computer program BNDSCO.

NOMENCLATURE

$a$ ..... Speed of Sound

$C_D$ ..... Drag Coefficient

$C_{D_o}$ ..... Zero-Lift Drag Coefficient

$C_L$ ..... Lift Coefficient

$C_{L_{max}}$ ..... Maximum Lift Coefficient

$D$ ..... Drag

$D_i$ ..... Induced Drag in Straight-and-Level Flight

$D_o$ ..... Zero-Lift Drag

$E$ ..... Specific Energy

$g$ ..... Acceleration due to Gravity

$h$ ..... Altitude

$h_{min}$ ..... Terrain Limit

$K$ ..... Efficiency Coefficient

$H$ ..... Variational Hamiltonian

$L$ ..... Lift

$M$ ..... Mach Number

$n$ ..... Normal Load Factor

$n_h$ ..... $n \sin\mu$

$n_L$ ..... Aerodynamic Load Limit

$n_{max}$ ..... Structural Load Limit

$n_v$ ..... $n \cos\mu$

$q$ ..... Dynamic Pressure

$S$ ..... Wing Surface Area

$t$ ..... Time

$T$ ..... Thrust

$T_{max}$ ..... Maximum Thrust

$V$ ..... Airspeed

$W$ ..... Weight

$x$ ..... Down-Range

$y$ ..... Cross-Range

## GREEK SYMBOLS

$\gamma$ ..... Flight-Path Angle

$\nabla$ ..... Relaxation Parameter

$\zeta$ ..... Lagrange Multiplier

$\eta$ ..... Throttle-Setting

$\lambda_{(.)}$ ..... Adjoint Variable

$\mu$ ..... Bank Angle

$\nu_{(.)}$ ..... Kuhn-Tucker Multiplier

$\rho$ ..... Air Density

$\sigma_{(.)}$ ..... Lagrange Multiplier

$\chi$ ..... Heading Angle

$\chi'$ ..... $\ln(|\chi|/\pi)$

## SUPERSCRIPTS AND SUBSCRIPTS

$(.)_C$ ..... Value at Corner Point

$(.)_D$ ..... Value at Dash Point

$(.)_e$ ..... Value at Entry Point

$(.)_E$ ..... Corresponding to Specific Energy

$(.)_h$ ..... Corresponding to Altitude

$(.)_f$ ..... Final Value

$(.)^{fb}$ ..... Feedback Value

$(.)_o$ ..... Initial Value

$(.)^r$ ..... Reduced-Order Value

$(.)_{ref}$ ..... Reference Value

$(.)_T$ ..... Target Value

$(.)_x$ ..... Corresponding to Down-Range

$(.)_y$ ..... Corresponding to Cross-Range

$(.)_\gamma$ ..... Corresponding to Path Angle

$(.)_\chi$ ..... Corresponding to Heading Angle

$(.)^*$ ..... Optimal Value

TABLE OF CONTENTS

LIST OF ILLUSTRATIONS

# CHAPTER 1. INTRODUCTION

Since the early days of flight, optimization of aircraft trajectories has been a challenging topic. The advances in sensing electronics and computing technology made in recent years have tilted the direction of research in trajectory optimization toward the exploration of a new and interesting problem: the on-board generation of real-time guidance commands to control and optimize aircraft flight profiles.

Due to the limited computational speed and storage capacity of current airborne computers, relatively fast algorithms are required for this purpose. Unfortunately, however, the nonlinear two-point-boundary-value problems (TPBVP) which arise in the application of optimal-control theory to atmospheric-flight-trajectory problems, are of tremendous computational complexity. Nevertheless, it is currently feasible to generate accurate open-loop solutions using sophisticated numerical methods [1,2]. While such numerical optimization techniques are of considerable value, they are usually rather intricate and computationally expensive, rendering them useless for real-time applications. On-board real-time guidance generally requires the optimal-control solution to be expressed in a closed-loop feedback form. Since it is usually not possible to derive closed-form feedback solutions for the "exact" system (describing say, the motion of a point-mass-modelled vehicle), approximate closed-form feedback solutions are sought.

One way to obtain closed-loop control is to compute optimal trajectories using highly simplified system models. For this reason reduced order concepts, in which fast dynamics, believed to have small effects on the solution behavior, are neglected, have received considerable attention. In problems dealing with atmospheric-flight-trajectory optimization, the earliest and best-known reduced-order concept is that of energy-state. In this concept the dominant state variable is specific energy (defined as the sum of potential and kinetic energy per unit weight). When Kaiser introduced this concept in connection with aircraft minimum-time climbs in 1944, it was rather intuitive in nature [3,4]. Although applied systematically to several aircraft performance optimization problems [5-10], it remained an ad-hoc engineering approach until the early seventies when it found a mathematical basis in the theory of singular perturbations [11-15].

In some applications the faster dynamics ignored in the reduced-order system models have a negligible effect on performance. In other cases the solutions of these simplified system models may not be sufficiently accurate, or may exhibit other undesirable features. In civil aviation, where the prime mission performance criteria are fuel-consumed and direct operating cost, reduced-order concepts generally provide an adequate basis for studying optimal flight trajectories [16-19]. This is a evidently a reflection of the fact that commercial aircraft generally maneuver in a restrained fashion. In military aviation, fighter aircraft perform a great variety of missions, both air-to-air and air-to-ground. In order to carry out their missions successfully, fighter aircraft often operate

at supersonic velocities and frequently indulge in rather violent maneuvering [20,21]. Reduced-order concepts are of limited value in the analysis of optimal flight paths of high-performance fighters.

One area of research in military aviation currently receiving considerable attention is that of air-to-air-combat analysis. The field of air-to-air combat analysis is characterized by many approaches to the problem, some of which are fundamentally different from each other [22]. The most realistic mathematical model of actual air-to-air combat is the differential game approach [23-24]. Most investigations of combat problems by differential game theory have focused on analysis of deterministic, two-player, zero-sum, perfect-information pursuit-evasion games. Although attempts to study air-to-air combat on the basis of even more general problem definitions have been made [25-29], the mathematical nature of the analyses involved is generally so complex that it is virtually impossible to obtain useful results for realistic dynamic models. In order to make the differential game approach tractable, simplifying assumptions with respect to dynamic model and/or role-specification are imperative. As a matter of fact a third-order system seems to be the highest order nonlinear differential game currently manageable [30-35]. Such highly simplified dynamic system models may be useful for evaluating relative aircraft performance; however, the resulting trajectories and optimal controls are of little use in the development of on-board real-time guidance schemes. The present research effort is limited to the early well-separated phase of a minimum-time intercept of a non-maneuvering target. Optimal-control theory provides an adequate framework wherein

such an initial phase can be studied. However, the end-game following this initial phase should allow for a maneuvering target. This end-game, not considered in the present effort, could be analyzed either by a differential game approach with a highly simplified system model, or by an optimal control approach with a more realistic system model.

By analyzing optimal-control problems in the framework of singular perturbations, more general problem formulations have become possible. Singular perturbation techniques have been extensively used to extend the validity of energy-state models by correcting for the neglected fast dynamics [11-15, 36-42]. This approach takes advantage of the time-scale separation of the state variables, by separating the dynamics into fast and slow modes (boundary-layer structure). This permits the solution of a high-order problem to be approximated in terms of solutions of a series of lower order problems. However, the application of singular-perturbation techniques is by no means a straightforward procedure. There is currently no rigorous method to identify time-scale separation in nonlinear dynamic systems. In most singular-perturbation analyses a boundary-layer structure is assumed based on ad-hoc time-scale separation judgment [43]. If all dynamical equations are ordered on separate time-scales, then it may be possible to obtain a closed-form feedback solution. This feature has attracted many researchers to cast trajectory-optimization problems in this particular singular- perturbation form in which there is a hierarchy of first-order boundary layers [44-50]. Unfortunately, in problems involving atmospheric flight, such distinct time-scale separation between state variables is an exception rather than

a rule. If, for instance, altitude and path-angle dynamics are considered on separate time-scales, these dynamics are effectively decoupled. However, it is well-known that altitude and path-angle dynamics are actually highly coupled [51]. On the other hand, if altitude and path-angle dynamics are considered on the same time-scale [14], the boundary-layer solution is not obtainable in feedback form. These features clearly indicate the limitations of singular-perturbation techniques. The occurrence of internal boundary-layers may further complicate matters [52]. Since time-scale separation is not complete the singular-perturbation solution is only suboptimal. Improved accuracy may be obtained, but this requires taking into account higher-order corrections. The method of matched asymptotic expansions provides recursive equations from which such terms can be computed [15,36]. Although feedback implementation of these correction terms seems feasible for planar flight [53,54], the prospects for 3-D flight are rather bleak.

Another approach to obtain approximate closed-form feedback control for realistic aircraft models is by neighboring-optimal-guidance technique [55-59]. In this approach perturbation-feedback control, i.e. control in the vicinity of a reference extremal, is considered. The resulting linear neighboring-optimal feedback guidance law controls the vehicle so as to follow a neighbor of the reference extremal. Most of the experience with this technique has been in the area of vehicle guidance in space flight [60-62]. In vehicle guidance in atmospheric flight, this technique has not found widespread application. This is primarily due to the fact that, in tactical situations, there is little a priori knowledge of the

flight path, which makes the selection of suitable reference paths difficult. In addition there are questions concerning the range of validity of the linear-feedback laws. A third drawback concerns the problems associated with estimating the index-time.

Yet another approach to feedback control proceeds by flooding the state-space with extremals (extremal-field approach). A closed-loop controller is then synthesized from the open-loop results. The drawback of this method is what has been termed the "curse of dimensionality". Even storing the solution to a planar interception problem requires an enormous amount of storage-space [63]. Efforts to extend this concept to three dimensions via energy-state approximation have been made [64]. However, the weaknesses of energy-state modeling are retained in this approach.

With this as background it is the objective of this study to investigate a concept for developing real-time computer algorithms to control and optimize three-dimensional aircraft flight profiles. The proposed concept, first sketched in Ref.65, has roots in all three approaches just mentioned: singular perturbations, neighboring-optimal guidance and extremal fields. By using elements of the three approaches in a more or less complementary fashion, one hopes that many of the weaknesses can be eliminated, and that a guidance scheme results that is still simple enough to lend itself to on-board implementation.

Use of singular-perturbation ideas is made in terms of the assumed hierarchical trajectory-family structure. A heading/energy family of ex-

tremals is used as the baseline in this scheme. However, in contrast to the singular-perturbation approach, this "reference" family is not built up from reduced-order extremals, but from point-mass-model extremals. Some of the extremal-field ideas are used in establishing this reference family. The next step is to generate a guidance law that will transfer the aircraft to the vicinity of the reference family. The control commands used for this purpose consist of the reference controls plus correction terms which are linear combinations of the altitude and path-angle deviations from reference values, weighted by precalculated gains. In this respect the proposed scheme resembles neighboring-optimal guidance. However, in contrast to the neighboring-optimal-guidance scheme, the reference control and state variables as well as the feedback gains are stored as functions of energy and heading in the presently-proposed approach.

To demonstrate feasibility, the proposed concept is applied herein to a long-range minimum-time intercept mission in 3-D. In this type of mission the initial separation between the interceptor and the target is assumed relatively large so that at least a portion of the interceptor's trajectory is flown at maximum velocity, i.e. a dash or cruise-dash arc is present. A guidance law is then developed providing the interceptor a time-range-optimal turn-climb to the dash point on the flight envelope, fairing into a steady-state cruise-dash.

The present effort was preceded by a study in which the concept was successfully applied to a climb-dash intercept mission in 2-D [66-67]. The present extension to 3-D is far from trivial. The extension adds a great

deal of complexity to the numerical resolution of the TPBVP as well as to the construction of the guidance laws, as will become apparent in the course of the analysis.

The formulation of the three-dimensional intercept problem as a minimum-time optimal-control problem is the starting point of the analysis. In this formulation significant order-reduction is obtained by analytic integration of some of the adjoint equations. This is of great importance in the numerical resolution of the TPBVP. The special form in which the problem is formulated is motivated by the well-known unstable behavior of state-Euler system solutions for a point-mass vehicle model. It is shown in the following that using this particular form no serious stability problems arise in the numerical resolution of the TPBVP. A brief description of the multiple-shooting algorithm (MSA), used to generate the point-mass model state-Euler solutions is presented. In order to expose the essential features of energy-management, an energy-state model is studied in some detail. The energy-state extremals are used subsequently to select the initial conditions for the point-mass-model extremals that span the reference family. The construction of the feedback laws is then described and some of their characteristic features are examined. Extensive numerical investigations comparing open-loop optimal and approximate feedback solutions, are presented. Some results on three-dimensional optimal-flight trajectories in the presence of a terrain-limit are reported in an appendix.

## CHAPTER 2. PROBLEM STATEMENT

### 2.1 EQUATIONS OF MOTION

The equations of motion for a point-mass model of an aircraft can be written as:

$$\dot{x} = V \cos\gamma \cos\chi \tag{1}$$

$$\dot{y} = V \cos\gamma \sin\chi \tag{2}$$

$$\dot{h} = V \sin\gamma \tag{3}$$

$$\dot{E} = (V/W)\,[T-D] \tag{4}$$

$$\dot{\gamma} = (g/V)\,[n_v - \cos\gamma] \tag{5}$$

$$\dot{\chi} = (g/V)\,[n_h / \cos\gamma] \quad , \tag{6}$$

where:

$$V = [2g(E-h)]^{1/2} \quad , \tag{7}$$

is to be regarded as eliminated in terms of E and h. The reason for selecting specific energy E as state variable is to obtain a better time-scale separation, which is especially important since further order reduction will be considered.

The equations of motion embody the assumptions of a constant-weight vehicle with thrust directed along the flight path and a flat non-rotating earth. The equations of motion are written here in a fixed coordinate frame that has its origin at the interceptor's final position and its

x-axis aligned with the projection of the target's velocity vector on the horizontal plane (see Fig.1). Heading is measured relative to the x-axis. The target is assumed to be travelling on a constant-heading course. Note that the present problem definition results in equations of motion which are completely independent of the target's dynamics and relative position. The control variables in these equations are $\eta$, $n_v$, $n_h$, where, $n_v$ and $n_h$ are defined as (see Fig.2):

$$n_v \equiv n\cos\mu \quad , \quad n_h \equiv n\sin\mu \tag{8}$$

The use of $n_v$ and $n_h$ as control variables is not very common (the more common choices are e.g. n and $\mu$ or $C_L$ and $\mu$,). The advantages of this selection for the present problem, will become apparent in the sequel.

## 2.2 AERODYNAMIC AND PROPULSIVE FORCE MODELS

The aerodynamic and propulsive forces are assumed to have the following form:

$$T = \eta T_{max}(M,h) \quad , \quad 0 \le \eta \le 1 \tag{9}$$

$$D = D_o + (n_v^2 + n_h^2)D_i \quad , \tag{10}$$

where $D_o$ is the zero-lift drag:

$$D_o = qSC_{D_o}(M) \tag{11}$$

and $D_i$ is the induced drag in straight-and-level flight ($n_v$=1; $n_h$=0):

$$D_i = K(M)W^2/qS \tag{12}$$

In the numerical examples a realistic aircraft model, representative of a high-performance fighter, is used. The fashion in which the functions $T_{max}$, $C_{D_o}$ and K(M) are represented is important in the computational work [66,67]. In the present effort all aircraft data as well as the atmospheric data have been represented by cubic splines and spline lattices [68]. This representation is sufficiently smooth to be used in conjunction with the 7-8th order Runge-Kutta-Fehlberg integration routine of the MSA. The Mach limit and dynamic-pressure limit are artificially enforced in the aircraft model by gently fairing off the thrust data. The functions $T_{max}(M,h)$, $C_{D_o}(M)$, K(M), $\rho(h)$ and a(h) are shown in Figs.3-7. It is noted that the function $T_{max}(M,h)$ corresponds to full-afterburner operation. Some of the other characteristic aircraft data are:

$$W = 37000 \text{ lbs} \quad , \quad S = 608 \text{ ft}^2$$

The resulting steady-state flight envelope can be seen in Fig.8.

## 2.3 OPERATIONAL CONSTRAINTS

The following constraints on the control variables are specified:

$$n \leq n_{max} \qquad \text{(structural limit)} \tag{13}$$

$$n \leq n_L \equiv (qS/W)C_{L_{max}} \qquad \text{(lift limit)} \tag{14}$$

Fig.9 shows $C_{L_{max}}$ as a function of M. The value of $n_{max}$ is 7.33. The load factor n is related to the control variables $n_v$ and $n_h$ by:

$$n = (n_v^2 + n_h^2)^{1/2} \tag{15}$$

It is noted that the bank angle $\mu$, related to $n_v$ and $n_h$ by:

$$\tan\mu = n_h/n_v \quad , \tag{16}$$

is an <u>unconstrained</u> variable. In addition to the constraints on the control variables, there are constraints on the state variables as well. As indicated earlier, the Mach limit and the dynamic pressure limit have been artificially enforced through data-manipulation in the present effort. The state-constraint remaining is the terrain limit:

$$h \geq h_{min} \tag{17}$$

This constraint, however, will be ignored in the trajectory computations needed for the construction of the feedback laws. The obvious reason for this is that, near the ground, flight-controls are dictated by considerations of safety rather than optimality. In Appendix A the influence of a terrain-limit on three-dimensional optimal flight trajectories is

studied. The results reveal some interesting features and may be useful in providing some qualitative guidelines.

## 2.4. OPTIMAL-CONTROL FORMULATION

The optimal-control problem to be solved is to determine the controls $\eta^*$, $n_v^*$ and $n_h^*$ such that, starting from the initial conditions,

$$x(t_o) = x_o \ , \qquad h(t_o) = h_o \ , \qquad E(t_o) = E_o \tag{18}$$

$$\gamma(t_o) = \gamma_o \ , \qquad \chi(t_o) = \chi_o, \tag{19}$$

the interceptor reaches the final conditions (dash-point),

$$x(t_f) = 0 \ , \qquad y(t_f) = 0 \ , \qquad h(t_f) = h_D \ , \tag{20}$$

$$E(t_f) = E_D \ , \qquad \gamma(t_f) = 0, \tag{21}$$

in minimum-time, $t_f$. The dash-point is indicated on the flight envelope in Fig.8. Note that the initial condition $y(t_o)$ and the final condition $\chi(t_f)$ are not prescribed, this despite the fact that a final heading $\chi(t_f) = 0$ is desired, in order to insure that the interceptor dashes in the direction of the target. The reason for this seemingly inappropriate formulation will become apparent in subsequent analysis; it will be shown that using this formulation it is still possible to reach (asymptotically) the desired final heading $\chi(t_f) = 0$.

The necessary conditions for optimality include the adjoint differential equations and transversality conditions:

$$\dot{\lambda}_x = -\partial H/\partial x \tag{22}$$

$$\dot{\lambda}_y = -\partial H/\partial y \quad , \quad \lambda_y(t_o) = 0 \tag{23}$$

$$\dot{\lambda}_h = -\partial H/\partial h \tag{24}$$

$$\dot{\lambda}_E = -\partial H/\partial E \tag{25}$$

$$\dot{\lambda}_\gamma = -\partial H/\partial \gamma \tag{26}$$

$$\dot{\lambda}_\chi = -\partial H/\partial \chi \quad , \quad \lambda_\chi(t_f) = 0 \quad , \tag{27}$$

where H is the variational Hamiltonian:

$$\begin{aligned} H = {} & \lambda_x V \cos\gamma \cos\chi + \lambda_y V \cos\gamma \sin\chi + \lambda_h V \sin\gamma + \\ & \lambda_E (V/W)[T-D] + \lambda_\gamma (g/V)[n_v - \cos\gamma] + \lambda_\chi (g/V)[n_h/\cos\gamma] + \\ & \nu_1[n_{max} - n] + \nu_2[n_L - n] \end{aligned} \tag{28}$$

Since the system is autonomous and the pay-off is the final time $t_f$, there is a first integral:

$$H = -1 \tag{29}$$

Substantial simplification of the TPBVP is obtained by closed-form integration of the adjoint Eqs.(22),(23) and (27). Using the transversality and final boundary conditions (20), the following expressions result

[64,69]:

$$\lambda_x = \text{Constant} \tag{30}$$

$$\lambda_y = 0 \tag{31}$$

$$\lambda_\chi = \lambda_x y \tag{32}$$

Going one step further, one can solve for $\lambda_x$ in terms of the parameter $\chi(t_f)$ by evaluating the first integral (29) at the final condition, assuming this is an equilibrium point:

$$H_{|t\,=\,t_f} = \lambda_x V_D \cos\chi(t_f) = -1 \quad ,$$

from which:

$$\lambda_x = -1/(V_D \cos\chi(t_f) \tag{33}$$

Assuming that the velocity-set is convex and the Euler solution nonsingular, the Minimum Principle can be used to express the optimal controls in terms of the state and adjoint variables [69]. The optimal throttle setting is given by:

$$\begin{aligned} \eta^* &= 1 \quad \text{if} \quad \lambda_E < 0 \\ &= 0 \quad \text{if} \quad \lambda_E > 0 \end{aligned} \tag{34}$$

The case $\lambda_E=0$ is singular and occurs at switchings between the throttle limits. Singular arcs, along which $\lambda_E=0$ over a nonzero time interval, may

appear with some system models, e.g. fuel-optimal or fuel-constrained, but are likely to occur for the present model only in isolated situations [14]. The optimal controls $n_v$ and $n_h$ are found from:

$$\partial H/\partial n_v = 0 \quad , \quad \partial H/\partial n_h = 0 \tag{35}$$

If neither of the load-factor constraints (13) or (14) is active, the Kuhn-Tucker multipliers $\nu_1$ and $\nu_2$ are identically zero and the following control expressions result:

$$n_v^* = [gW\lambda_\gamma]/[2\lambda_E D_i V^2] \tag{36}$$

$$n_h^* = [gW\lambda_\chi/\cos\vartheta]/[2\lambda_E D_i V^2] \tag{37}$$

If instead of $n_v$ and $n_h$, n and $\mu$ had been used as control variables, the resulting control expressions would have been more complex. This is a consequence of the fact that such expressions would involve $\tan\mu$ rather than $\mu$ directly, with the obvious complication of multiple roots.

If one of the load-factor constraints is active, it can be used in conjunction with the optimal-control conditions (35), to solve for $n_v$, $n_h$ and the multiplier corresponding to the active constraint (the multiplier corresponding to the inactive constraint is identically zero). The optimal controls $n_v$ and $n_h$ in the case of an active load-factor constraint are:

$$n_v^* = -[\lambda_\gamma][\inf(n_L, n_{max})]/[(\lambda_\chi/\cos\gamma)^2 + \lambda_\gamma^2]^{1/2} \tag{38}$$

$$n_h^* = -[\lambda_\chi/\cos\gamma][\inf(n_L, n_{max})]/[(\lambda_\chi/\cos\gamma)^2 + \lambda_\gamma^2]^{1/2} \tag{39}$$

If both load-factor limits are met simultaneously, Eqs. (13) and (14) can be solved for the "corner velocity" at any given energy level:

$$V_c = [2Wn_{max}/qSC_{L_{max}}]^{1/2} \tag{40}$$

By evaluating the corner velocity over the entire range of specific energy, a unique curve in the (V,h)-space called the "corner-velocity locus", is obtained (see, e.g., Fig.10). The significance of this curve is two-fold [14]. Firstly, the corner-velocity locus features maximum <u>instantaneous</u> turn rate at any given energy level. Secondly, this curve separates two distinct regions in the (V,h)-space: above the corner-velocity locus the load factor is constrained by the lift limit (14); below the corner-velocity locus the load factor is constrained by the structural limit (13).

It should be noted that only the multiplier $\nu_2$ is needed in the evaluation of the right members of the adjoint equations (24) and (25). This is a consequence of the fact that the structural constraint (13), in contrast to the aerodynamic constraint (14), does not depend on the state variables E and h. This feature, clearly advantageous in numerical work, would not have been present if, e.g., $C_L$ had been selected as control variable.

The TPBVP, determined by the system of state and adjoint equations with the appropriate boundary and transversality conditions, can be solved in open-loop form only. A closed-form feedback solution can be obtained if the intercept problem is treated in reduced-order (so-called "energy-state") approximation.

## CHAPTER 3. ENERGY-STATE MODEL

### 3.1 SINGULAR-PERTURBATION APPROACH

In the energy-state approach , it is assumed that there is a time-scale separation such that $(h,\gamma)$ behave as fast variables as compared with $(x,y,E,\chi)$. This suggests order-reduction by letting $\dot{h},\dot{\gamma} \to 0$ in Eqs. (3) and (5), resulting in the algebraic constraints [14]:

$$\gamma^r = 0 \tag{41}$$

$$n_v{}^r = 1 \tag{42}$$

The remaining four state equations (1), (2), (4) and (6) form the reduced-order system. The control variables in the energy-state model are $\eta$, $n_h$ and h. Application of the Minimum Principle to the reduced-order problem results in the following optimal-control expressions, assuming the load factor is within its permissible range:

$$n_h{}^r = [gW\lambda_\chi]/[2\lambda_E D_i V^2] \tag{43}$$

$$h^r = \arg\min_h [H] \quad , \tag{44}$$

where the expression (28) for H is still valid. As a result of the order-reduction not all of the boundary conditions imposed on the state variables in the original problem can be satisfied. Consistent with

singular-perturbation theory, the boundary conditions on the "slow" variables are retained, while the boundary conditions on the "fast" variables are met by allowing discontinuities ("jumps") at $t = t_o$ and $t = t_f$. Since the min-H operation (44) leads to the dash-point on the flight envelope [8,14], no jumps occur at $t = t_f$ in the present formulation.

Since $n_v(t) \equiv 1$, the load-factor constraints (13) and (14) are very simple to enforce in the energy-state approach. The expression for the optimal throttle-setting (34) for the point-mass model applies to the energy-state model as well. Also, since the geometry of the intercept remains unchanged in the energy-state model, the expressions for the adjoints (30)-(33) are still valid. As a result only one adjoint equation (governing $\lambda_E$) needs to be integrated in the energy-state approach. If we consider symmetric flight only ($n_h(t) \equiv 0$), no adjoint equations need to be integrated at all. In Ref.8 it is shown that for the so-called energy-range climb the energy adjoint is given by:

$$\lambda_E = (V - V_D)/(V_D\dot{E}) \tag{45}$$

The right member of Eq.(45) is clearly singular when evaluated at the steady-state dash-point. In the energy-state approximation the equilibrium-point is reached only asymptotically.

## 3.2 EXTREMAL-FIELD SOLUTION

The particular form in which the energy-state model is written allows a family of trajectories to be generated using an extremal-field approach. Starting from the terminal manifold the state-Euler equations are integrated backward in time, with an assumed value for the final heading. By slightly varying the value of final heading, the state-space is flooded with extremals. The only unknown parameter at the terminal manifold is the final value of the energy adjoint. However, the parameter $\lambda_E(t_f)$ can be obtained by evaluating Eq. (45) for the energy-range climb. This parameter can be used for the evaluation of the remaining members of the family as well (it is recalled that $\lambda_\chi(t_f) = 0$ and as a consequence of Eq.(43), $n_h(t_f) = 0$ for all turn-climb trajectories).

## 3.3 GENERAL FEATURES

In Fig.10 several extremals in the (V,h) space are sketched. In Fig.11 some ground tracks are shown. If final heading is chosen identically zero the (symmetric) energy-range climb path is obtained. The remaining members of the family (obtained by very small variations in final heading) all reveal a similar behavior in retro-time: starting from the dash-point the trajectories closely follow the energy-range path (in near-symmetric flight), but, when the turn is initiated, altitude increases (possibly discontinuously) until the corner-velocity locus is reached. The trajectories will subsequently "ride" the corner-velocity locus, with heading-to-go increasing in retro-time. The optimal throttle-setting generally

is full thrust; however, for large heading-to-go, throttle-switching may occur.

It is observed that the turn-climb trajectories lie almost entirely within a corridor formed by the corner-velocity locus and the energy-range climb path. A similar corridor was noted in the energy-modelled study of Ref.71. The behavior demonstrated by the extremals is fairly transparent. In the optimization process the optimal trade-off between the conflicting requirements of a high turn rate and a high energy-range rate is established. It is evident that, for large heading-to-go, the turn rate is emphasized and hence control actions are such that flight is on or near the corner-velocity locus. As heading-to-go is decreased the emphasis shifts towards high energy and range rates and the control actions are such that the flight is directed generally towards the energy-range climb path.

Fig.12 shows some extremals in the (χ,E)-space. It is noted that the extremals provide simple covering of the region, i.e. the mapping is one-to-one. In other words, the optimal-control solutions of the energy-state family can be expressed as functions of specific energy E and heading angle χ , i.e. $\eta^r = \eta^r(E,\chi)$, $n_h{}^r = n_h{}^r(E,\chi)$ and $h^r = h^r(E,\chi)$. The energy/heading family of energy-state solutions, seemingly is an attractive candidate to serve as a "reference family" in a feedback-guidance scheme. Unfortunately, however, the energy-state model exhibits several undesirable features which impair its suitability for such an application. One of the most unrealistic features in the energy-state model is

the frequent occurrence of instantaneous jumps in altitude, not only at the endpoints (to meet the the boundary conditions) but also internally. Another weakness of energy-state modelling is that it results in a zero path-angle approximation. It should be noted that a different path-angle estimate is produced if a different selection of "slow" and "fast" variables is used in the energy-state analysis. This is shown for the symmetric range-open energy climb in Ref.72, where a transformation of state variables is proposed with the objective of enhancing time-scale separation. Although the fidelity of the reduced-order solution could be improved with this technique for this particular problem, the approach will sometimes be impractical for more complex system models, since the transformations involved are defined by complex partial differential equations. Singular-perturbation techniques may be used to overcome some of the weaknesses in the energy-state model. For example, boundary-layer corrections can be used to generate smooth transients from the initial conditions to what, in singular-perturbation theory, is termed the "outer" solution (reference family). However, as pointed out in the Introduction, these procedures are not without problems.

## CHAPTER 4. POINT-MASS MODEL

### 4.1 REFERENCE FAMILY

The alternative procedure proposed in Ref.65, which avoids many complications but is nontheless simple enough to lend itself to on-board implementation, will now be applied to three-dimensional minimum-time intercept. In the proposed scheme a hierarchical structure similar to that of the energy-state model is assumed: trajectories of an energy/heading family (reference family) funnel into a steady-state cruise-dash; trajectories of an altitude/path-angle family (boundary-layer transients) funnel into individual members of the energy/heading family. The present 3-D scheme differs from the 2-D scheme of Refs. 66 and 67 only in that a family of reference extremals is used instead of a single reference path.

Rather than to use energy-state solutions to build up the reference family (as in the usual singular-perturbation approach), one may employ a family of point-mass-modelled state-Euler solutions. The energy-state solutions are used to select the initial conditions for the individual point-mass-model trajectories that form the reference family. Since we desire a reference family extending over the widest range of energy and heading possible, initial heading-to-go for the individual trajectories is selected as $180^{\circ}$ (this choice provides a complete $360^{\circ}$ range of heading, due to symmetry). The energy-state solutions suggest a zero initial

path-angle and an initial altitude on the corner-velocity locus. Initial range-to-go is selected sufficiently large to allow an asymptotic approach of the equilibrium point for each individual member of the family (700 kft). Since one assumes the behavior of the point-mass-model trajectories to be similar to that of the energy-state model, one anticipates heading to asymptotically reach zero and with the prejudice of foresight Eq.(33) reduces to:

$$\lambda_x = -1/V_D \tag{46}$$

## 4.2 NUMERICAL SOLUTION OF THE TPBVP

Using the results (30)-(32) and (46) the TPBVP is reduced to a set of 10 differential equations, 9 of which are given by Eqs.(1)-(6),(24)-(26). A tenth differential equation results if the parameter $t_f$ is treated as a state variable:

$$\dot{t}_f = 0 \tag{47}$$

The 10 boundary conditions needed to solve these equations are given by Eqs.(18)-(21).

As mentioned earlier, state-Euler solutions are generated using a multiple-shooting algorithm (MSA). The main advantage of this procedure is that numerical-error growth is suppressed by dividing the integration

interval into a number of subintervals. Since the state-Euler system associated with the point-mass model is highly unstable, this is an important feature. The MSA is described in detail in Ref.1. Here only the principles of the basic algorithm (without the complication of switching functions) are briefly outlined.

The multiple-shooting algorithm can be used to solve nonlinear TPBVP's of the form:

$$\dot{z} = f(z,t) \tag{48}$$

$$g[z(t_o), z(t_f)] = 0 \quad , \tag{49}$$

where z(t) is the n-vector of state and adjoint variables and g the n-vector of initial and final boundary conditions. The interval is divided into m subintervals by introducing the grid points:

$$0 = t_o < t_1 < \ldots < t_m = t_f \quad , \tag{50}$$

where, without loss in generality, it is assumed that $t_o = 0$. In each subinterval $t \in [t_j, t_{j+1}]$, j=0,...,m-1 the initial-value problem:

$$\dot{z} = f(z,t) \quad , \tag{51}$$

is solved with the initial conditions:

$$z(t_j) = Z_j \tag{52}$$

Starting with an initial guess $Z_j^{(0)}$, $j=0,\ldots,m-1$, the problem then consists of finding values for $Z_j$ such that the solutions are continuous across the subintervals and the boundary conditions are satisfied. In other words, the function:

$$r = [r_0, r_1, \ldots, r_{m-1}]^T \quad , \tag{53}$$

where:

$$r_j = z(t_{j+1}, Z_j) - Z_{j+1} \quad , \; j = 0,\ldots,m-2 \tag{54}$$

$$r_{m-1} = g[Z_0, z(t_m, Z_{m-1})] \quad , \tag{55}$$

must vanish. The 1st m-1 components of r are the jumps across the grid points. Applying the Newton method for adjusting the $Z_j$, the linear system:

$$\begin{bmatrix} G_0-I & 0 & \ldots & \ldots & 0 \\ 0 & G_1-I & & & 0 \\ \vdots & & & & \vdots \\ 0 & & & G_{m-2}-I & 0 \\ A & 0 \ldots & & \ldots 0 & BG_{m-1} \end{bmatrix} \begin{bmatrix} \Delta Z_0 \\ \Delta Z_1 \\ \vdots \\ \Delta Z_{m-2} \\ \Delta Z_{m-1} \end{bmatrix} = - \begin{bmatrix} r_0 \\ r_1 \\ \vdots \\ r_{m-2} \\ r_{m-1} \end{bmatrix} \tag{56}$$

has to be solved for $\Delta Z_j$ with:

$$G_j = \partial z[t_{j+1}, Z_j]/\partial Z_j \tag{57}$$

$$A = \partial g/\partial z(t_o) \quad , \quad B = \partial g/\partial z(t_f) \tag{58}$$

and I is the identity matrix. After solving for $\Delta Z_j$, the new values for $Z_j$ are computed from:

$$Z_j^{(k)} = Z_j^{(k-1)} + \delta \Delta Z_j \quad , \tag{59}$$

where $\delta$ is the relaxation factor of the Newton method. The band structure of the linear system (56) allows the system to be reduced in size. This reduced system can be solved for $\Delta Z_0$. The remaining terms $\Delta Z_j$ can then be obtained from recursive equations. Although the reduced size of the system appears to be an attractive feature, it is not used in the presently-employed algorithm. The reason why solving the original large system is preferred over solving the reduced system is that the large system is much better conditioned. In the MSA a Broyden method is used to update the Jacobian, thus largely reducing the computational burden. One of the major advantages of the MSA is that it is well-suited to handle multi-point-boundary-value problems which, for instance, arise in optimal control problems involving state-constraints. A disadvantage of the method is that a relatively good initial estimate to the solution is required. However, by using the MSA in conjunction with a continuation procedure (on the initial conditions), this problem can be substantially alleviated. In the present effort the first turn-climb trajectory was obtained by using the symmetric energy-range climb of Ref.67 as initial guess and by gradually increasing the initial heading.

Stability considerations play not only an important role in the selection of a numerical optimization method, but also in the formulation of the

TPBVP itself. Especially the formulation of a three-dimensional problem requires carefull attention. problem. As mentioned earlier, in the present effort the final heading is not prescribed, despite the fact that that zero final heading is desired. The special form in which the problem is formulated allows the desired final heading to be reached asymptotically. If one were to specify final heading, then the initial value of the heading adjoint would require iterative calculation. The state-Euler system is extremely sensitive to this parameter and severe stability problems result [67]. In the present approach the initial cross-range is iterated upon, and no serious stability problems result. One of the most important contributions of the present research effort is that the heading adjoint, a major source of stability problems, has been completely eliminated from the problem by paying careful attention to aspects as location and orientation of the reference frame, stipulation of boundary conditions, closed-form integration of some of the adjoint equations and use of first integrals.

Some of the point-mass trajectories of the reference family are shown in Fig.13. The energy-management features observed earlier in the energy-state model are confirmed by these point-mass model results. It is noted that all trajectories in the reference family are flown with full throttle. In Fig.14 a typical 3-D trajectory is shown. The ground track of this trajectory is sketched as well.

# CHAPTER 5. FEEDBACK SOLUTION

## 5.1 GUIDANCE SCHEME

The next step is to generate a near-optimal guidance law that will transfer the interceptor to the vicinity of the reference family. A closed-loop controller, based on linear feedback of altitude and path-angle errors (where error is defined as the difference between the actual and the nominal value) is synthesized along the lines contemplated in Ref.65. The resulting feedback laws are of the following form:

$$n_v^{fb} = n_{v_{ref}}(E,\chi') + \frac{\partial n_v}{\partial h}(E,\chi')\,[h - h_{ref}(E,\chi')] + \frac{\partial n_v}{\partial \gamma}(E,\chi')\,[\gamma - \gamma_{ref}(E,\chi')] \tag{60}$$

$$n_h^{fb} = n_{h_{ref}}(E,\chi') + \frac{\partial n_h}{\partial h}(E,\chi')\,[h - h_{ref}(E,\chi')] + \frac{\partial n_h}{\partial \gamma}(E,\chi')\,[\gamma - \gamma_{ref}(E,\chi')] \tag{61}$$

where $\chi'$ is defined as:

$$\chi' \equiv \ln(|\chi|/\pi) \tag{62}$$

Evidently the control commands $n_v^{fb}$ and $n_h^{fb}$ must be subjected to the constraints (13) and (14). The decision to initiate a left or a right turn, i.e. the sign of $n_h^{fb}$, depends on the sign of the measured heading

angle ($-\pi \leq \chi \leq \pi$). The sign of $n_h^{fb}$ is selected such that $|\chi|$ decreases in time. The reference variables, i.e. altitude, flight path-angle, the controls and the feedback gains, are functions of two variables, E and $\chi'$. The particular choice of the non-dimensional variable $\chi'$ accounts for the exponential character of the heading transient and insures that the reference variables can be accurately represented by spline-lattices over the entire range of energy and heading.

## 5.2 REFERENCE-VARIABLE MAPPING

Figs. 15 and 16 show the maps of altitude, $h_{ref}(E,\chi')$ and of reference path-angle $\gamma_{ref}(E,\chi')$. As far as the mapping of the remaining reference variables is concerned, an indirect approach is used in the present effort. As indicated in the introduction, there is no unique choice of control variables. It turns out that it is advantageous to use a different set of control variables for the reference data. The disadvantage of using $n_v$ and $n_h$ as control variables is that they are coupled by the constraints (13) and (14). If on the other hand n and $\mu$ are used as control variables, only one of the variables (n) is affected by the constraints. This is the reason why the set n and $\mu$ is used for generating the database. By using the following transformations, the reference variables needed in the evaluation of the feedback laws (60) and (61), can be obtained from the precomputed data:

$$n_{v_{ref}} = n_{ref}\cos\mu_{ref} \quad , \quad n_{h_{ref}} = n_{ref}\sin\mu_{ref} \tag{63}$$

$$(\partial n_v/\partial h) = \cos\mu_{ref}(\partial n/\partial h) - n_{ref}\sin\mu_{ref}(\partial\mu/\partial h) \quad (64)$$

$$(\partial n_v/\partial\gamma) = \cos\mu_{ref}(\partial n/\partial\gamma) - n_{ref}\sin\mu_{ref}(\partial\mu/\partial\gamma) \quad (65)$$

$$(\partial n_h/\partial h) = \sin\mu_{ref}(\partial n/\partial h) + n_{ref}\cos\mu_{ref}(\partial\mu/\partial h) \quad (66)$$

$$(\partial n_v/\partial\gamma) = \sin\mu_{ref}(\partial n/\partial\gamma) + n_{ref}\cos\mu_{ref}(\partial\mu/\partial\gamma) \quad (67)$$

At this stage one might wonder why the set n and μ is not used directly in the feedback scheme. As a matter of fact such a scheme has been examined; however, in numerical simulation runs it proved to be inferior to the currently-recommended scheme, especially for large deviations from the nominal state. For a certain type of maneuver (high-speed yo-yo), the alternative scheme broke down altogether. This was a result of the fact that the linear corrections terms caused the load factor to become negative for large deviations from the reference, which by definition is impossible (see Eq.(15)). For these reasons the set $n_v$ and $n_h$ was retained.

In Figs. (17) and (18) the reference control maps are shown. The regions where the load factor is constrained (either by Eq.(13) or (14)) are cross-hatched in Fig.17. The gap separating the two constrained-control areas has been the subject of speculation. In this region the aircraft accelerates through the transonic region with the aid of gravity, while executing a rather hard turn at the same time. It is conjectured that load factor is slightly reduced below its constrained level in order to temper

the effect of the transonic drag-rise. For this reason this area will be referred to as the "transonic region".

The precomputed feedback gains are in effect the partials of the control variables n and $\mu$ with respect to the "fast" state variables h and $\gamma$, with E and $\chi$ held constant. They are obtained numerically in difference-quotient approximation as the average of the forward and backward differences [67]. To this end, for each initial condition calculations are redone with small perturbations from the reference values in altitude and flight-path angle. The feedback gains are evaluated along the reference trajectories by successively treating intermediate points as "new" initial conditions. From the viewpoint of computational efficiency as well as accuracy, it is natural to use the grid points of the MSA (assuming they are appropriately distributed over the interval) as the "new" initial conditions. It should be noted that, in order to compute the feedback gains accurately, highly accurate state-Euler solutions are needed [67]. The MSA proved to be an extremely powerful tool in this respect.

The four gains are shown as functions of E and $\chi'$ in Figs.18-21. In the regions where the reference load factor is constrained, no partials of the load factor are evaluated. As a matter of fact it may not even be possible to evaluate those partials as they may not be defined. This is for example the case on the corner-velocity locus where a discontinuity in the partial of the load factor with respect to the altitude, appropriate to the values of lift and structural limit, is occasioned. Ref.55, which deals with neighboring-optimal guidance, furthermore shows that the

presence of inequality constraints on control variables generally leads to nonlinear control behavior. This clearly is an unwelcome complication and one may consider a simple alternative approach instead. This approach entails the following: in those regions in the ($\chi'$,E)-space where the reference load-factor is constrained, the value zero is assigned to the partials of the load factor. This amounts to using open-loop control (at least with respect to n) as long as the reference load-factor is constrained.

## 5.3 REFERENCE-DATA REPRESENTATION

The reference variables are computed preflight, but are to be stored as functions of E and $\chi'$ for on-board use. This requires bivariate or, possibly, linearly-interpolated fits for double-table-look-ups. Among the many methods, bicubic-spline fitting is a commonly employed technique. However, this method requires the use of a rectangular grid for the coordinate variables. From Fig.12 it is clear that in the present case the data points are irregularly distributed. There are two ways to go about solving this problem. Firstly, a local splining technique, capable of handling irregularly distributed data, can be used. Secondly, the irregularly-distributed sample-data points can be used to estimate the values of the mapped variables at the nodes of a specified rectangular grid by interpolation between surrounding data points. Once the rectangular grid has been generated, the bicubic spline technique can be used. Both options have been examined to some extent. The bivariate fit, described in Ref.73, calculates an interpolating function which is a

fifth-degree polynomial in each triangle of a triangulation in the coordinate-plane. The interpolating function is continuous and has continuous first-order partial derivatives. Unfortunately, however, the routine implementing this method [74], did not perform satisfactorily for the present problem and some very undesirable features, most notably excessive "wiggling" of the splined functions, were noticed. The second approach proved to be much better in this respect. A rectangular grid was generated using the nearest neighbor method, described in Ref.75. A nearest neighbor method can be used to estimate the value of the mapped variable at a specified grid node by searching for the n nearest sample data points regardless of their radial distribution around that node. In the present effort the value of the mapped variable at a grid-point is estimated by a distance-weighted average of 8 nearby sample data points. After gridding, the bicubic spline routine of Ref.74, implementing the method of Ref.76, can then be used to represent the data. The maps presently employed have been generated using this second approach.

It is evident that the number of data points has a profound impact on the accuracy of the representation. For establishing the grid values of the control and state variables approximately 1500 data points on 26 extremals were used. In order to obtain a nearly uniform distribution of sample data points across the map, the coordinate variable E is rescaled in the spline routine, so that it is of the same order of magnitude as $\chi'$. The evaluation of the feedback gains requires the solution of five TPBVP's at each sample point. It is evident that a tremendous computational effort would be required if a density of sample points similar to that of the

reference control and state variables were to be used for the gains. In order to curtail the computational effort, approximately 100 data points on 8 extremals, were used to estimate the grid values for the feedback gains. The size of the specified grid-matrix is 27 × 21 (= 567 nodes), with an equal spacing in each coordinate direction. This representation proved to be satisfactory for the purpose of digital simulation of a point-mass system model driven by the feedback laws.

## 5.4 IMPLEMENTATION ASPECTS

It is observed that the heading transient is rather fast and this suggests that the assumed ordering of "slow" and "fast" variables in the energy-state model may not be correct. This discrepancy has been noticed in the literature. Ref.43 gives as reasons for treating $\chi$ as a "slow" variable, the fact that certain maneuvers such as "high- and low-speed yo-yo's", can be better modeled and the fact that the inclusion of $\chi$ in slower subsystems is relatively easy, since the adjoint equation associated with $\chi$ can be analytically integrated. In the present approach a reason of at least equal importance is that $\chi$ varies monotonically during a maneuver, which makes it such a suitable coordinate-variable for reference-variable mapping in the first place.

Nevertheless, the fast behavior of the heading transient does pose some serious problems in a "real-world" situation. These problems stem from the fact that the feedback laws require accurate measurements of the heading angle. In an airborne implementation, where measurement errors

are inevitable, it may therefore actually be required to replace measured values of $\chi$ by predicted values, in particular for small heading-to-go when the relative measurement-errors are large. Such predictions can be made for instance by assuming that the heading transient can be described by an exponential function of time, with a time-constant to be estimated and updated on-line. In digital simulation of a point-mass system model, the implementation of the feedback laws does not present any problems.

The range of the coordinate $\chi'$ in the reference-variable maps extends from -10 to 0. However, due to the exponential behavior of the heading transient, the value of $\chi'$ will eventually move out of this range as the maneuver progresses. The selection of the range of $\chi'$ for the reference variable maps, is not just arbitrary. The range of $\chi'$ is selected such as to insure that the altitude and path-angle transients can be as good as completed within that range. If $\chi'$ becomes too small and moves out of the range, a simple switch to 2-D symmetric flight ($n_h \equiv 0$) is made. The feedback law for 2-D symmetric flight is essentially the same as the one described in Refs.66 and 67, however with $n_v$ replacing $C_L$ as control variable.

In the "transonic region" some of the feedback gains may vary rather rapidly, reach high peak-values and even change sign (see Figs.19-22). As a result unstable flight conditions may occur for trajectories emanating from or passing through this transonic region, if no preventative measures are taken. Similar unstable situations may occur for trajectories emanating from the region in the $(\chi', E)$-space, where $\partial\mu/\partial\gamma$ is nega-

tive (see Fig.22). One of the measures that could be taken to alleviate such instability problems is to bound the magnitude of the altitude/path-angle perturbations. However, such a measure would clearly affect flight-paths originating outside the transonic region as well. For this reason we have opted for another measure, namely to bound the feedback gains. The following bounds have been adopted:

$$\partial n_v/\partial h \leq 10^{-4} \ (m^{-1}) \quad , \quad \partial n_v/\partial \gamma \leq 1 \ (rad.^{-1}) \tag{68}$$

$$|\partial n_h/\partial h| \leq 0.25 \ 10^{-4} \ (m^{-1}) \quad , \quad |\partial n_h/\partial \gamma| \leq 1 \ (rad.^{-1}) \tag{69}$$

The values of the bounds evolved from extensive numerical simulation of the point-mass system model, driven by the feedback laws. The values of the bounds are such that the gains outside the indicated unstable regions in the $(\chi', E)$-space are not or hardly affected, while undesired flight conditions within those regions can be avoided. The occurrence of unstable flight situations is one of the more unpleasant complications in the extension to 3-D. A more serious stability study of the point-mass system model driven by the feedback laws clearly is of interest for future research.

It is noted that the control laws (21) are independent of the cross-range y. Execution of these laws during an engagement may therefore actually cause the interceptor to fly parallel to, rather than behind the target, in the dash phase of the mission. Assuming that the initial cross-range

is small compared to the total range-to-go a simple offset correction can be devised to overcome this problem. The offset correction is obtained by adding a correction term:

$$\Delta\chi = \arctan[y/(x_f - x)] \quad , \tag{70}$$

to the measured heading angle. The effect of the correction term is very limited if heading-to-go is large; however, if the heading error is almost closed the correction term becomes dominant and actually dictates a new course: a collision course. The coordinates of the collision point are $(x_f,0)$, where $x_f$ is the projected down-range position of the target. Fig. 23 illustrates the effects of the offset correction incorporated in the feedback strategy with $x_f = 0$.

It is evident that the constant-weight assumption made in the formulation of the point-mass system model is violated in actual flight due to fuel expenditure. In particular, if the aircraft operates with full afterburner, as in the presently considered mission, fuel consumption will, in fact, decrease the aircraft weight rapidly. Since weight variations obviously affect the aircraft's control strategy, corrective actions are called for. Due to high fuel consumption, the aircraft can operate with full afterburner for a very brief period only. Optimal control strategies are therefore imperative, if the airplane is to prove effective during this brief period of afterburning operation. A very simple way to account for weight variations is by computing the feedback control laws for two different aircraft weights: a high weight and a low

weight. The control commands for the (estimated) actual weight are then determined by interpolation between the high- and low-weight solutions. In eventual on-board real-time implementation of the scheme contemplated, similar corrections for off-nominal ambient temperature and winds-aloft are called for as well. Another issue that has to be addressed before a practical implementation of the controller could take place is to evaluate and compensate for the effects of changes in the aircraft configuration, due to the release of external stores for instance, on the guidance scheme.

## CHAPTER 6. POINT-MASS SIMULATION

The guidance scheme was tested in digital simulation runs using a point-mass system model. The range of validity of the feedback laws was examined by comparing approximate feedback solutions to open-loop optimal solutions for a wide variety of initial flight conditions.

In the present effort the initial flight-path angle for the reference extremals was selected as zero. As indicated in Chapter 3 a different selection, for example the path-angle corresponding to unaccelerated flight, can be argued. This raises the question as to what extent this choice influences the performance of the controller. To address this issue the following numerical experiment was conducted. For a given reference extremal ($E_o$= 70 kft) the initial path-angle was varied while the remaining initial conditions remained unchanged. Using the feedback laws the point-mass model was simulated starting from the very same initial conditions. For the open-loop optimal as well as the closed-loop approximate solutions, the performance index (time-of-flight) was recorded. The results are presented in Fig.24. From the results it is evident that the feedback laws perform quite satisfactorily even for large initial deviations from the zero reference value of path angle. It therefore seems safe to state that the effect of a particular choice of the initial path-angle for the reference extremals on the performance of the controller is limited. It is interesting to note that the local maximum on the curve in Fig.24 corresponds to the state-Euler solution with

the initial path-angle free ($\mu = 90^{\circ}$). State-Euler solutions with very large initial path-angles are difficult to obtain. This is caused by the singularity in the equation of motion (6) for $\gamma = \pm 90^{\circ}$. The convergence of the MSA is very poor for near-singular values of the flight-path angle occuring anywhere along the extremal. The singularity in the equations of motion defined by Euler angles can be avoided by using quaternions instead [77]. However, by doing so the possibility of additional singular subarcs in the optimal- control solution is introduced, a clearly unwelcome complication. The present equations of motion (1)-(6) are adequate to describe most 3-D maneuvers of interest, as will become clear from the examples presented.

The feedback laws do not only perform satisfactorily for large perturbations in path-angle, but also for large perturbations in altitude as well as for combined path-angle/altitude perturbations. To illustrate this, five numerical examples featuring a variety of maneuvers are presented. Fig.25 shows the solutions in the (V,h)-space for the five examples. For each of the examples the characteristic features will be shown in more detail. The initial conditions for <u>example 1</u> are:

$$x_o = -700 \text{ kft} \quad , \quad h_o = 7.5 \text{ kft} \quad , \quad E_o = 10 \text{ kft}$$
$$\gamma_o = 0^{\circ} \quad , \quad \chi_o = -170^{\circ}$$

The results are shown in Figs.26-32. There is only a small initial deviation in path-angle from nominal (see Fig.27), but the initial deviation in altitude is about 3000 ft above nominal (see Fig.26). The optimal-

control histories are shown in Figs.28 and 29; however, these results are perhaps better understood if the load-factor and bank-angle histories (Figs.30 and 31) are examined first. Since the trajectory starts above the corner-velocity locus, load factor is constrained by the lift limit in the initial phase. The feedback load-factor history shows an overshoot which is compensated for by an earlier onset of the decay. The "wiggles" in the load-factor history are caused by the aircraft passing through the transonic region. The initial bank-angle is close to $180^{\circ}$, which is characteristic for maneuvers starting at altitudes far above nominal. In particular at high energy levels, when transients are not as rapid, the initial phase of such maneuvers tends towards a split-S (also see example 2 of Ref.78), reaching path-angles close to $-90^{\circ}$. At low energy levels, as in this example, heading transients are generally rather fast, as can be observed in Fig.32. The time-of-flight for the optimal trajectory is $t_f$=374.20 sec. The feedback trajectory takes about 0.80 sec (or 0.2%) more. The initial conditions for example 2 are:

$$x_o = -700 \text{ kft} \quad , \quad h_o = 0 \text{ kft} \quad , \quad E_o = 25 \text{ kft}$$
$$\gamma_o = 0^{\circ} \quad , \quad \chi_o = -150^{\circ}$$

Some of the results are shown in Figs.33 and 34. In this example the initial altitude is about 16000 ft below nominal. The aircraft executes a rather steep climbing turn, losing speed, before fairing into the reference flight-path. The optimal-control solution of this type of maneuvers has some very distinct features. This will be demonstrated by example 4, which has similar, but more pronounced features. The difference in

time-of-flight between the optimal solution and the feedback approximation is only about 1.03 sec (or 0.3%). The initial conditions for example 3 are:

$$x_o = -700 \text{ kft} \quad , \quad h_o = 40 \text{ kft} \quad , \quad E_o = 48 \text{ kft}$$
$$\gamma_o = 0^o \quad , \quad \chi_o = -145^o$$

This particular example serves to demonstrate a trajectory that originates in the transonic region. Maneuvers of this type are among the most difficult to be performed by the guidance scheme. Figs.35-37 show some of the results for this example. The initial deviations from nominal are considerable, both in altitude and path-angle. The most striking feature of a "transonic maneuver" as presented in this example can be seen in the load-factor history of Fig.37. The optimal load-factor history has two very distinct peaks. The feedback solution "reproduces" those peaks actually rather well. As a result the difference between the optimal solution and the feedback approximation is only about 1.8 sec (or 0.5%). The initial conditions for example 4 are:

$$x_o = -700 \text{ kft} \quad , \quad h_o = 27.5 \text{ kft} \quad , \quad E_o = 70 \text{ kft}$$
$$\gamma_o = 45^o \quad , \quad \chi_o = -135^o$$

Example 4 is representative for another category of "difficult" maneuvers: high-speed yo-yo's. Several interesting details of the solution for this particular example are shown in Figs.39-43. Initial altitude is about 12000 ft below nominal, while the path-angle is about $65^o$ above nominal.

Similar to example 2, the maneuver starts out with a climbing turn with speedloss. However, unlike example 2, the aircraft subsequently converts altitude back into kinetic energy (see Fig.38). From the viewpoint of energy management such behavior is perfectly logical: by converting kinetic energy into altitude, the flight is directed towards the corner-velocity locus, resulting in improved turning performance. Once the turn has been nearly completed, the excess potential energy (altitude) can be reconverted into kinetic energy (velocity) in order to improve range and energy rates. Fig.40 shows that the feedback control $n_v$ lags the optimal control $n_{v_*}$. From Figs.42 and 43 it is clear that this is mainly caused by a lag in bank angle. The bank-angle history of Fig.43 is typical for a high speed yo-yo maneuver: initially bank angle is below $90^\circ$, followed by a brief period in which bank angle is above $90^\circ$ and finally bank angle decays to zero. The behavior of the optimal bank-angle history is quite different from the reference bank-angle history which probably accounts for the fact that this type of maneuver is difficult to perform. Nevertheless the guidance scheme is capable of handling this type of maneuver quite satisfactorily. A difference in time-of-flight of about 2.6 sec (or 0.8%) for this particular example clearly supports this claim. The initial conditions for <u>example 5</u> are:

$$x_o = -700 \text{ kft} \quad , \quad h_o = 55 \text{ kft} \quad , \quad E_o = 110 \text{ kft}$$
$$\gamma_o = 0^\circ \quad , \quad \chi_o = -140^\circ$$

The purpose of this particular example is to demonstrate a maneuver starting at a high energy level. Like example 1, the initial altitude is

substantially above nominal (about 9000 ft for this example). The initial path-angle is about $25^{\circ}$ above nominal. Some of the results are shown in Figs.44-48. One interesting feature that can be observed is that the transients of this maneuver are much slower than the transients for similar maneuvers initiated at much lower energies (compare for instance to example 1). Another interesting feature is that the control variable $n_v$ behaves rather mildly. The time-of-flight for the optimal trajectory is $t_f$=330.67 sec. The difference in time-of-flight between the optimal solution and the feedback approximation is about 0.33 sec (or 0.1%).

In all more than a hundred simulation runs were made for a variety of initial conditions. <u>All</u> examples examined (with $-45^{\circ} \leq \gamma_o \leq 45^{\circ}$) had an accuracy of 1% or better, a rather impressive result.

## CHAPTER 7. CONCLUSIONS

An automatic guidance scheme for a three-dimensional aircraft intercept mission has been developed. The scheme employs state-Euler solutions for a point-mass model, but makes use of singular-perturbation ideas in terms of a hierarchical trajectory-family structure. Indeed the turn-climb schedules that emerge fair gracefully into a cruise-dash. Numerical examples revealed that, despite their linear nature, the feedback laws perform accurately even for large departures from the nominal state.

The flight paths for the sample aircraft, representing a high-performance fighter, revealed some surprising features. One of the most striking features was that all examined trajectories with a heading-to-go of $180^{o}$ or less were flown full-throttle. A second surprising feature was the wide range of flight-path angles observed in many maneuvers. It is believed that these characteristics may be the result of the particular aircraft model used, featuring a rather high thrust-to-weight ratio.

Several attempts to develop an automatic guidance scheme for three-dimensional intercept missions have been made in recent years, mostly using singular perturbation techniques [47,48]. The singular-perturbation procedures employed essentially decompose the original 3-D problem into vertical and horizontal sub-problems. The resulting guidance laws are vectorial compositions of the orthogonal 2-D guidance laws. However, such guidance laws have some serious deficiencies. First of all, the decom-

position of the 3-D problem into two 2-D sub-problems can be justified only if the assumption $\cos\gamma = 1$ holds, which is clearly not the case, as our results bear out. Secondly, relating to the vertical sub-problem, the artificial time-scale separation between the strongly coupled altitude and path-angle dynamics is difficult to justify. And thirdly, there is the problem of altitude jumps in the outer solution, calling for separate internal boundary layers. Some ad-hoc engineering approaches to alleviate some of these deficiencies have been suggested recently [79]. However, the validity of all of these feedback laws is still largely untested.

The presently proposed scheme does not suffer from any of these deficiencies. Moreover, its validity is demonstrated by comparison with exact solutions. Nevertheless there are some weaknesses in the present approach as well. Unlike the nonlinear feedback laws obtained using singular perturbation techniques, the present scheme is rather inflexible with respect to variations in design factors, operational constraints and atmospheric conditions. Corrective measures along the lines of Chapter 5 are possible, but do require a significant amount of storage space. Due to this lack of flexibility the present scheme is also less suitable for applications involving rapid systematic parametric studies, such as preliminary design or performance estimation. Another weakness is that the missions considered are restricted to long-range operations. On the other hand the concept does hold promise for extension to other mission performance indices, such as a weighted combination of time and fuel-consumed.

On the indication of the results presented herein, the guidance scheme constitutes itself as a very attractive candidate for real-time implementation on-board advanced fighter aircraft. The potential of the in-flight trajectory algorithm could be fully evaluated by real-time simulation experiments, such as the pilot-in-the-loop simulations reported in Ref.80, and eventually by actual flight testing.

## APPENDIX A. OPTIMAL 3-D TRAJECTORIES IN THE PRESENCE OF A TERRAIN LIMIT

Despite its simple form, the enforcement of the altitude constraint (17) is a far from straightforward procedure. This is a consequence of the fact that the altitude constraint is a pure state constraint, i.e. the controls do not enter explicitly. The altitude constraint:

$$S = h_{min} - h \leq 0 \ , \tag{A-1}$$

is of second order, as follows from:

$$\dot{S} = 0 \quad \rightarrow \quad \dot{\gamma} = 0 \tag{A-2}$$

$$\ddot{S} = 0 \quad \rightarrow \quad \dot{\gamma} = (g/V)[n_v - \cos\gamma] = 0 \tag{A-3}$$

The last expression actually determines a control law for the variable $n_v$ on the constrained arc: $n_v \equiv 1$. Following Bryson and Ho [70], the constraint (A-3) is formally adjoined to the Hamiltonian using the multiplier $\zeta$. Since this constraint is adjoined in the same way as the system equation (5), the computational procedure is largely simplified. The optimal control expression for $n_v$ given by Eq.(36) is simply modified to:

$$n_v = gW[\lambda_\gamma + \zeta]/[2V^2 D_i \lambda_E] \ , \tag{A-4}$$

from which for $n_v = 1$:

$$\zeta = [2V^2 D_i \lambda_E]/[gW] - \lambda_\gamma \qquad \text{(A-5)}$$

Note that $\zeta=0$ in the case that the altitude constraint is not active. The adjoint equations are modified by simply replacing $\lambda_\gamma$ by $\lambda_\gamma+\zeta$. The entry conditions for a constrained arc are:

$$h_{min} - h = 0 \quad , \quad \gamma = 0 \qquad \text{(A-6)}$$

The entry conditions, treated as interior-point constraints, give rise to the following "jump conditions" at the entry time $t_e$:

$$\lambda_h(t_e^+) = \lambda_h(t_e^-) - \sigma_1 \qquad \text{(A-7)}$$

$$\lambda_\gamma(t_e^+) = \lambda_\gamma(t_e^-) - \sigma_2 \quad , \qquad \text{(A-8)}$$

where $\sigma_1$ and $\sigma_2$ are constant multipliers. At the exit point the following condition applies:

$$\zeta = 0 \qquad \text{(A-9)}$$

Due to the lack of uniqueness of the adjoints on the constrained arc, a different set of conditions can be arrived at [70]. In the above analysis the existence of a constrained arc is assumed. However, typical of second order state constraints, there can be optimal paths that touch the constraint boundary at only one point. Such touch-point problems are actually more simple, since there are fewer conditions to be satisfied at the touch point:

$$h_{min} - h = 0 \tag{A-10}$$

$$\gamma = 0 \tag{A-11}$$

$$\lambda_h(t_e^+) = \lambda_h(t_e^-) - \sigma_1 \tag{A-12}$$

The constrained-arc and touch-point conditions have been incorporated in the control logic of the MSA algorithm. Since the lift and structural constraints may be active as well, the control logic is quite complicated. The possibility of throttle-switching complicates matters even further. The MSA is extremely well-suited to handle state constraints. The only disadvantage is that the sequence of constrained arcs (or touch points) and unconstrained arcs needs to be known (or assumed) a priori. Also the program has no capability to test whether there will be a constrained arc or a touch point. This information has to be specified a priori as well. As a result some trial-and-error efforts will generally be required.

Our research efforts concerning state constraints have focussed on maneuvers taking place below the corner-velocity locus. Consequently the lift limit does not come into play, thus simplifying the problem significantly. Our results bear out that most of the altitude-constrained maneuvers are of the touch-point type. As a matter of fact it was quite difficult to generate examples featuring constrained arcs. The only way such examples could be generated was by stipulating very large values for the terrain limit.

The boundary conditions for the example selected are:

$x_o = -620$ kft , $h_o = 44.3935$ kft , $E_o = 88.95$ kft

$\gamma_o = -16.8293^\circ$ , $\chi_o = -180^\circ$

$x_f = 0$ , $y_f = 0$ , $h_f = h_D$ , $E_f = E_D$ , $\gamma_f = 0$

The altitude history for the unconstrained problem can be seen in Fig. 49. In this figure two constrained solutions are indicated as well. The solution corresponding to $h_{min} = 30.5$ kft features a touch point. The solution corresponding to $h_{min} = 31.5$ kft features a constrained arc. The constrained arc has a duration of about 3 sec. It is evident that the values used for the terrain limit have no physical meaning; however, they do illustrate the occurrence of constrained arcs. For more realistic values of $h_{min}$ (corresponding to sea level, for instance), the constrained solution will always feature a touch point. This is achieved by shifting the emphasis in the initial phase of the maneuver from turning in the horizontal plane to turning in the vertical plane. It is believed that for less powerful aircraft or for lower initial speeds the possibility of constrained-altitude arcs at sea level does exist.

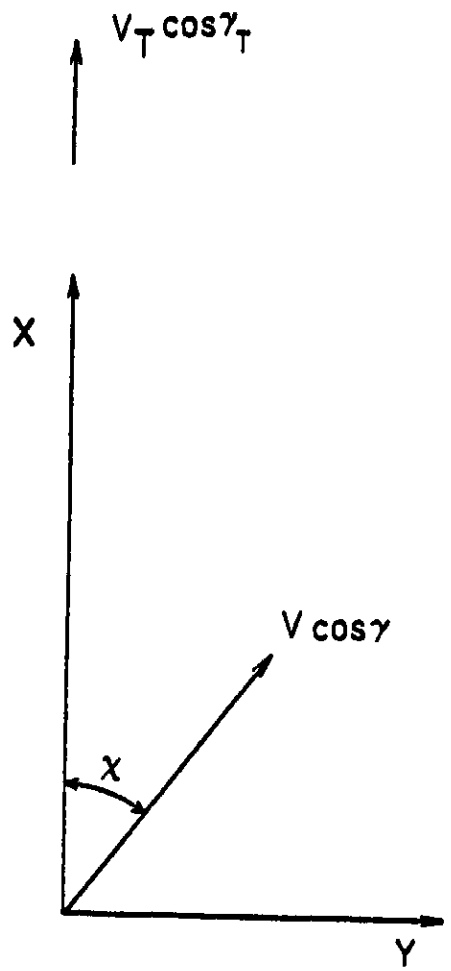


Figure 1. Horizontal plane geometry.

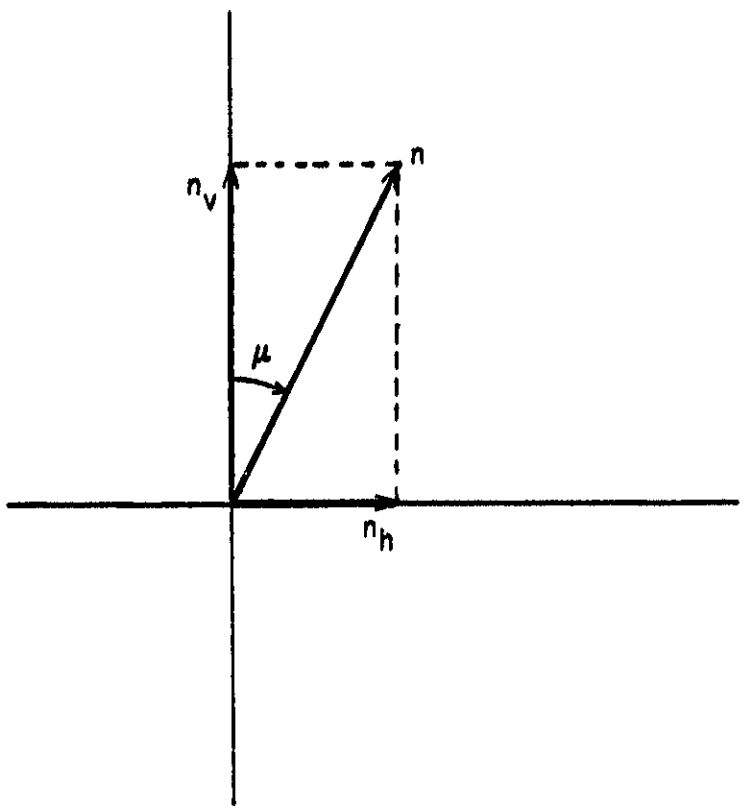


Figure 2. Definition of $n_h$ and $n_v$.

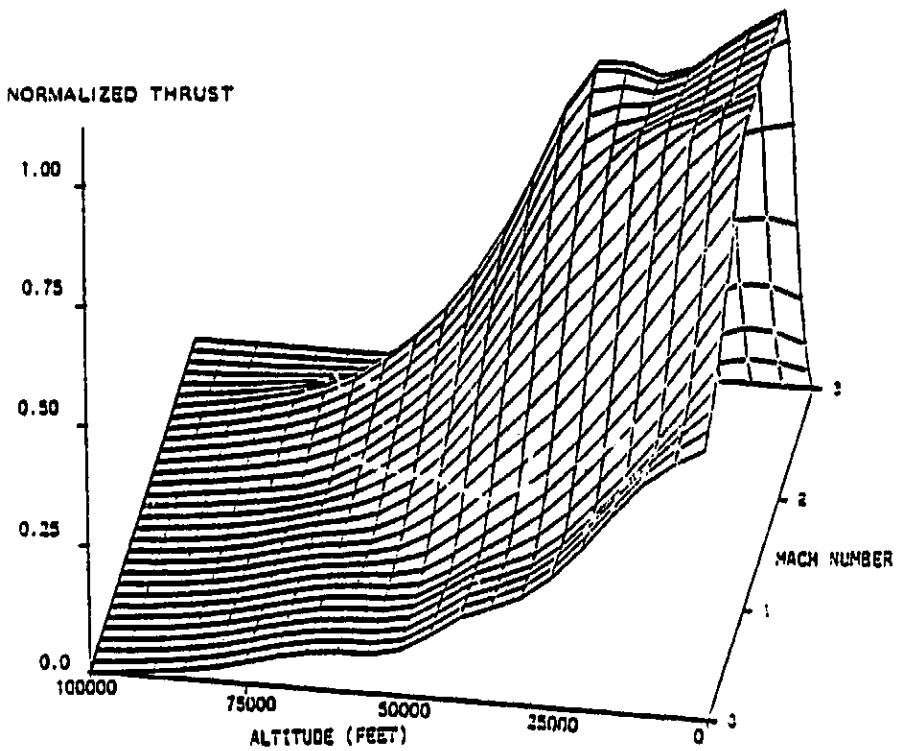


Figure 3. Maximum afterburning thrust vs. Mach number and altitude.

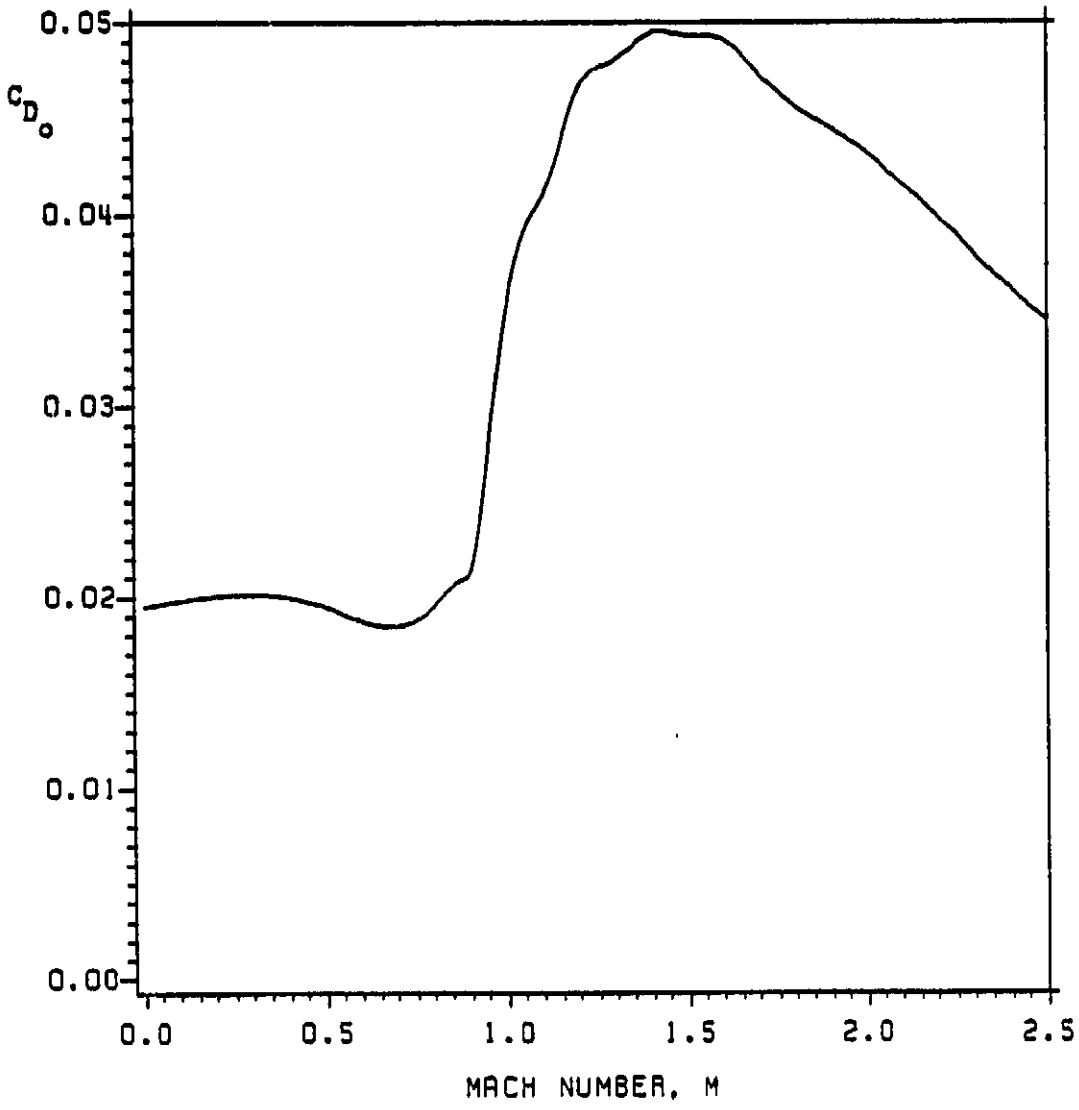


Figure 4. Aircraft zero-lift drag coefficient as a function of Mach number.

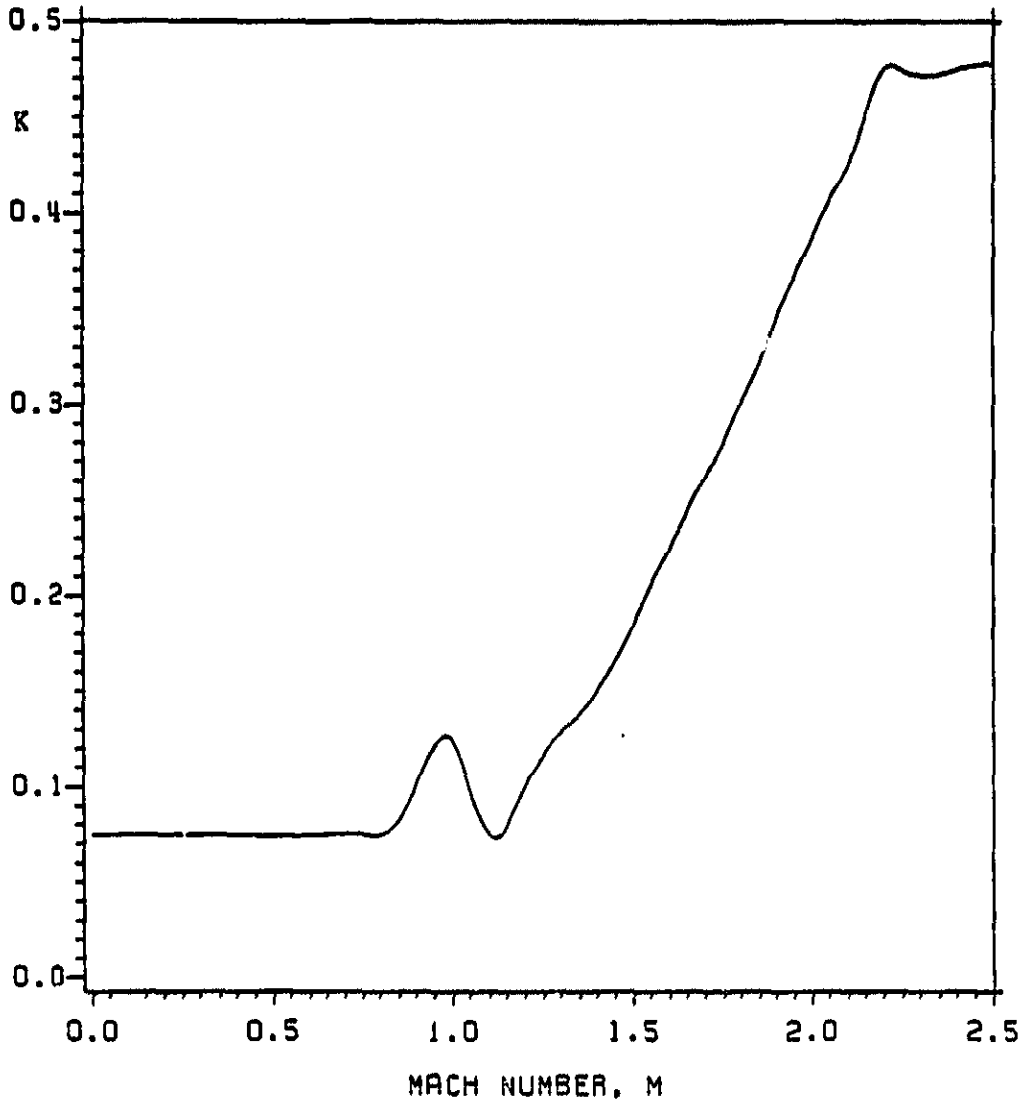


Figure 5. Aircraft efficiency coefficient as a function of Mach number.

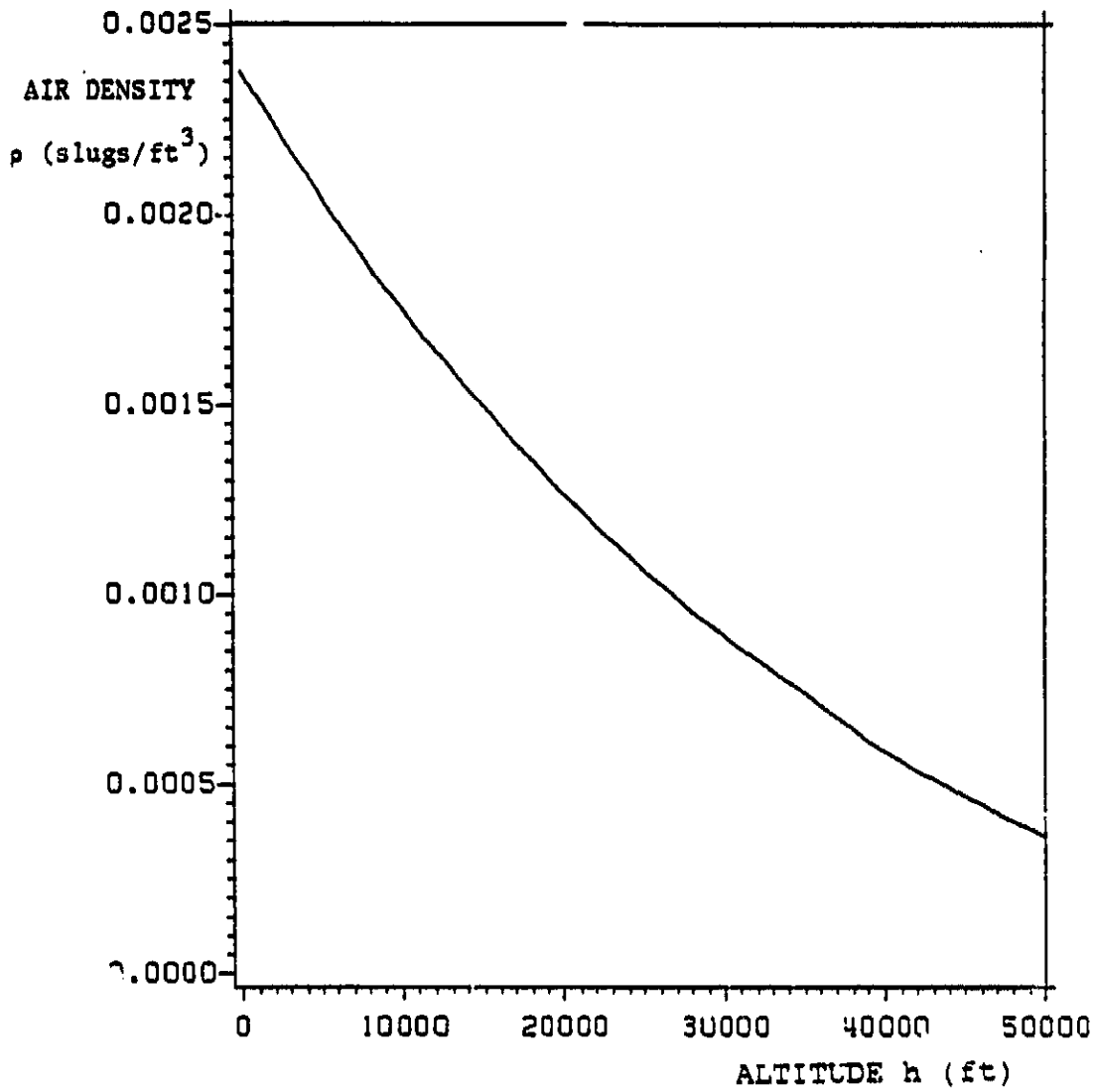


Figure 6. Air density as a function of altitude.

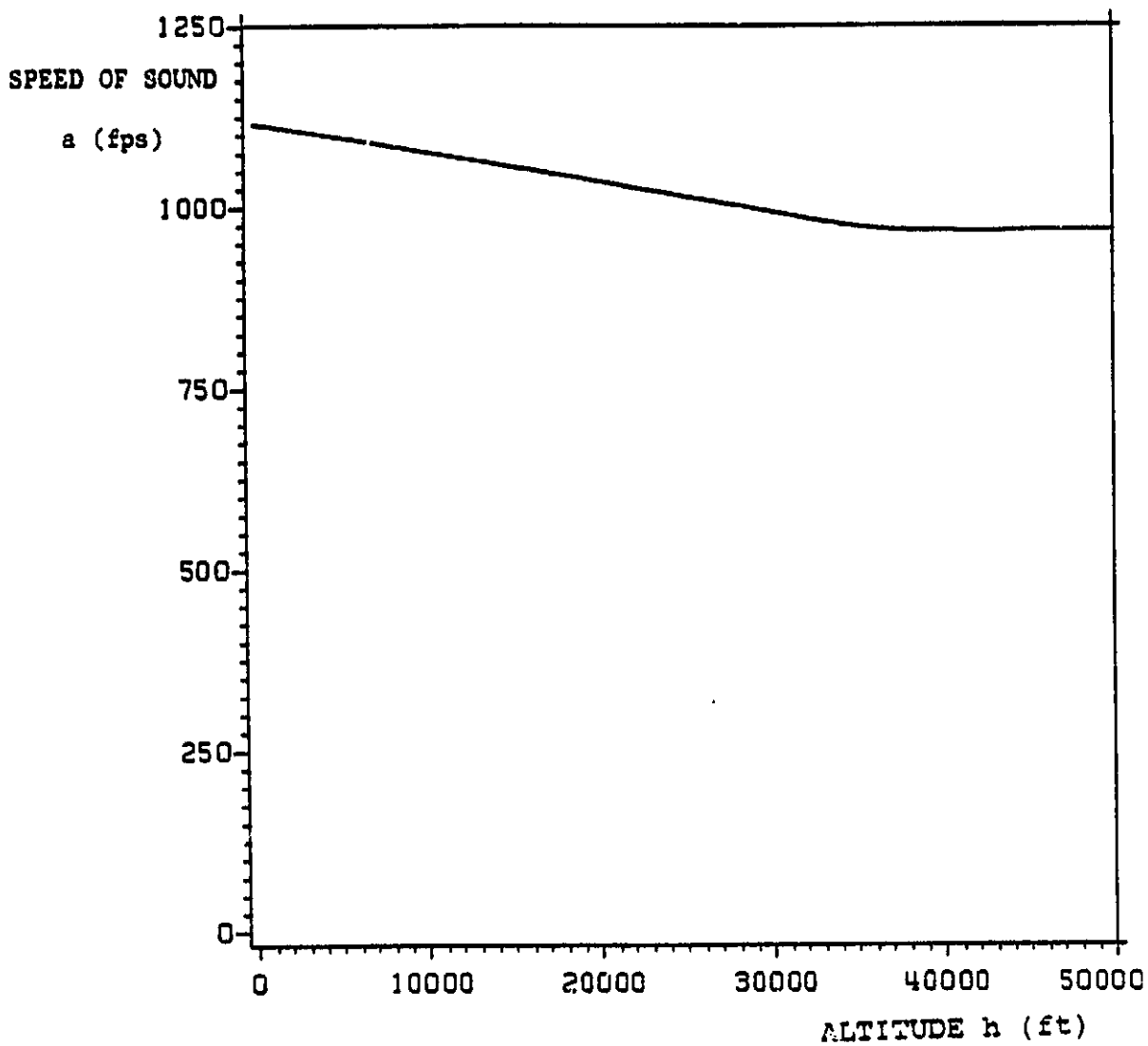


Figure 7. Speed of sound as a function of altitude.

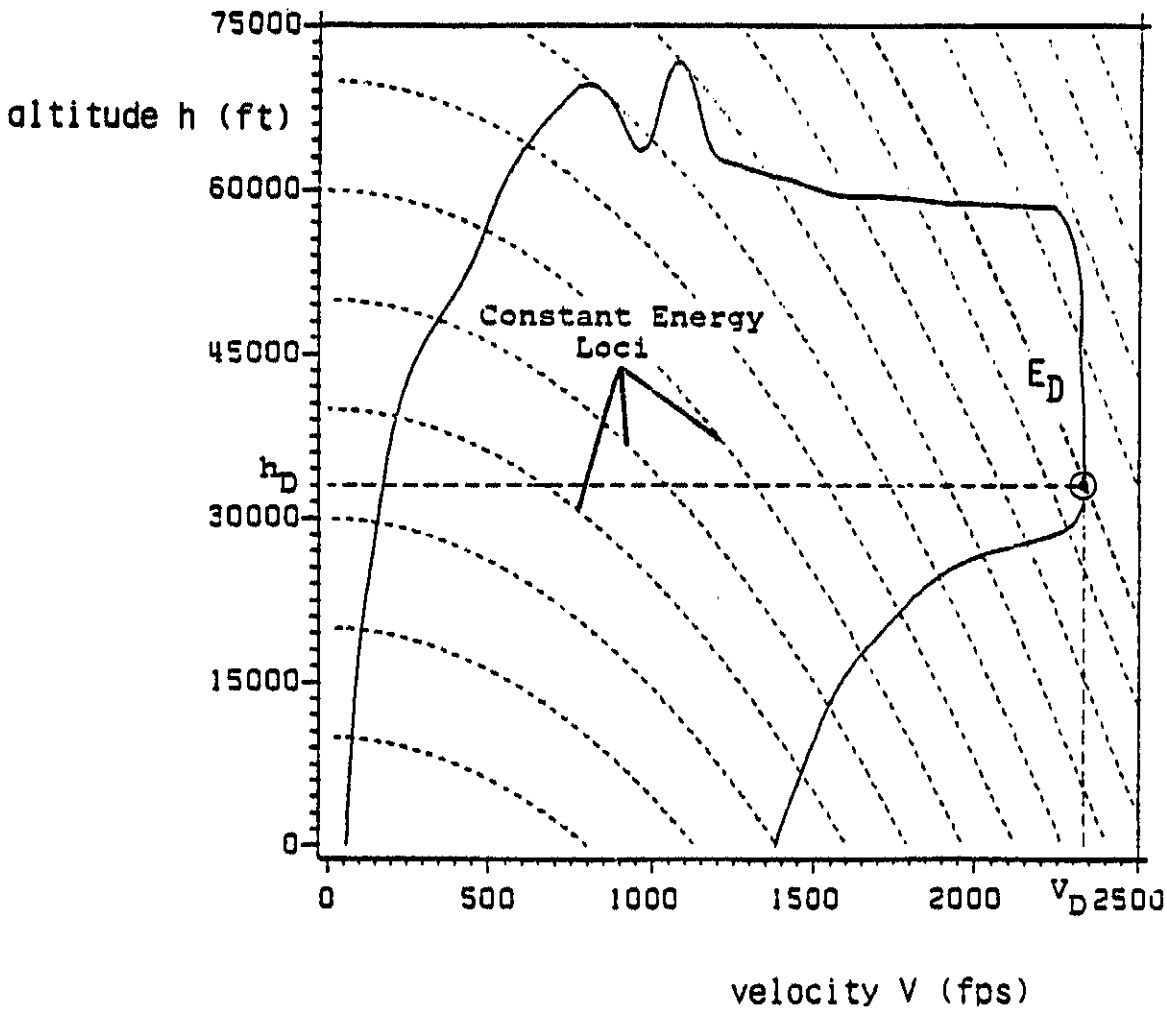


Figure 8. Steady-state flight envelope with dash-point.

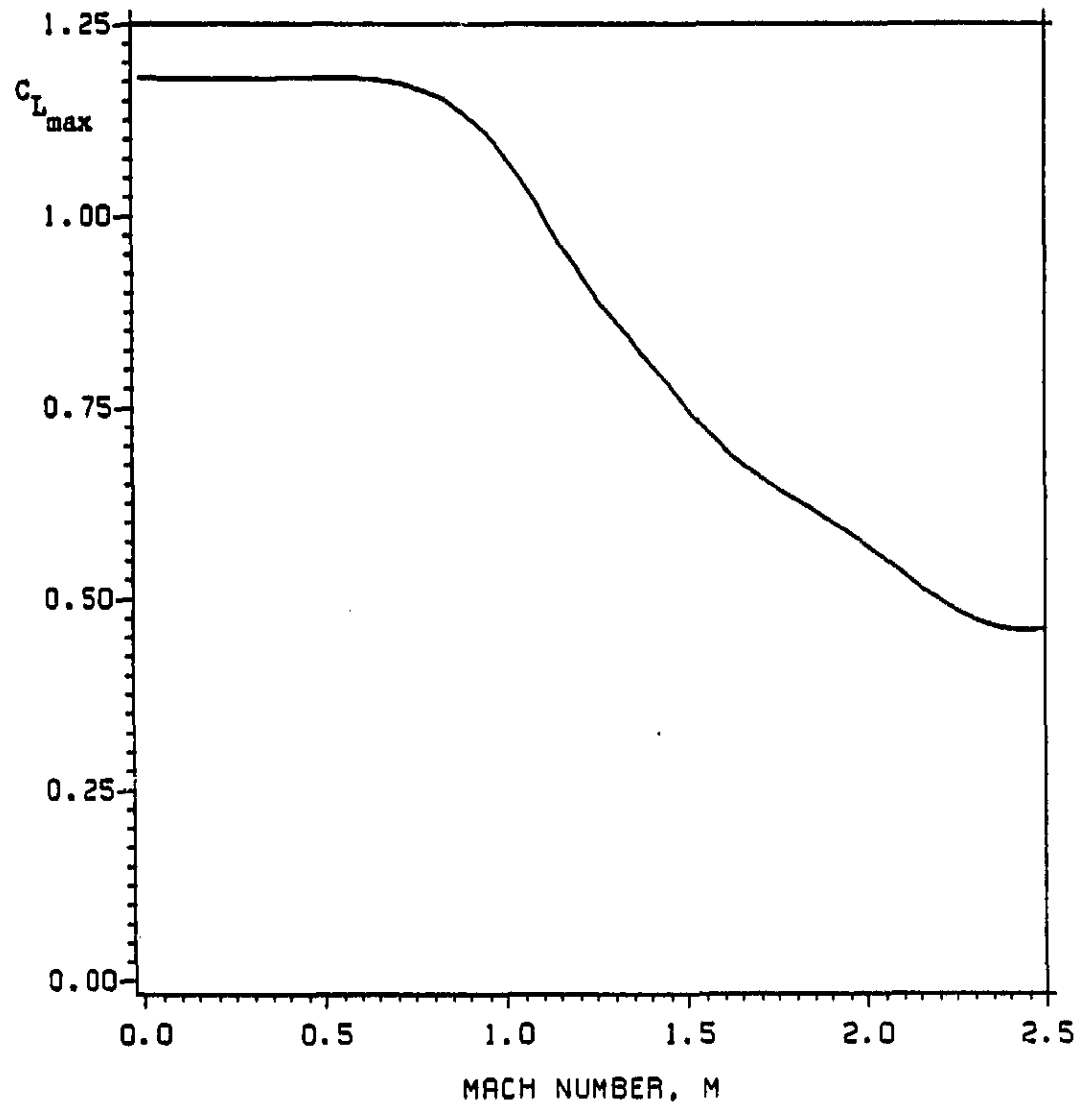


Figure 9. $C_{L_{max}}$ as a function of Mach number.

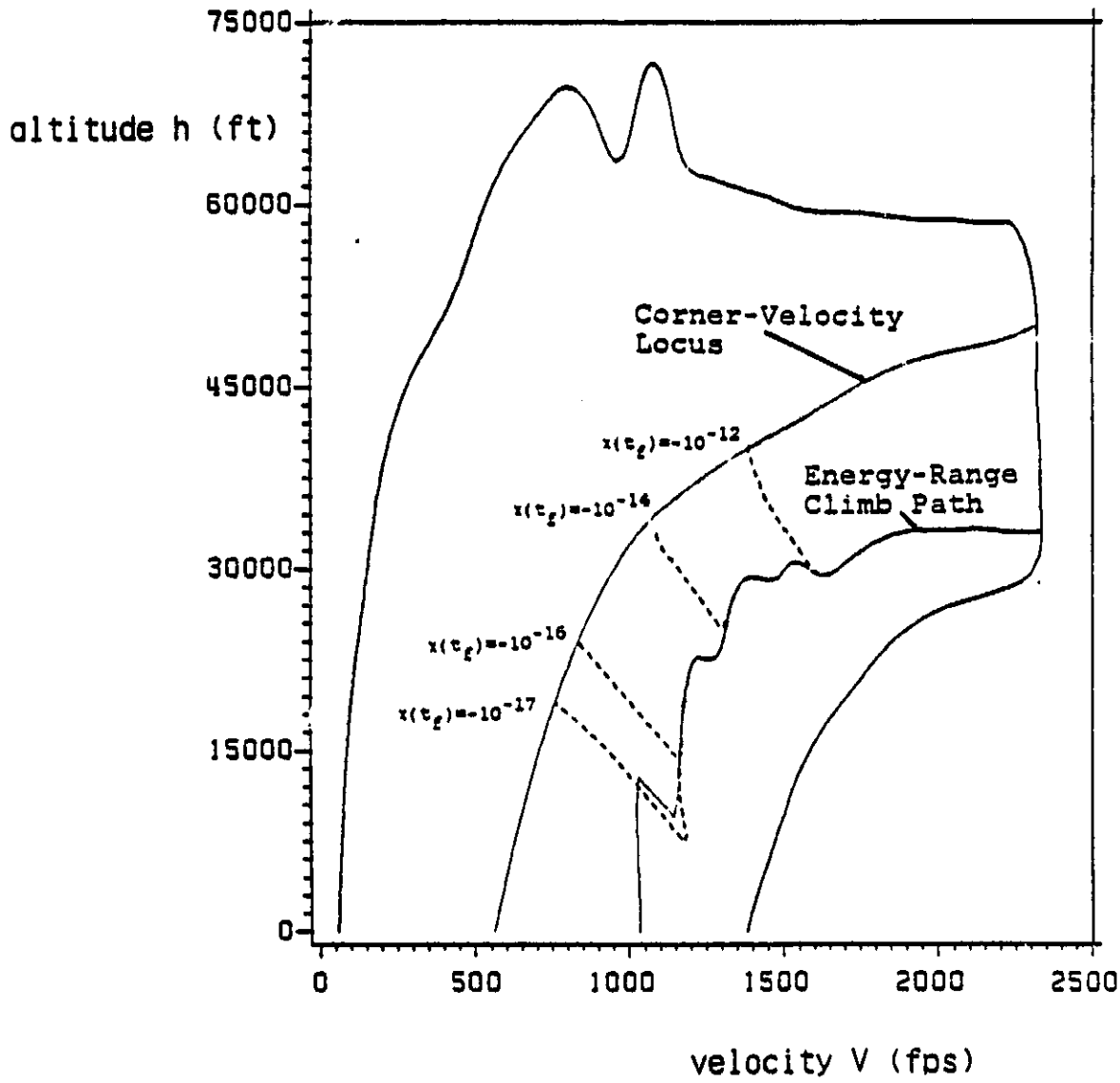


Figure 10. Energy-state solutions in the (V,h)-space.

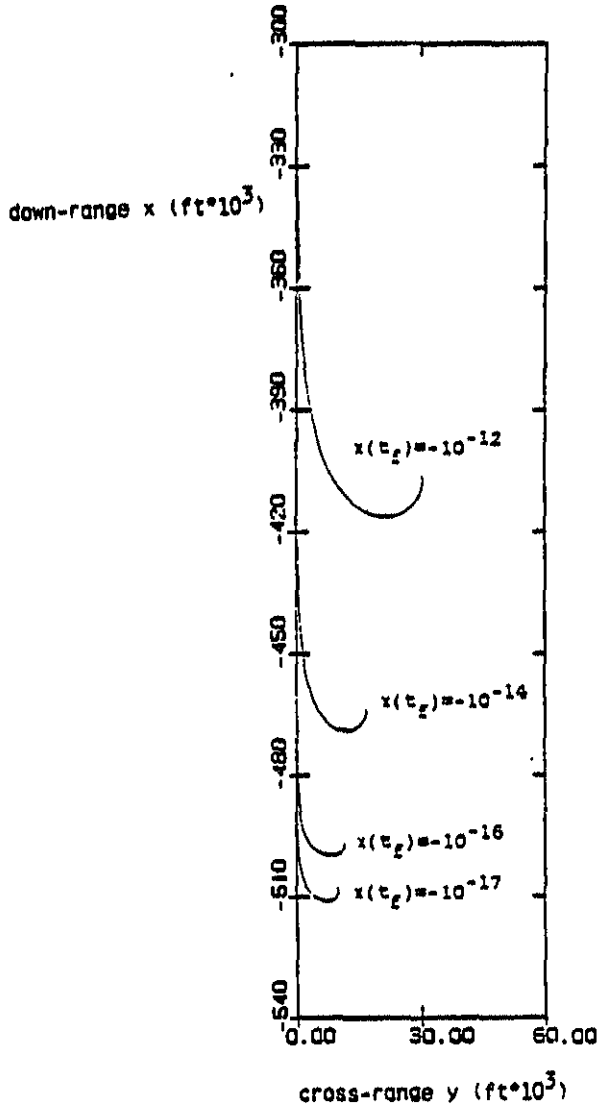


Figure 11. Ground tracks of energy-state solutions.

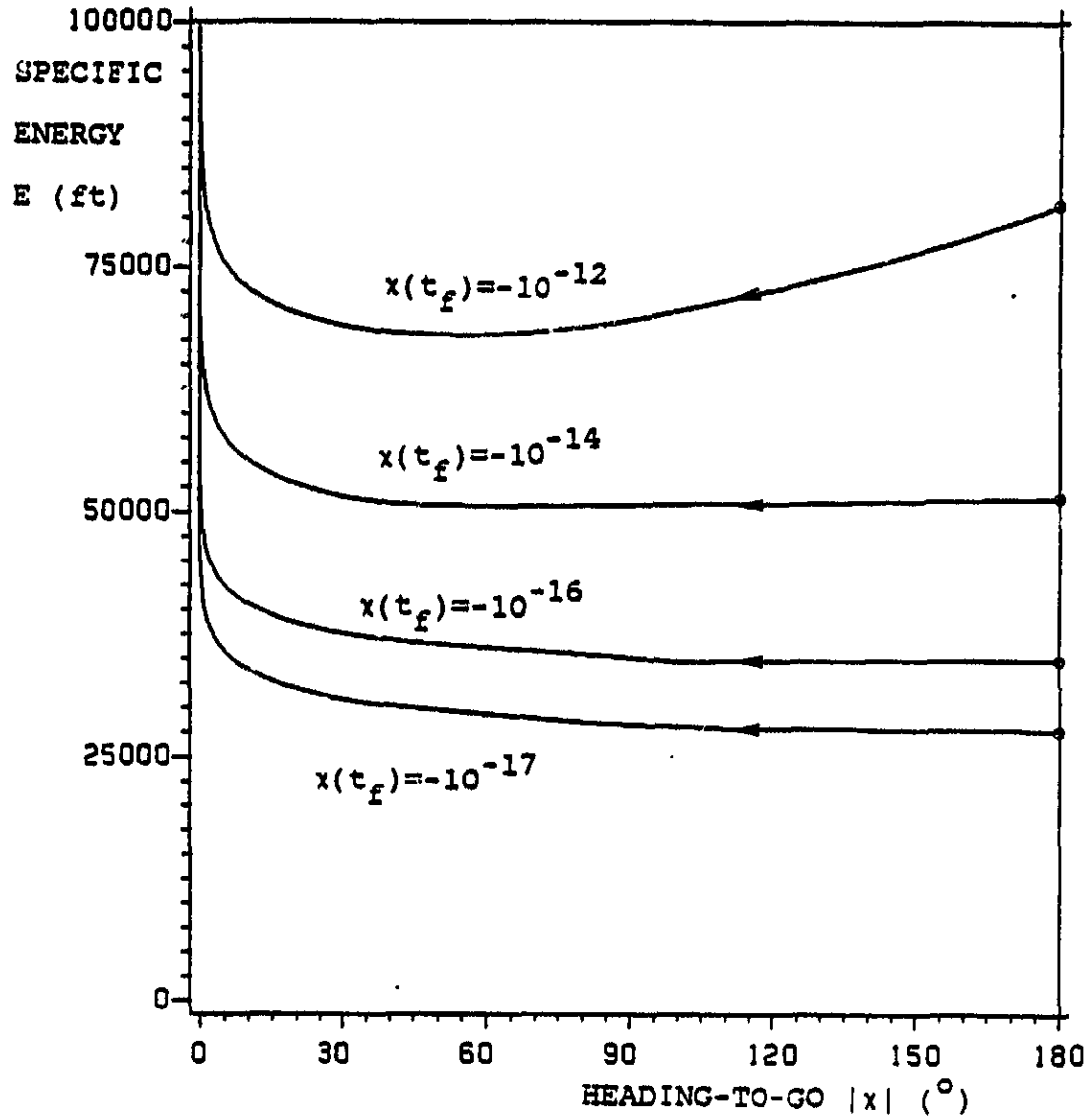


Figure 12. Energy-state solutions in the (X,E)-space.

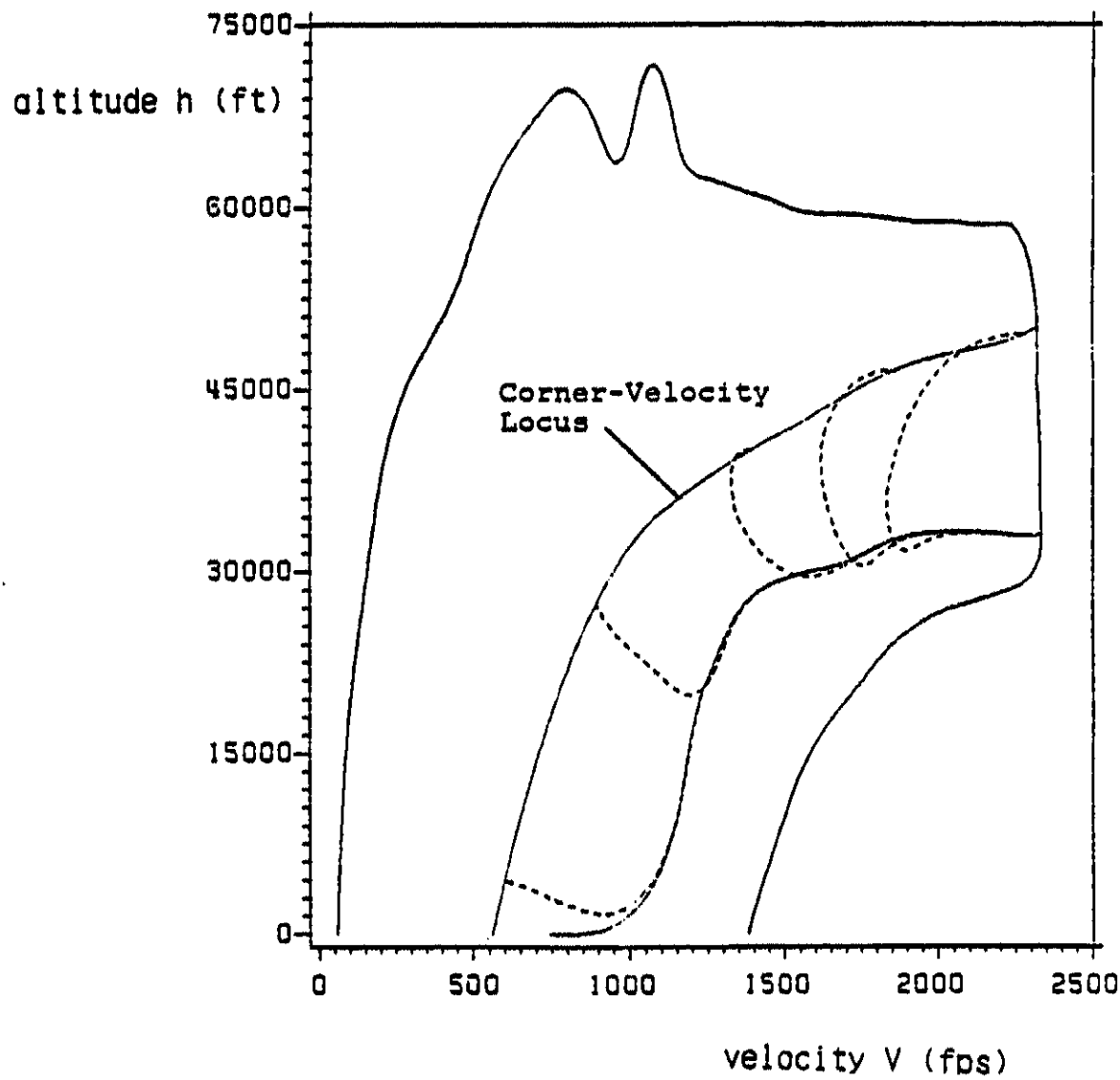


Figure 13. Point-mass state-Euler solutions in the (V,h)-space.

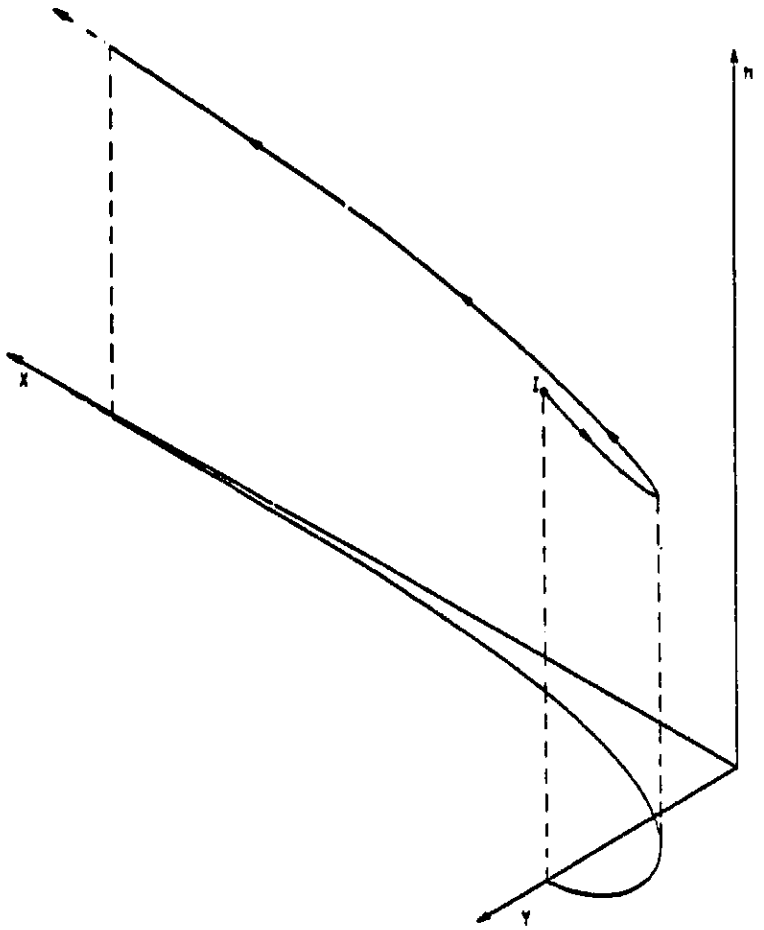


Figure 14. A typical 3-D trajectory and its ground track.

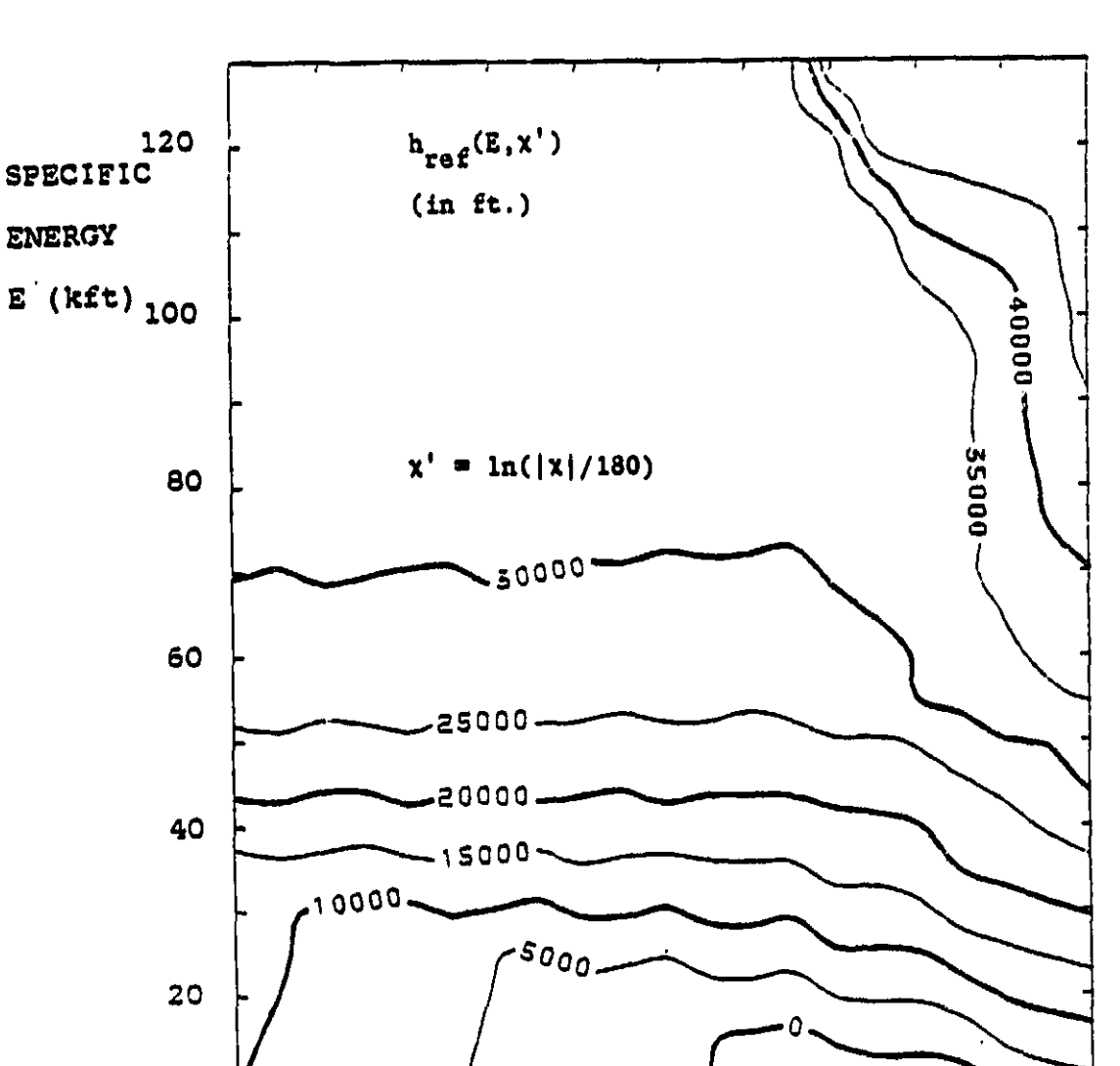


Figure 15. Map of $h_{ref}(E,\chi')$.

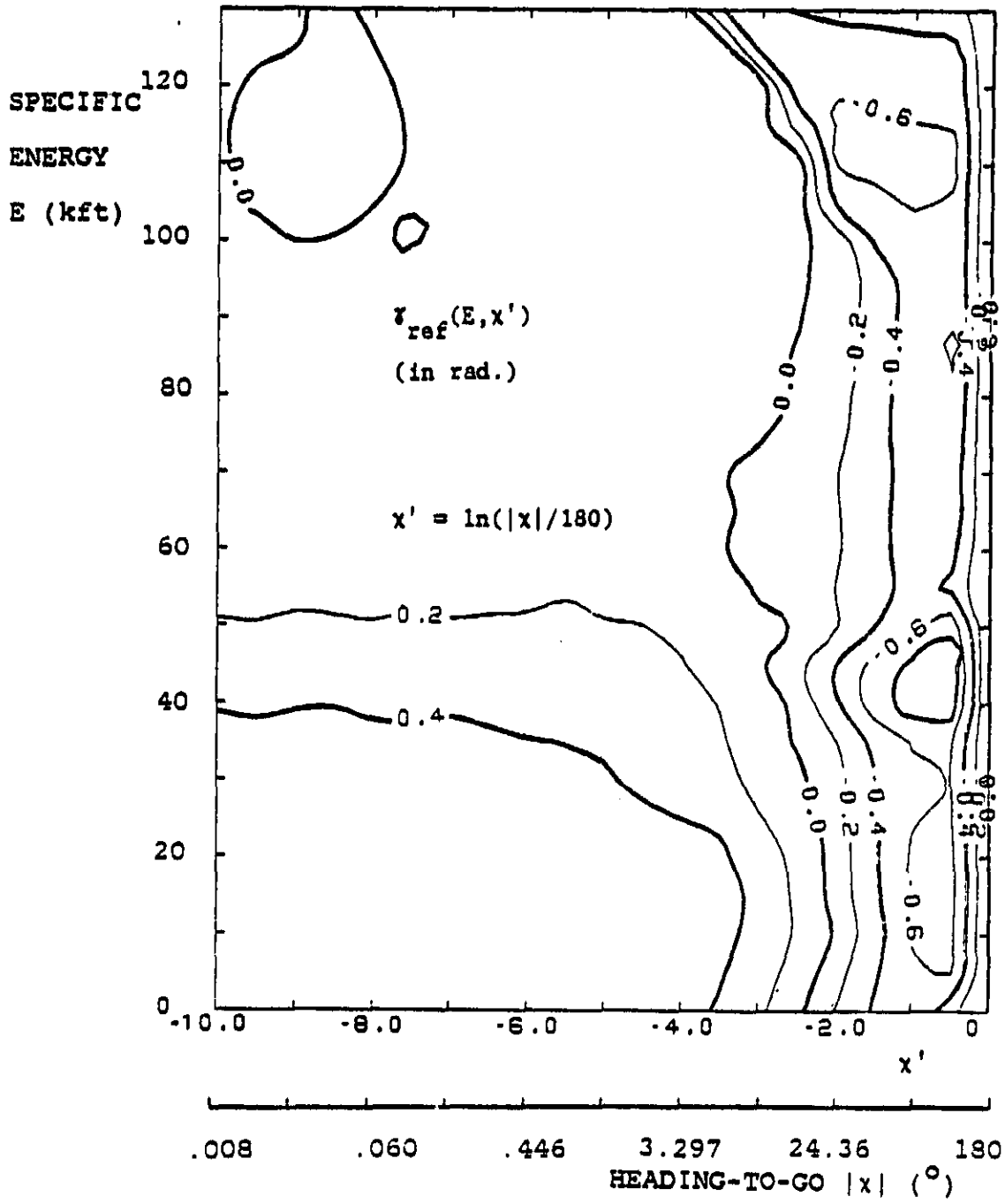


Figure 16. Map of $\gamma_{ref}(E,x')$.

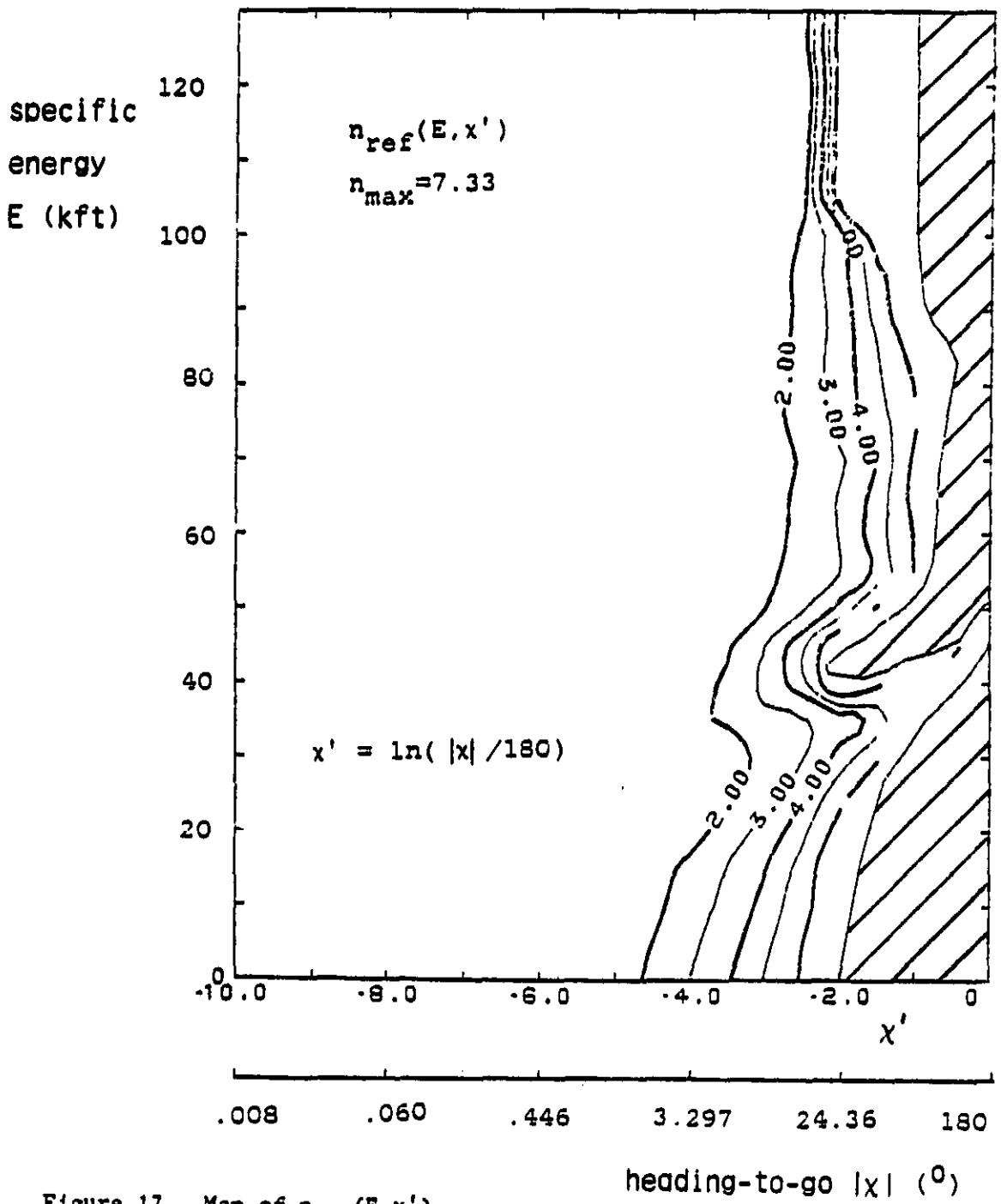


Figure 17. Map of $n_{ref}(E,x')$.

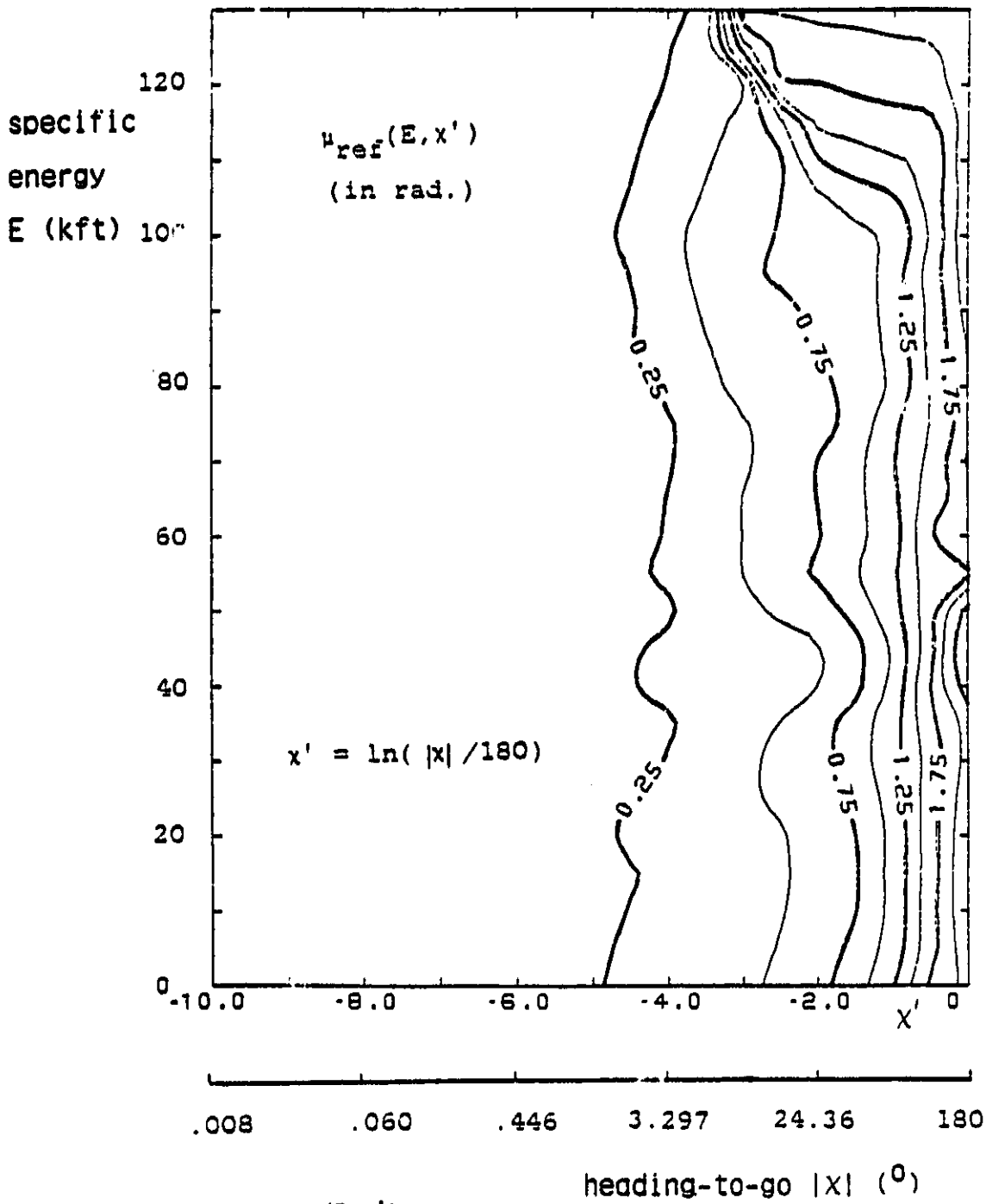


Figure 18. Map of $\mu_{ref}(E,x')$.

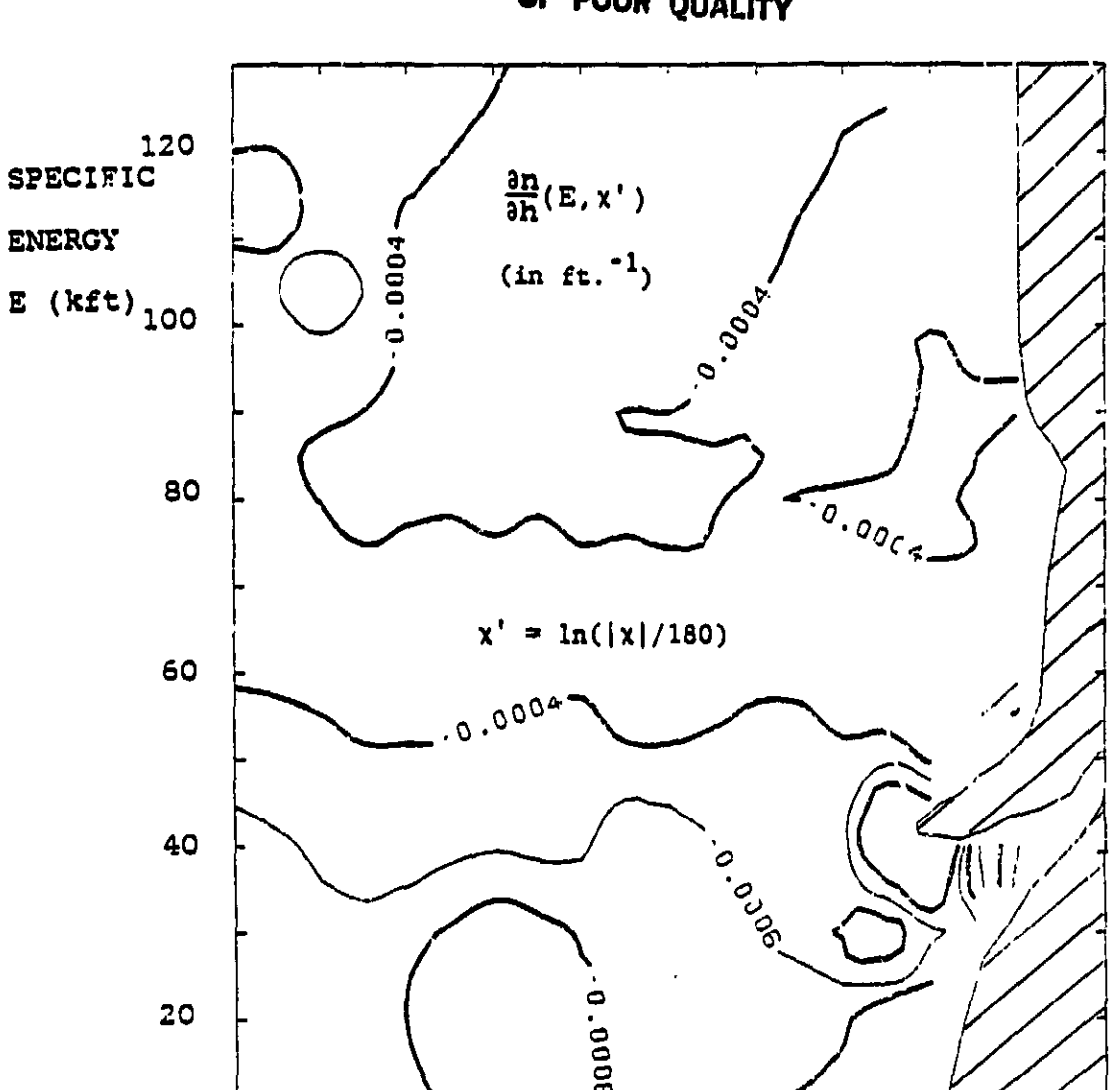


Figure 19. Map of $\partial n/\partial h(E,x')$.

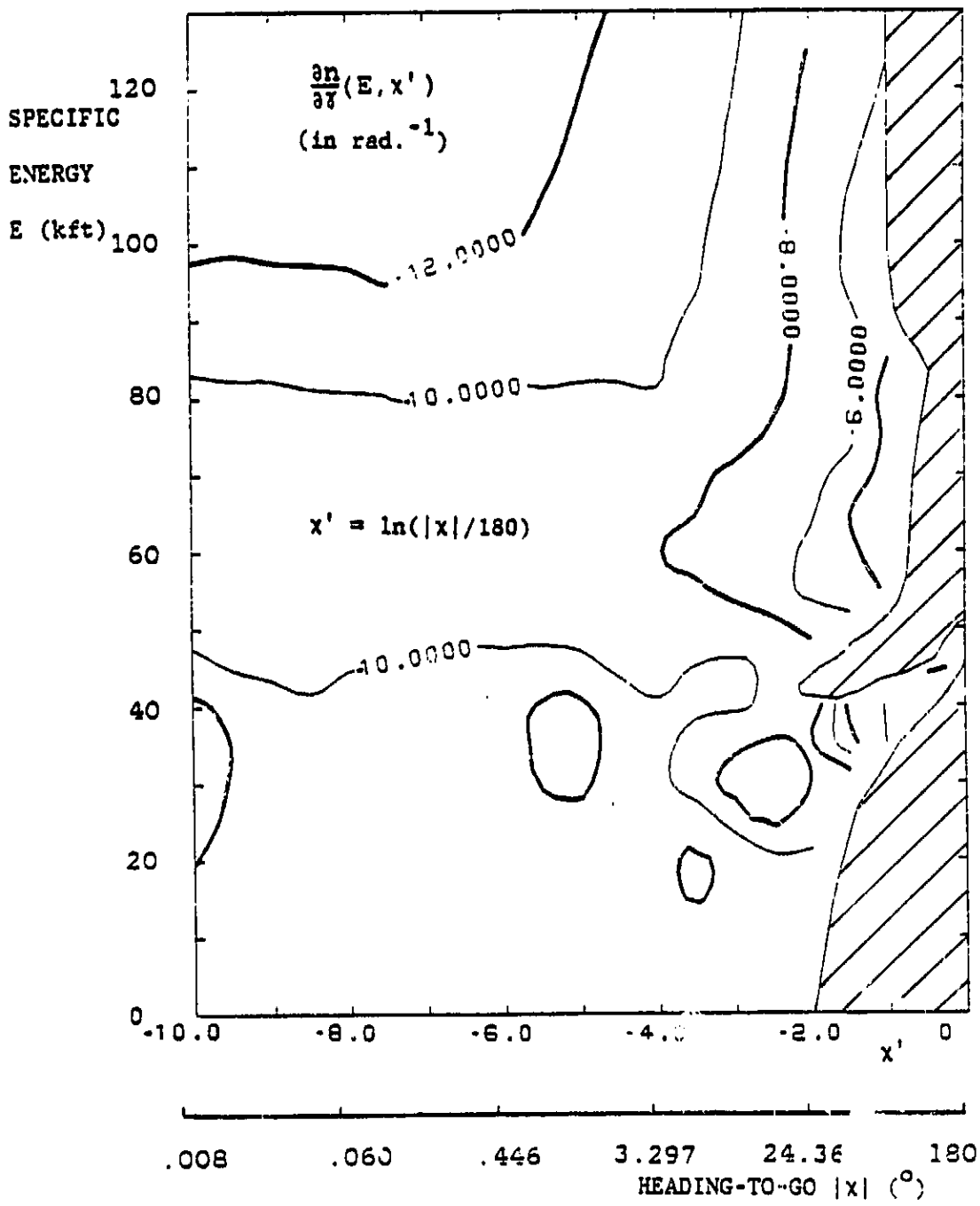


Figure 20. Map of $\partial n/\partial \gamma(E,x')$.

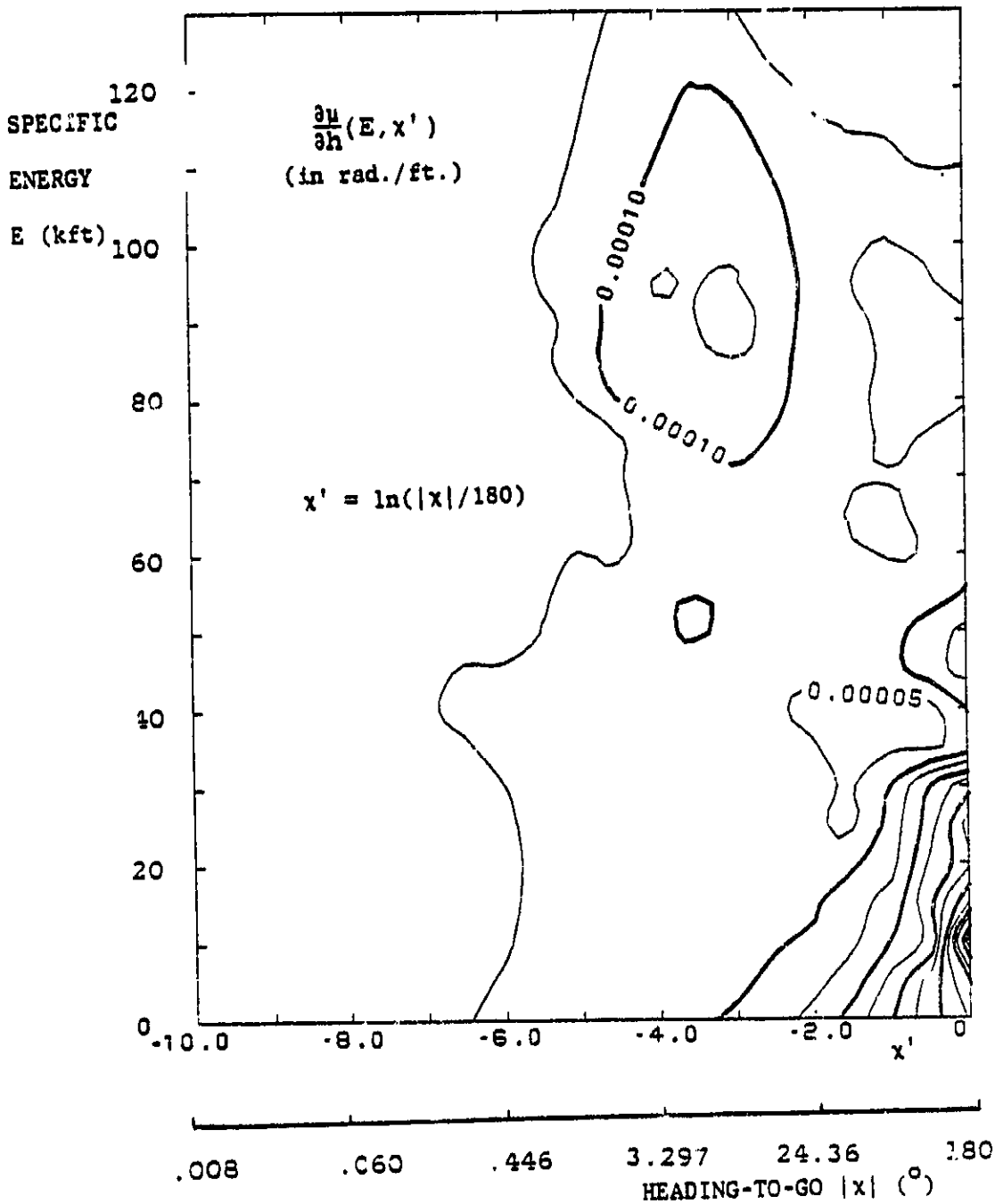


Figure 21. Map of $\partial u/\partial h(E,x')$.

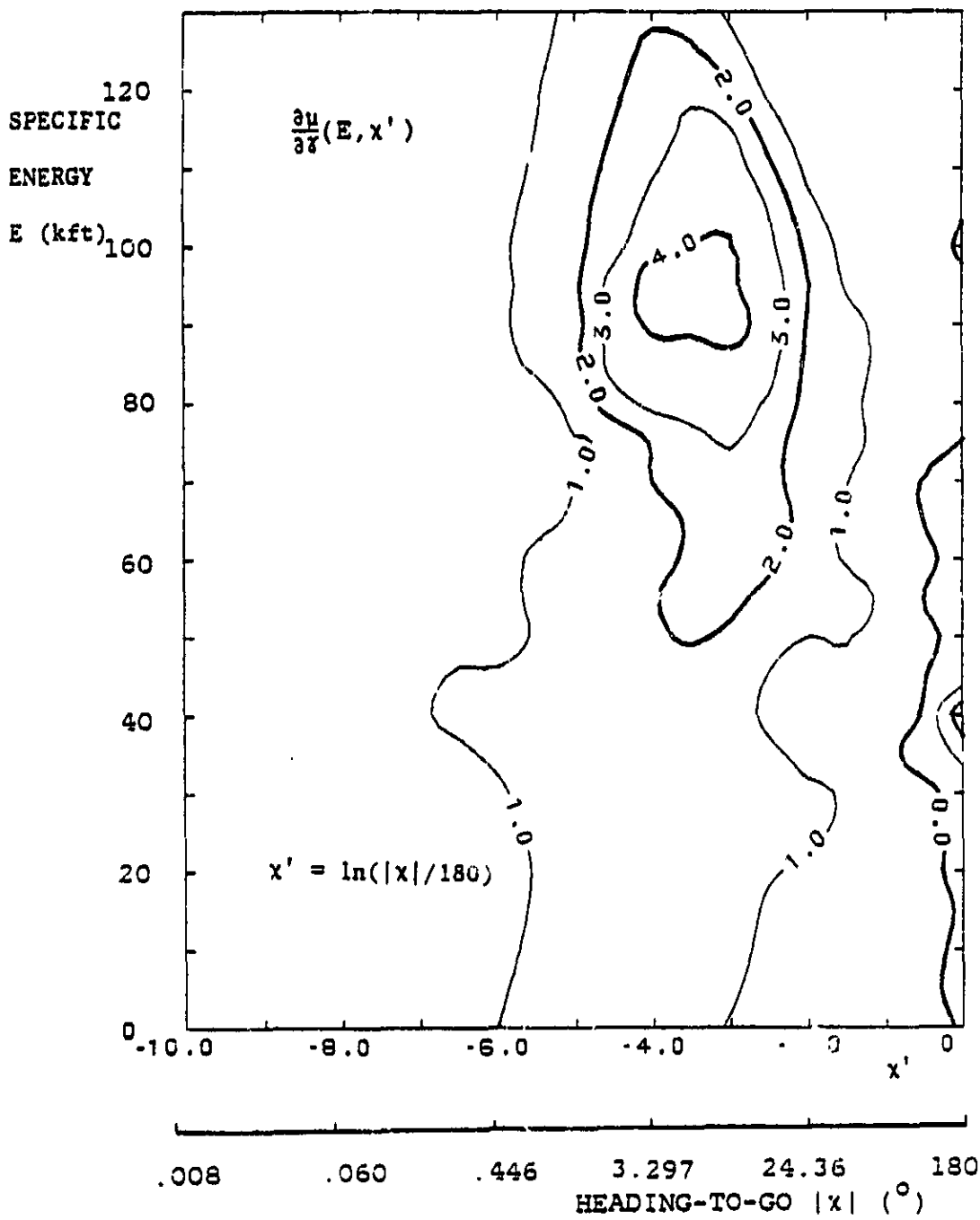


Figure 22. Map of $\partial\mu/\partial\gamma(E,x')$.

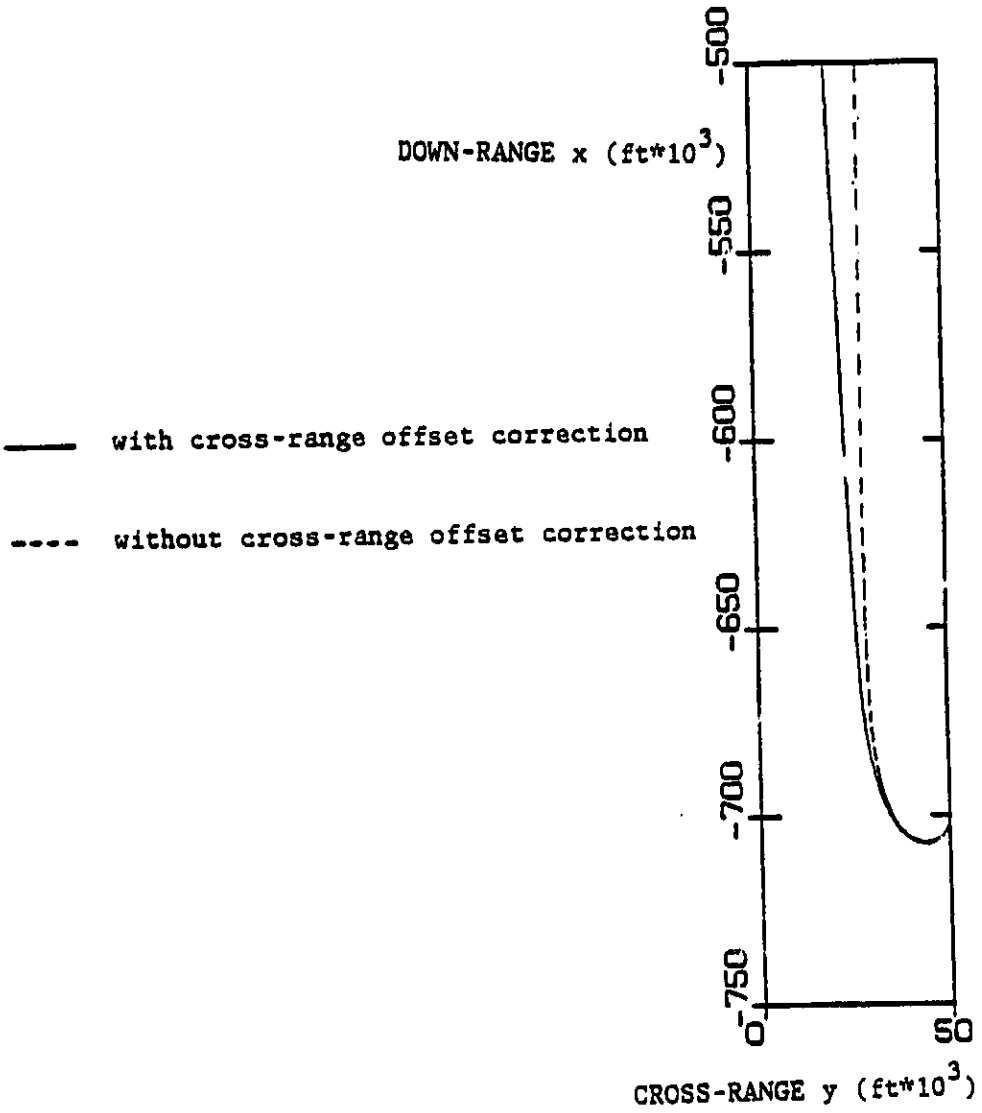


Figure 23. The effect of the cross-range offset correction.

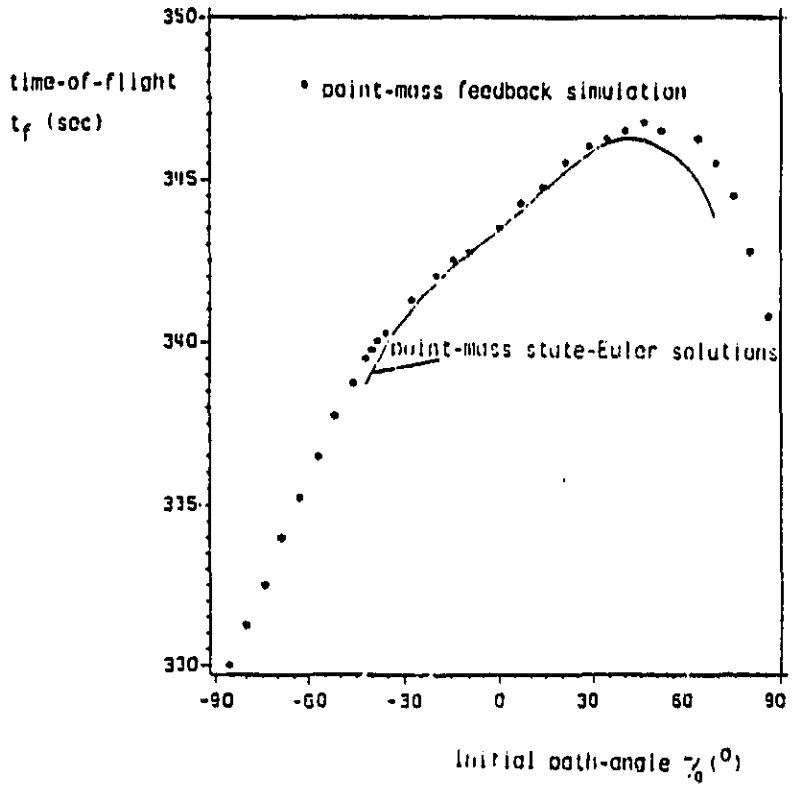


Figure 24. Open-loop optimal and approximate feedback solutions for a reference flight-path with variable initial path-angle.

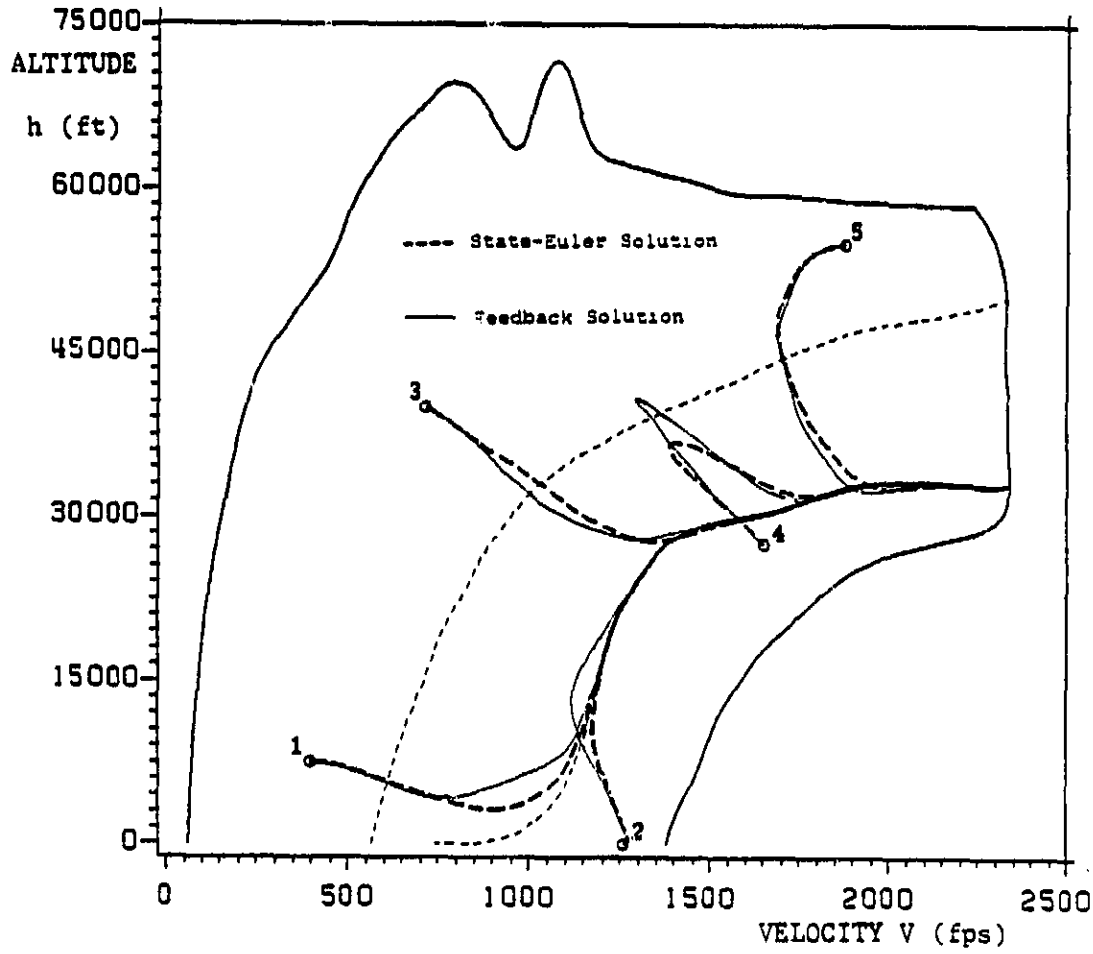


Figure 25. Solutions in the (V,h)-space for examples 1 through 5.

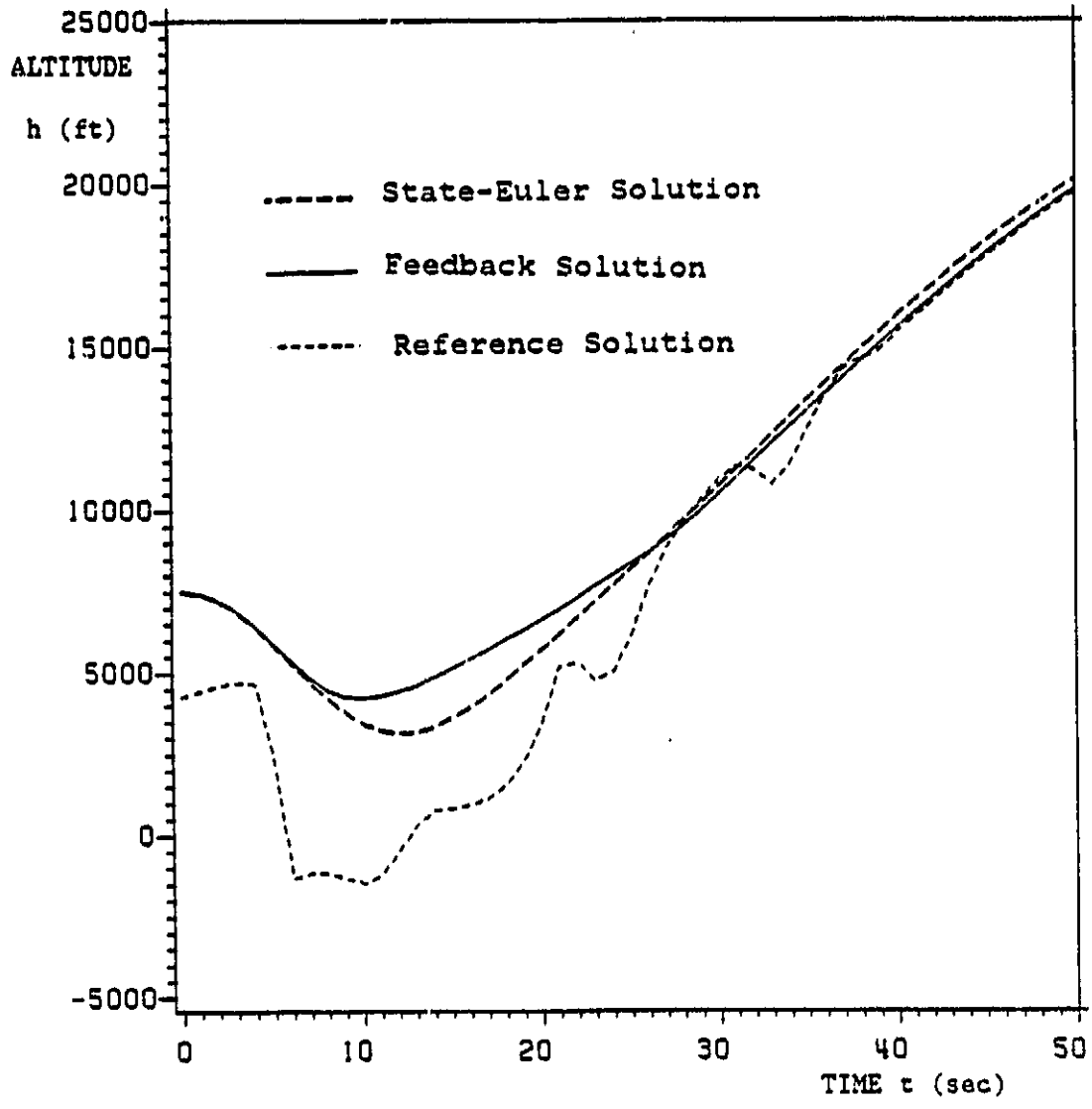


Figure 26. Altitude history for example 1.

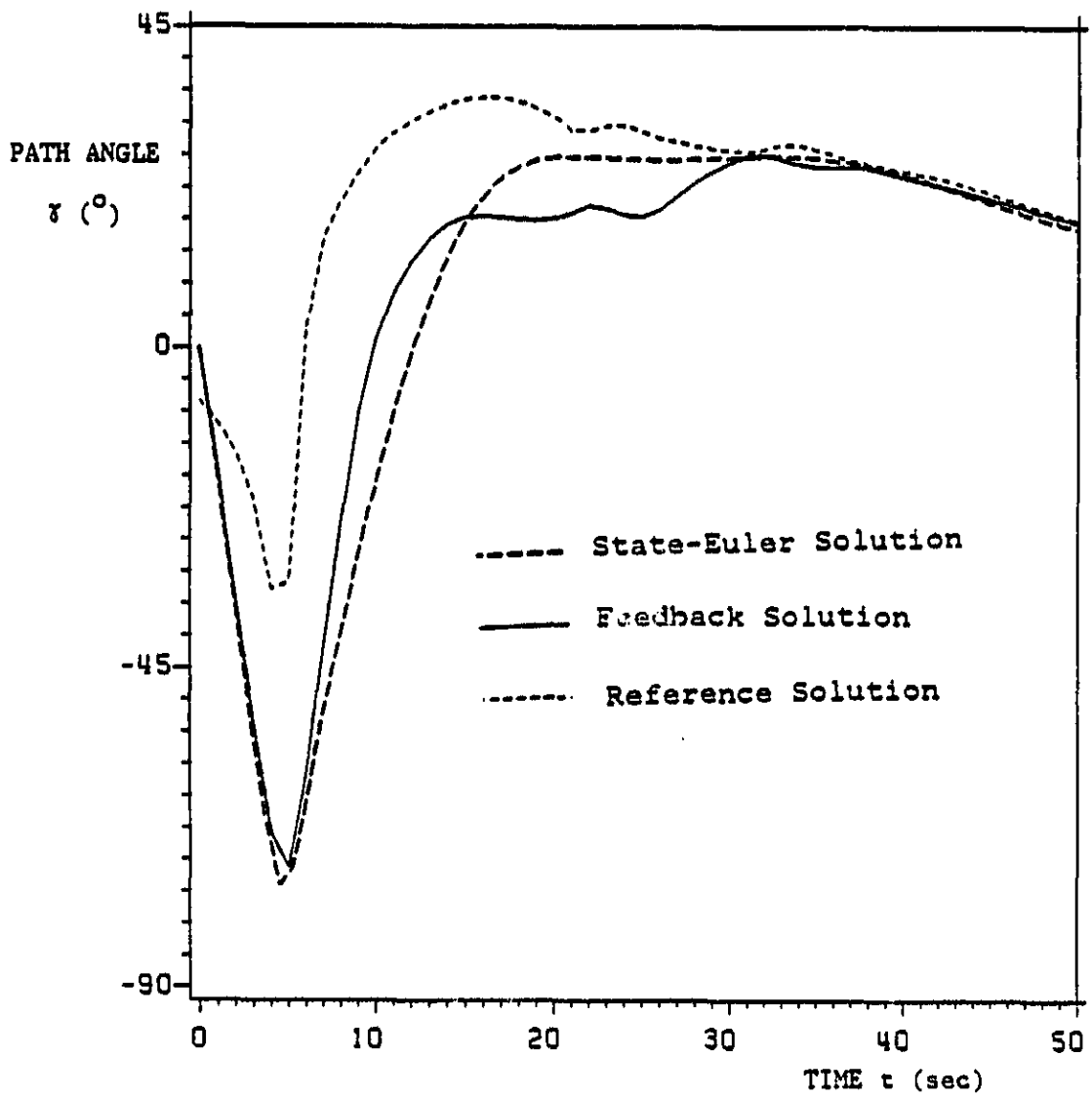


Figure 27. Path-angle history for example 1.

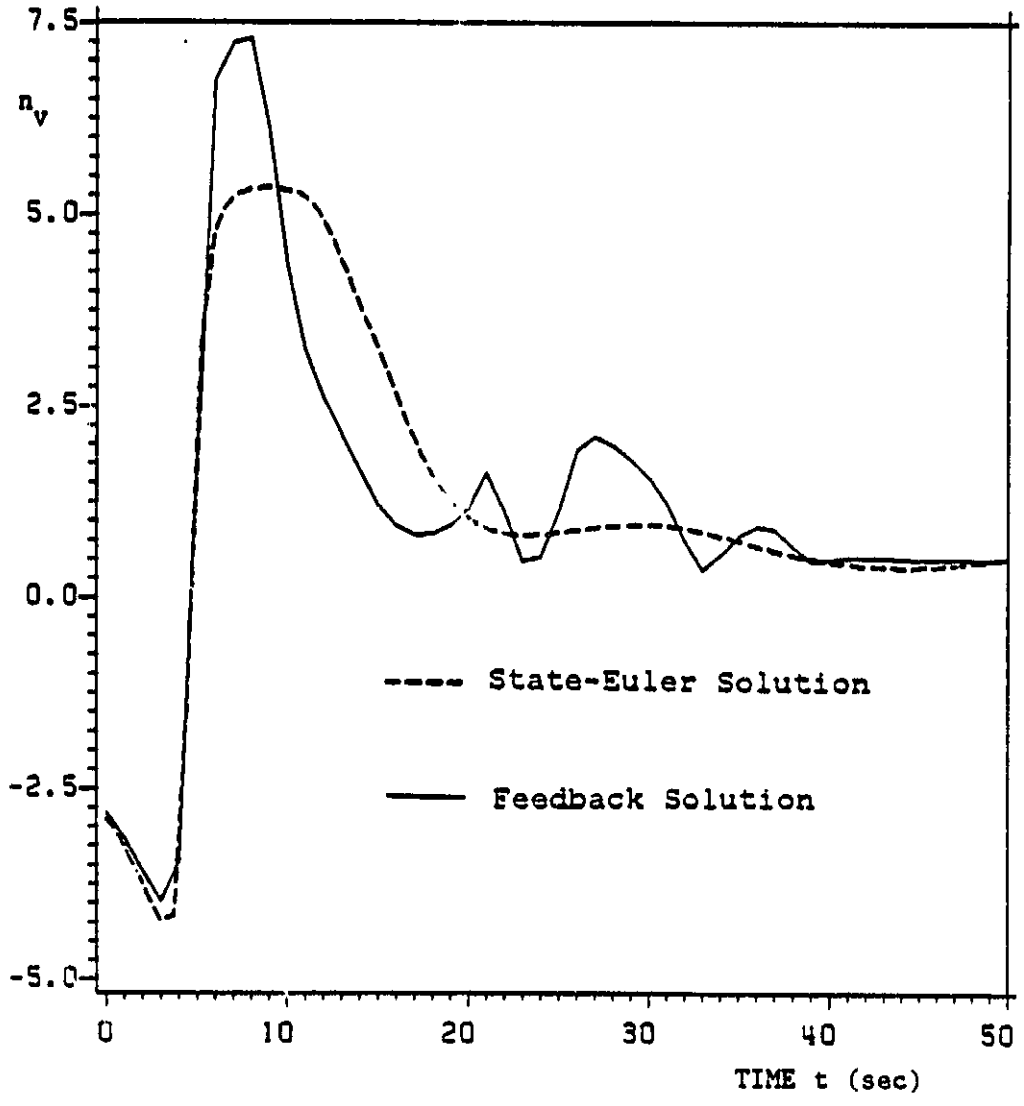


Figure 28. $n_v$ history for example 1.

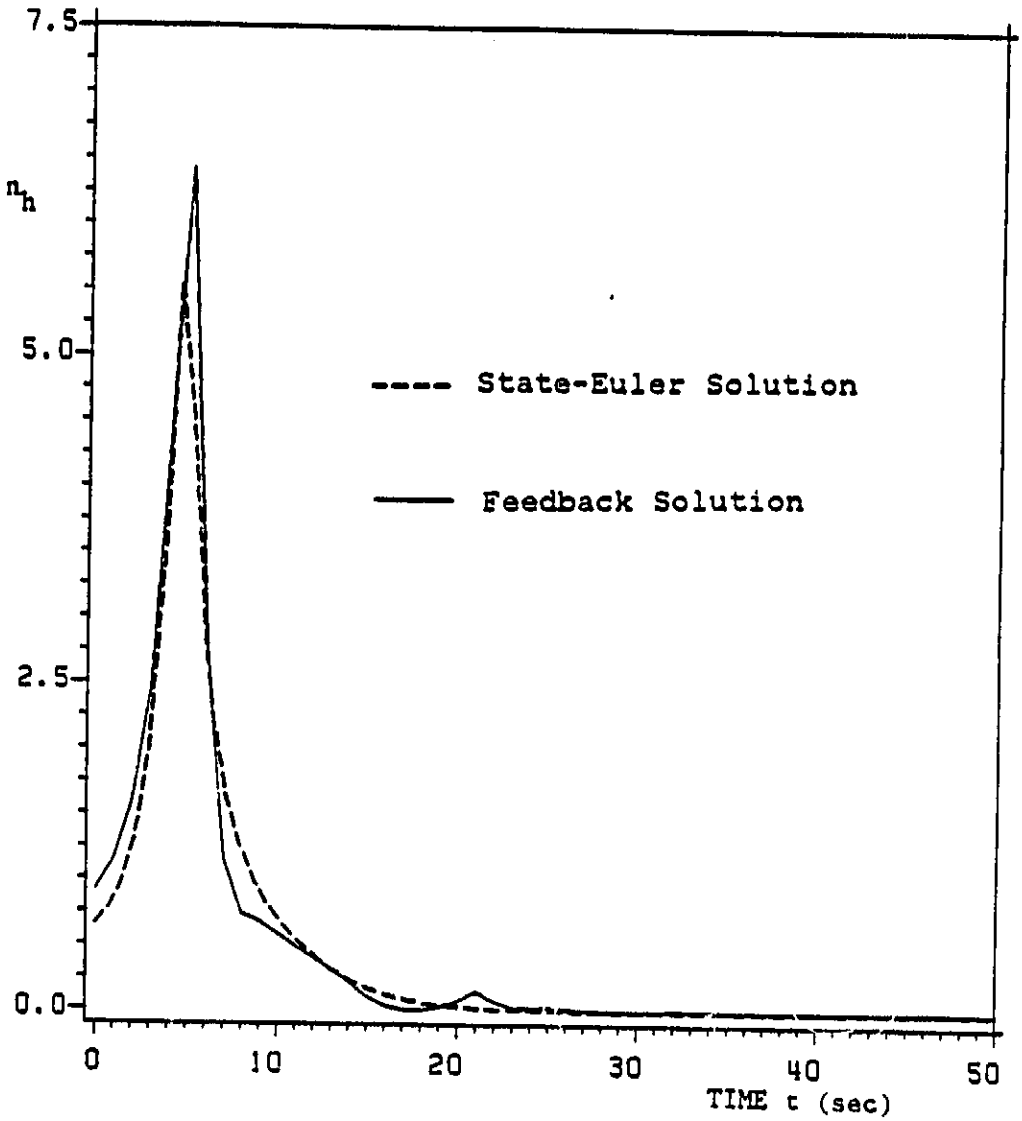


Figure 29. $n_h$ history for example 1.

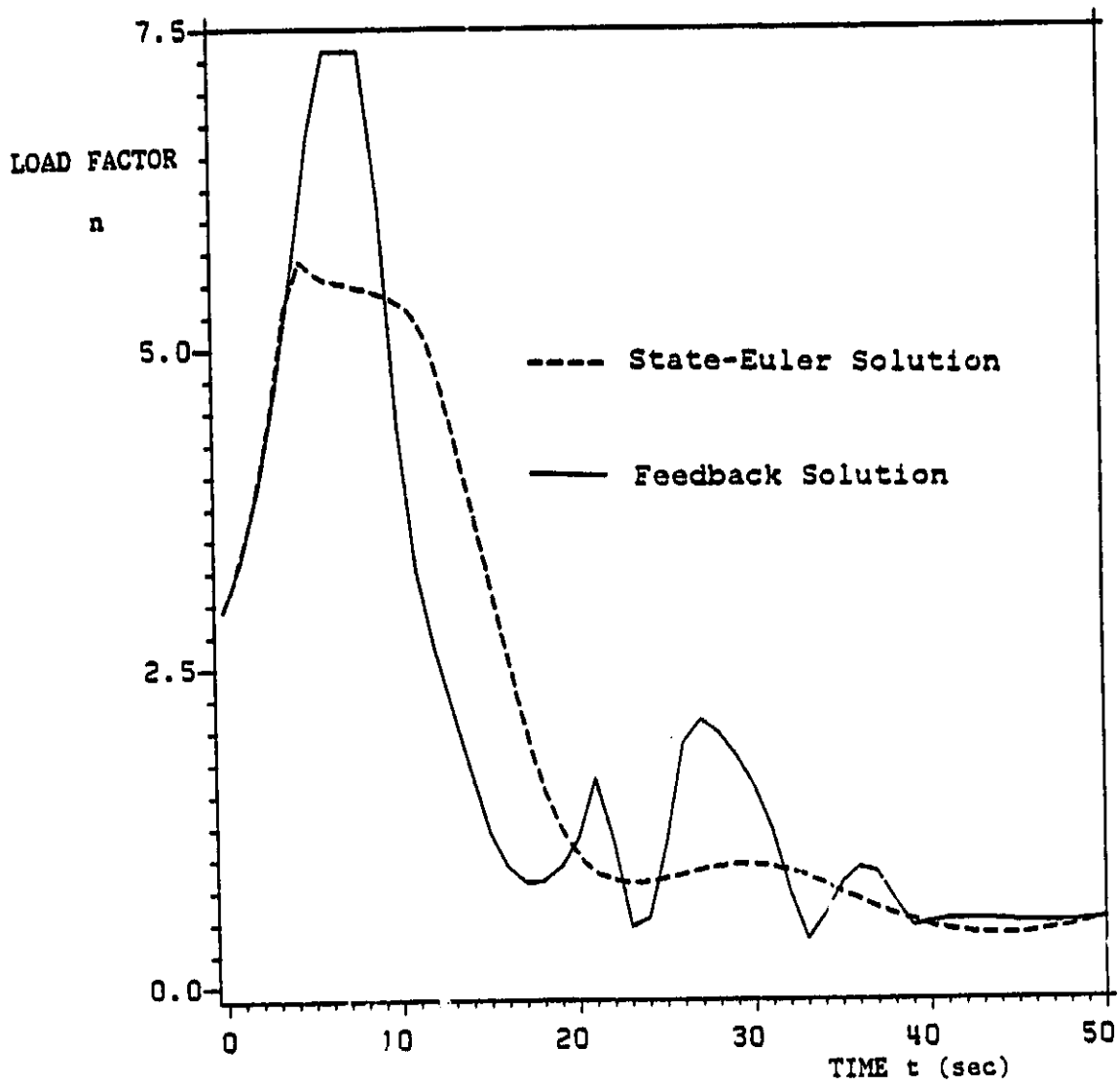


Figure 30. Load-factor history for example 1.

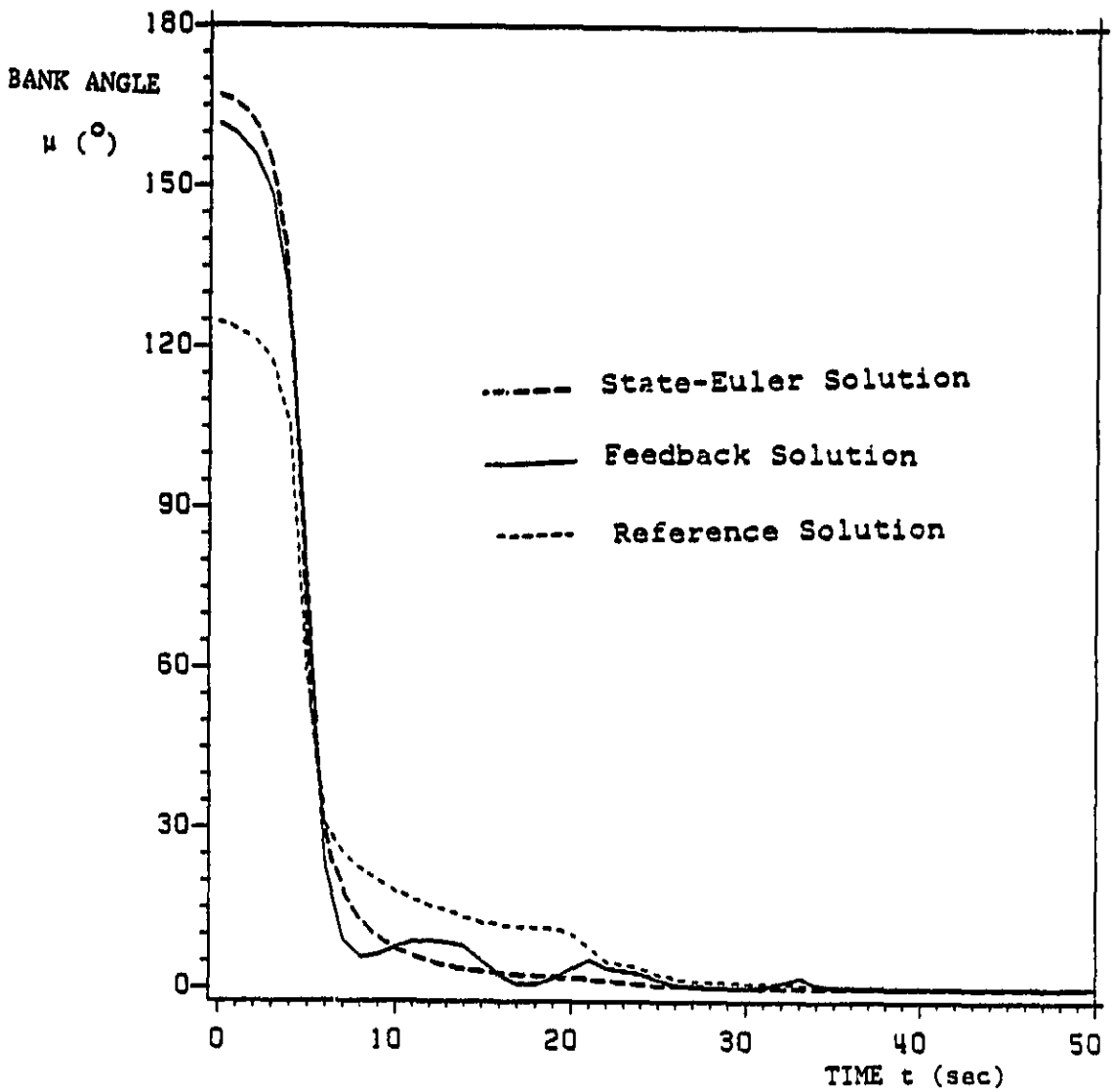


Figure 31. Bank-angle history for example 1.

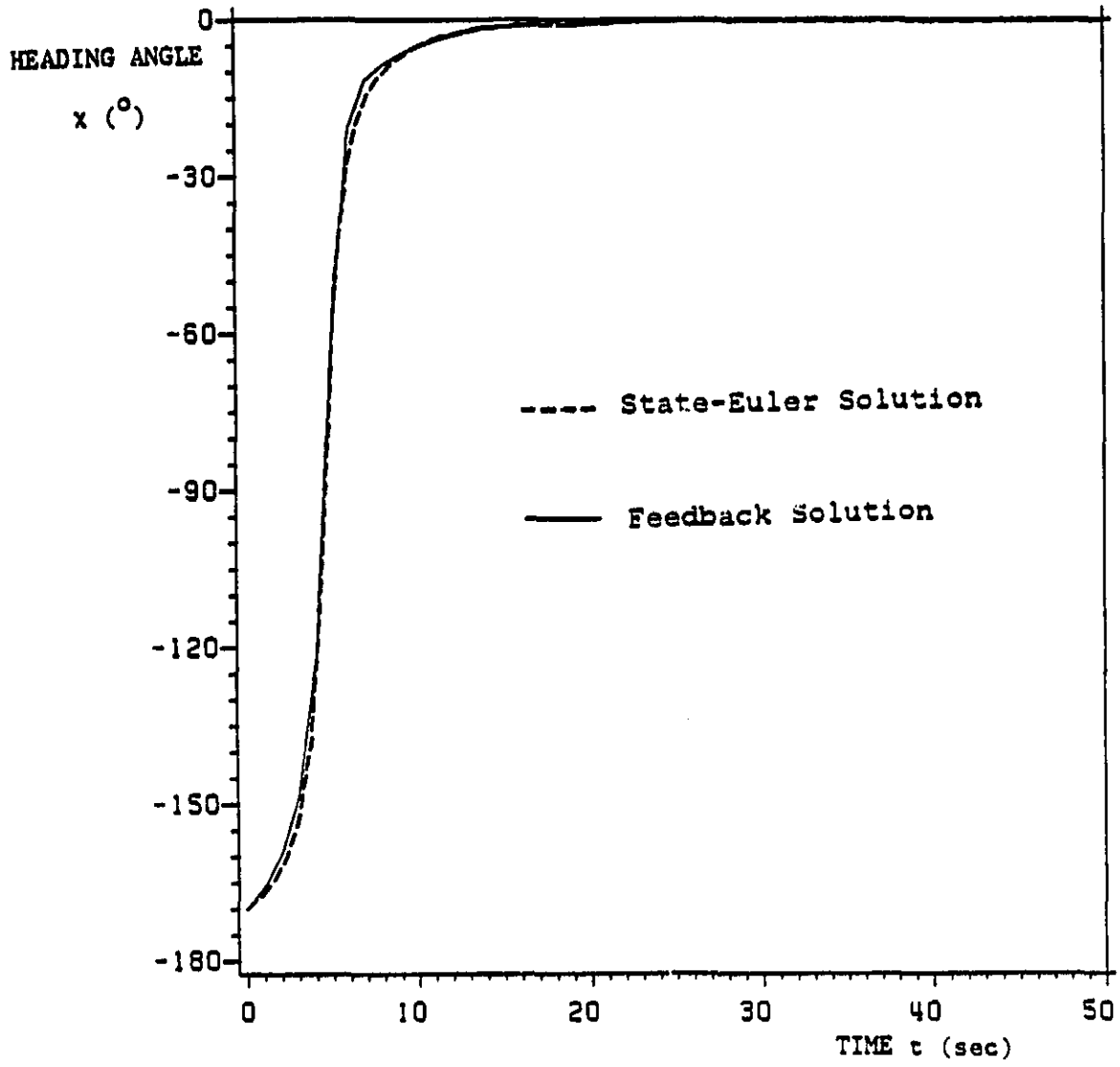


Figure 32. Heading-angle history for example 1.

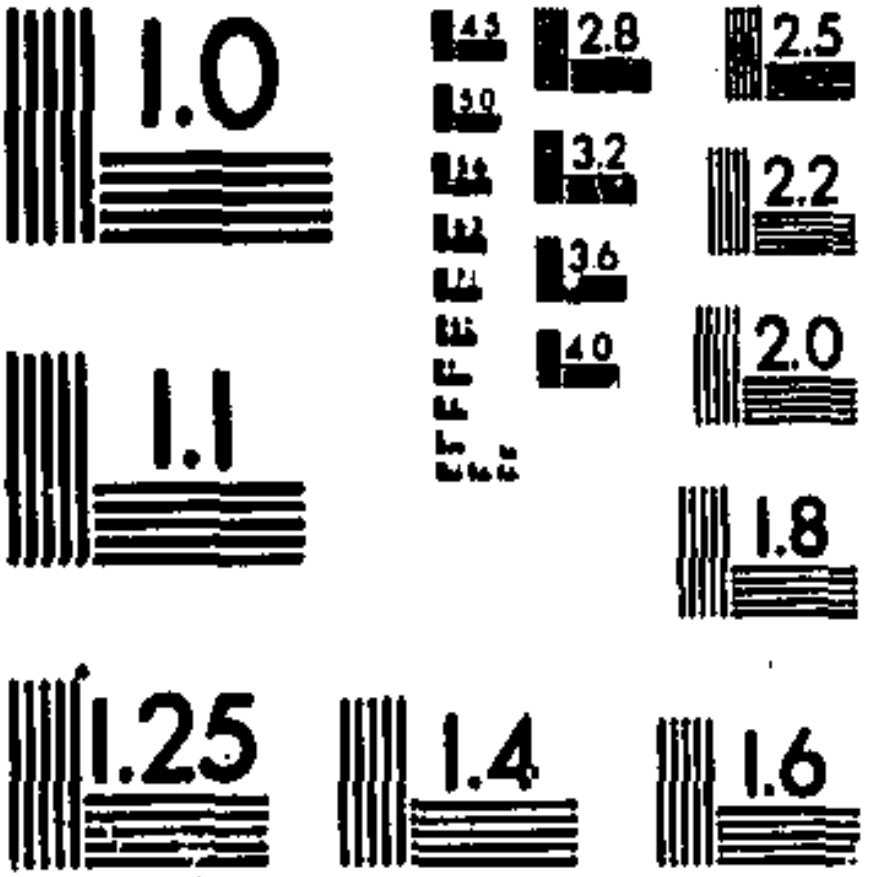


MICROCOPY RESOLUTION TEST CHART
NATIONAL BUREAU OF STANDARDS
STANDARD REFERENCE MATERIAL 1010a
(ANSI and ISO TEST CHART No. 2)

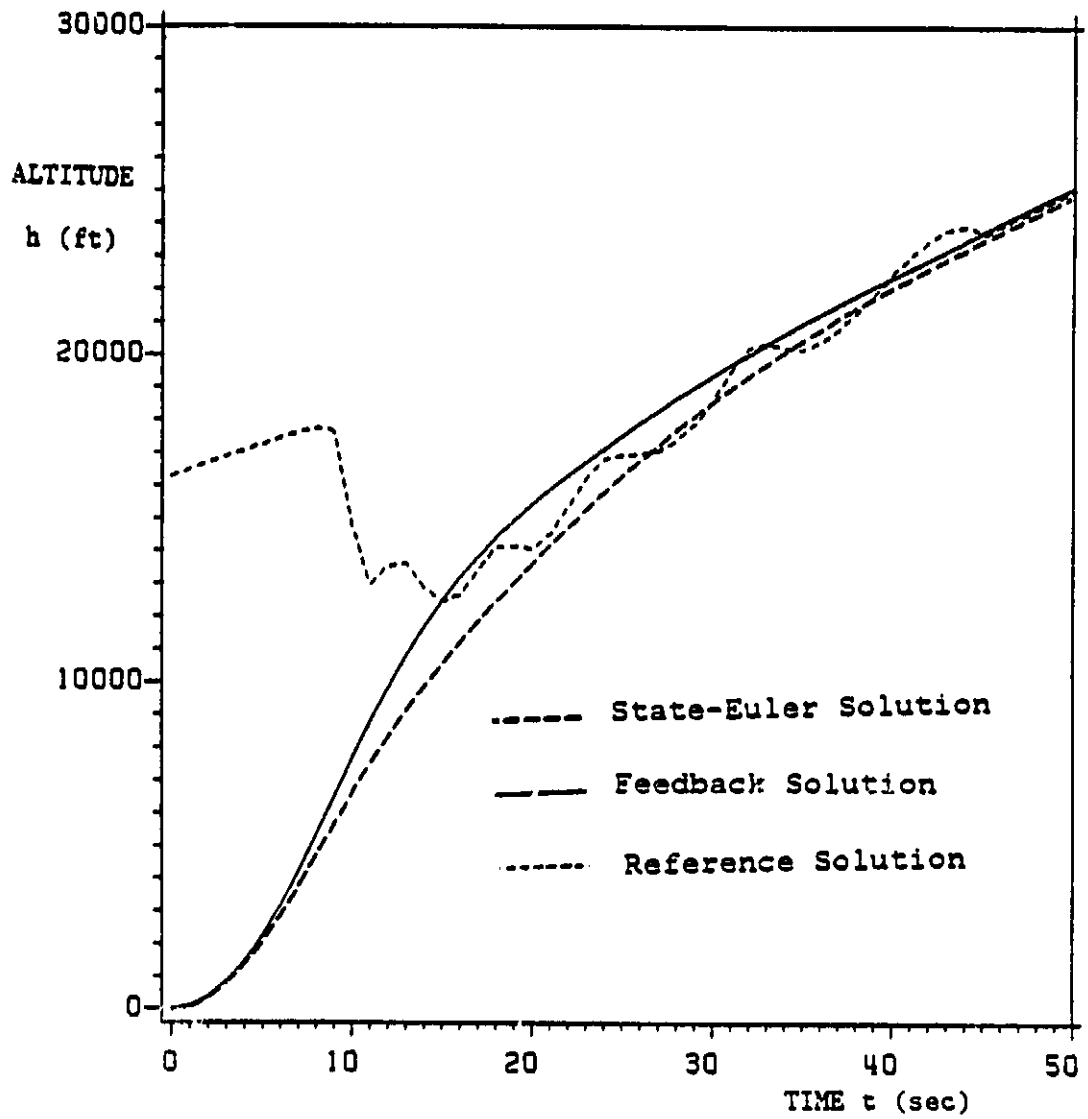


Figure 33. Altitude history for example 2.

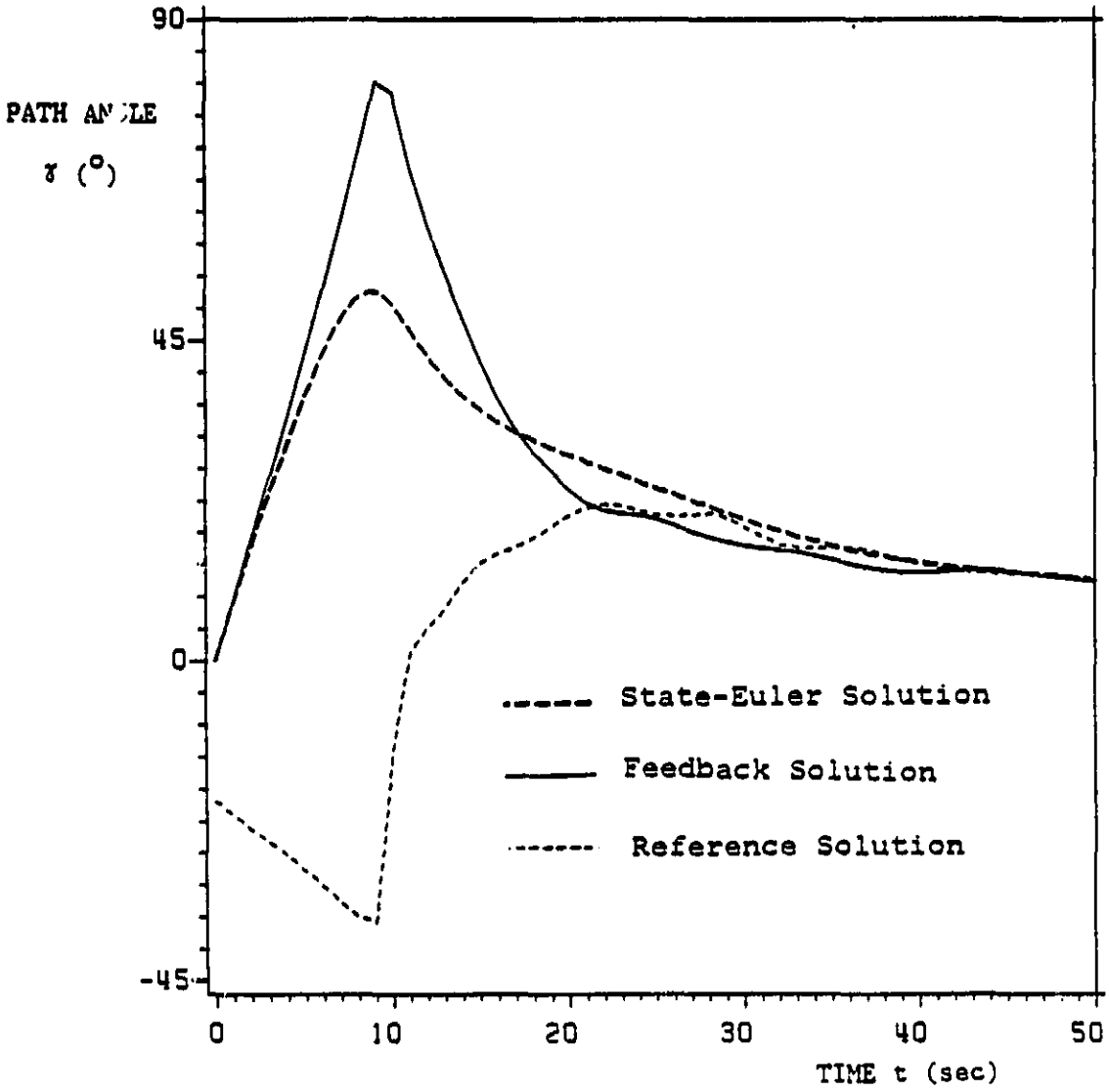


Figure 34. Path-angle history for example 2.

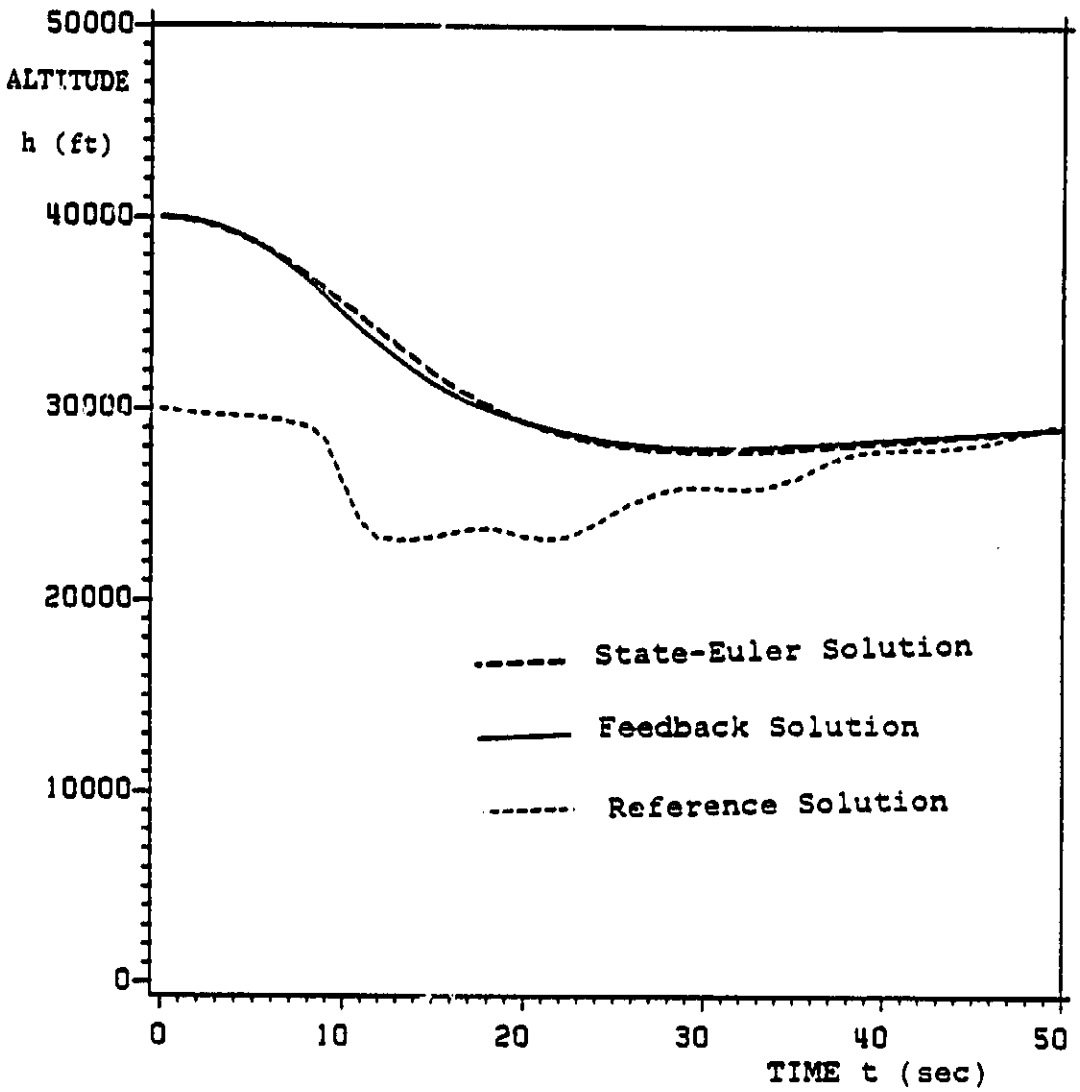


Figure 35. Altitude history for example 3.

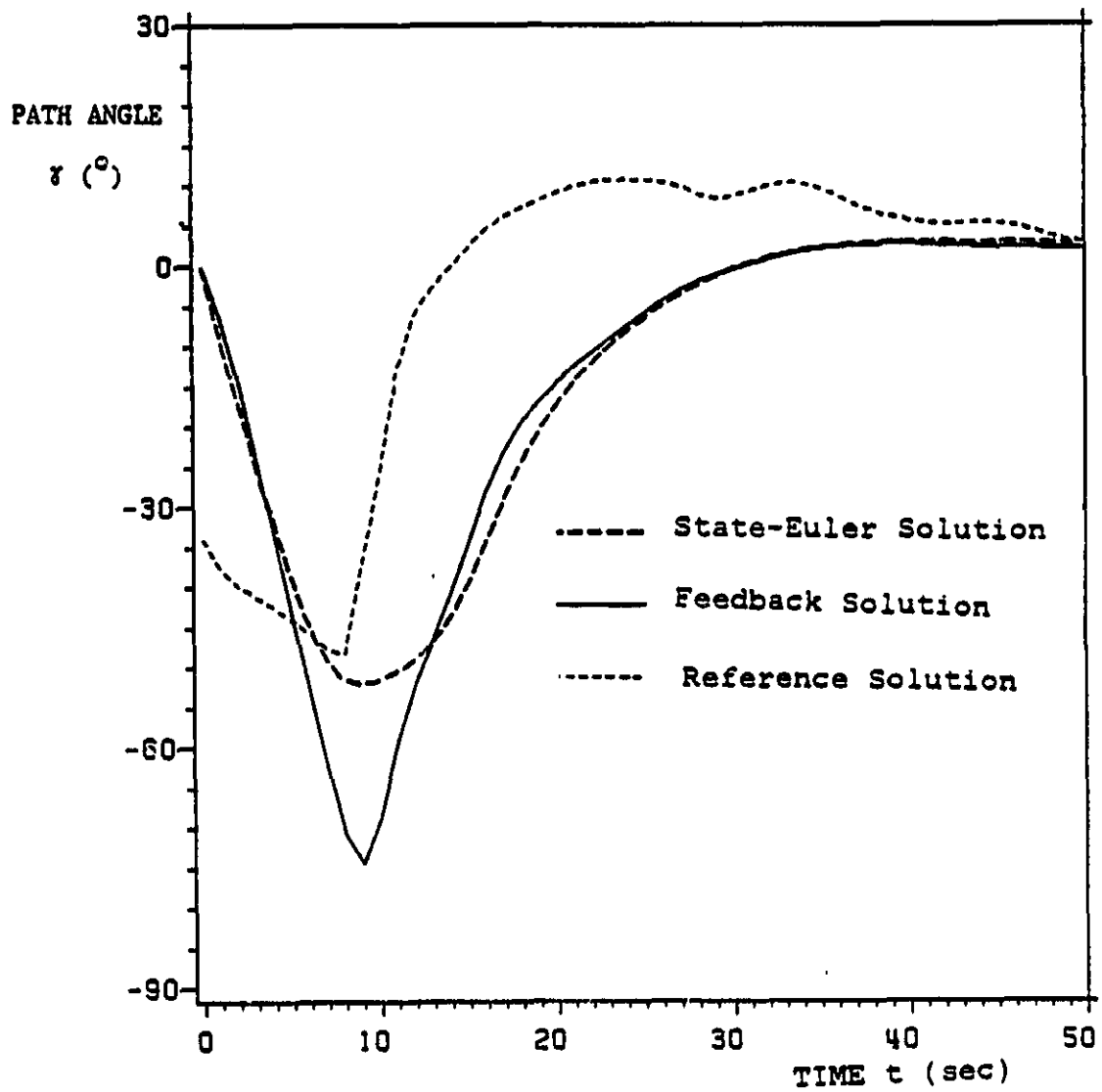


Figure 36. Path-angle history for example 3.

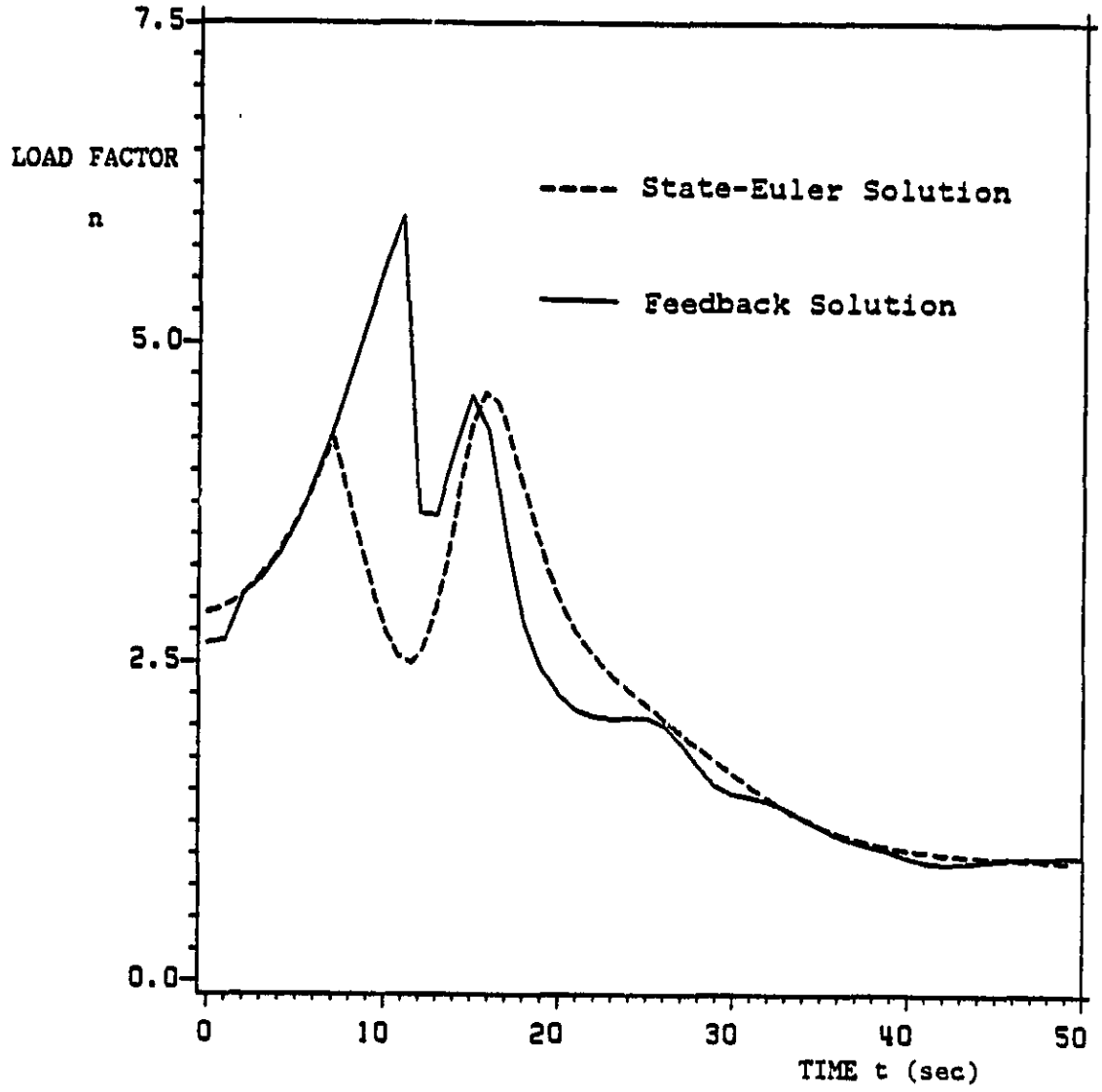


Figure 37. Load-factor history for example 3.

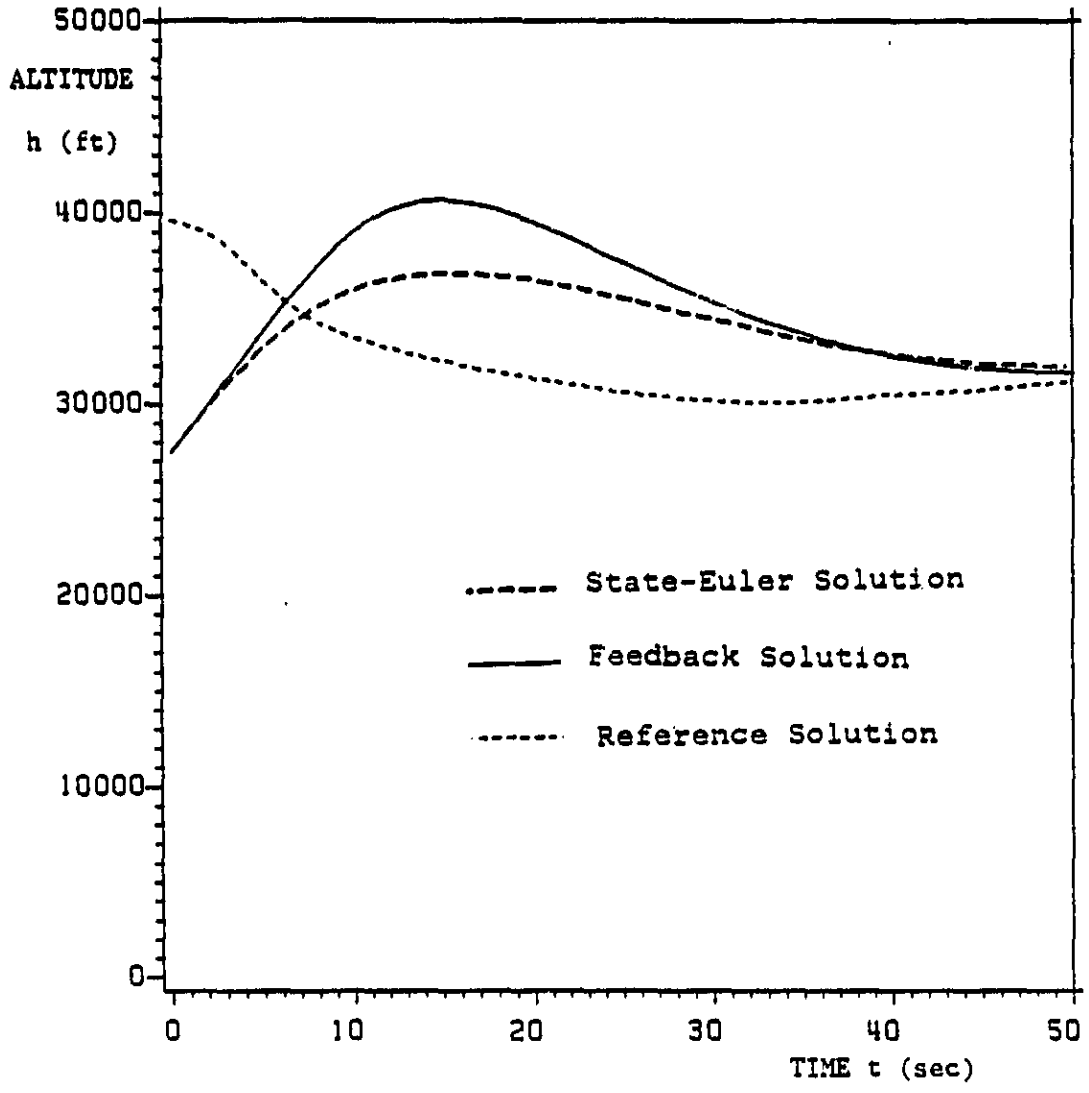


Figure 38. Altitude history for example 4.

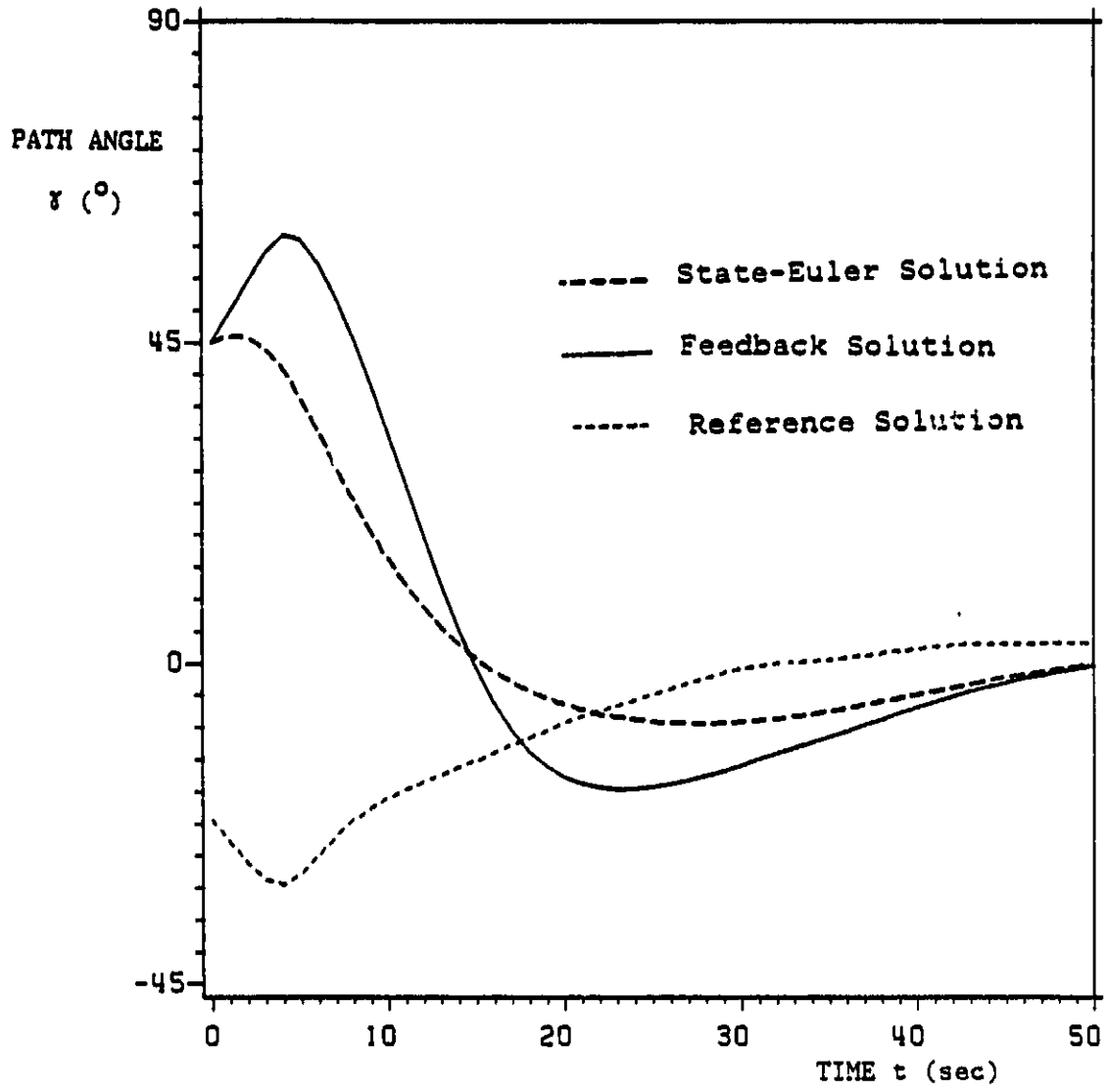


Figure 39. Path-angle history for example 4.

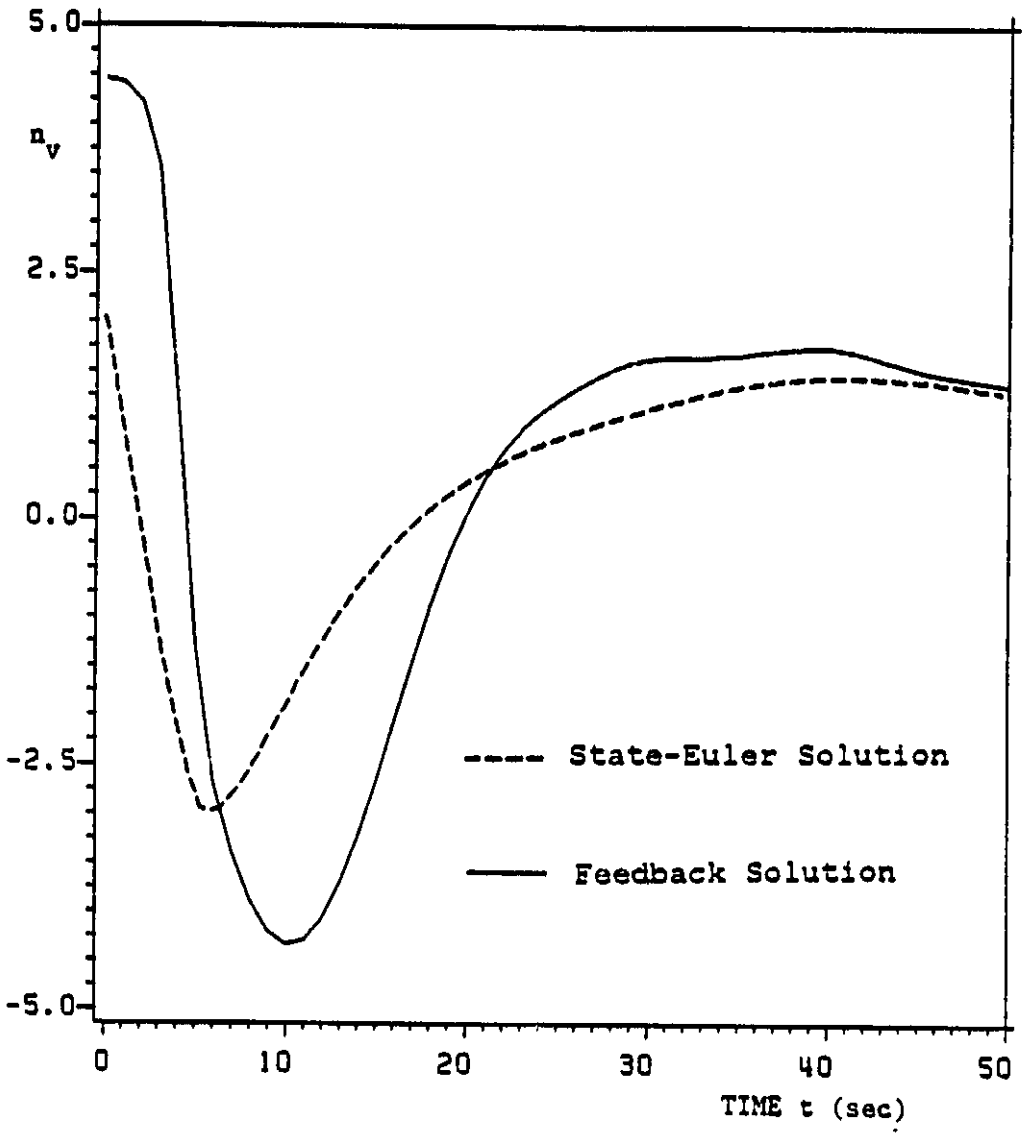


Figure 40. $n_v$ history for example 4.

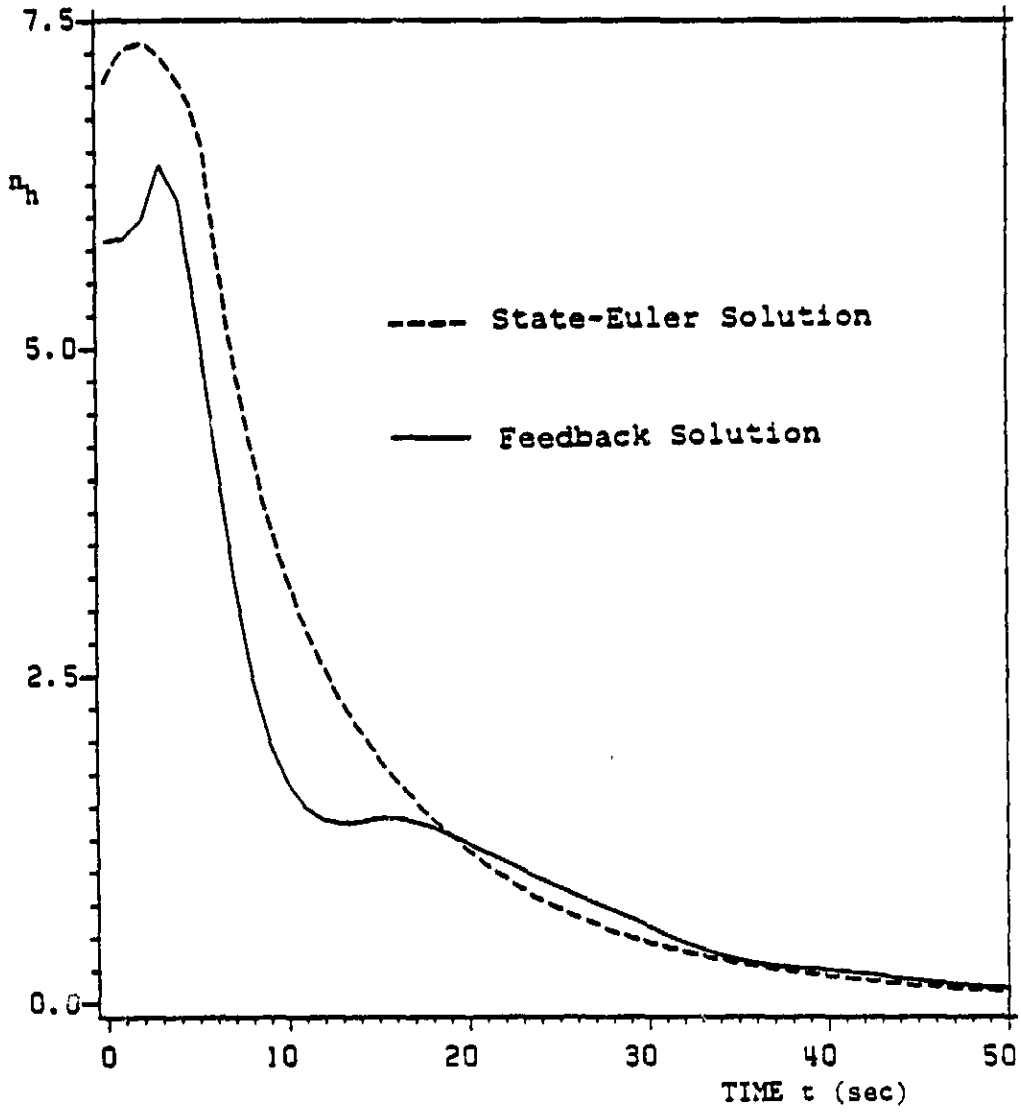


Figure 41. $n_h$ history for example 4.

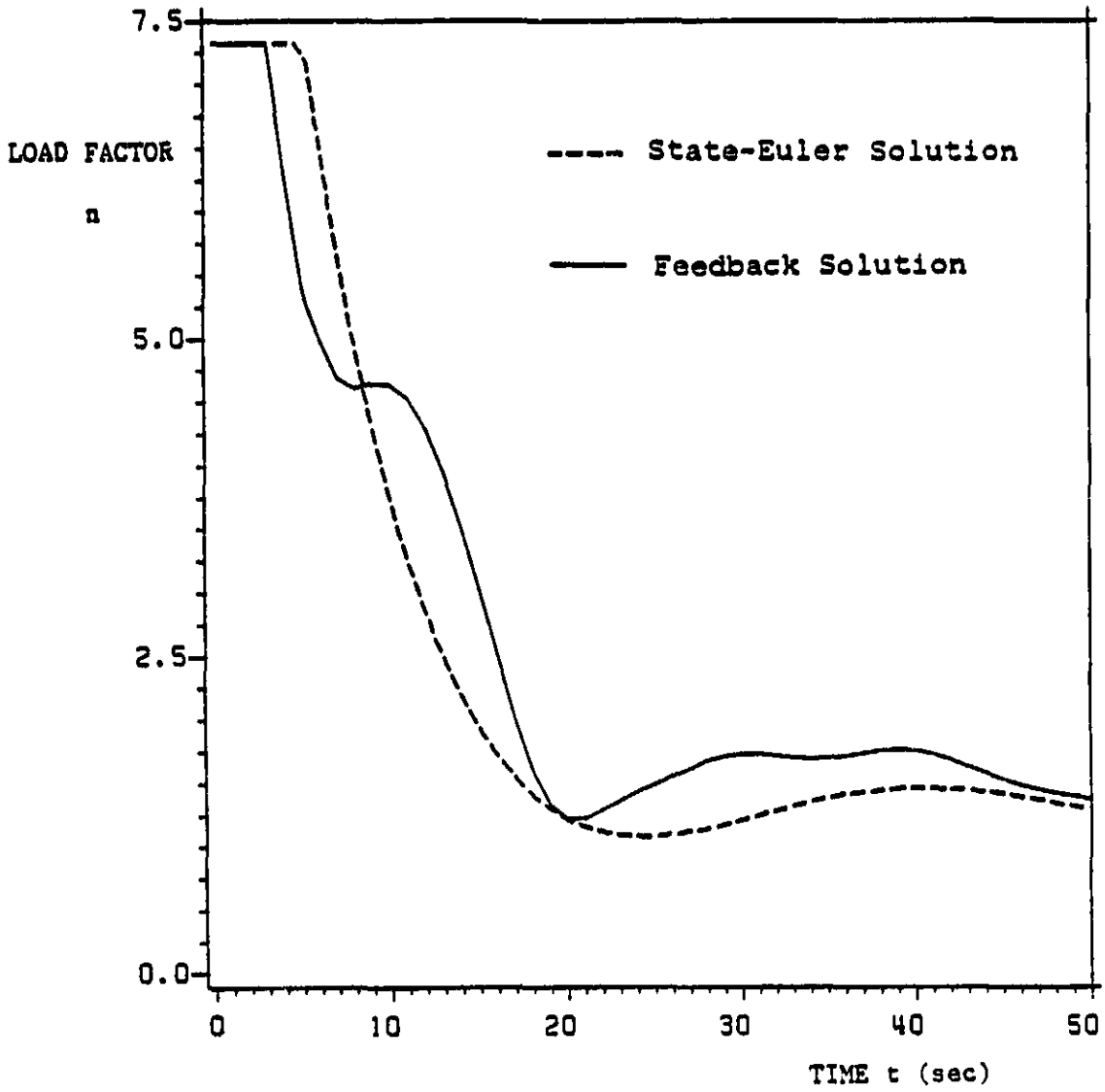


Figure 42. Load-factor history for example 4.

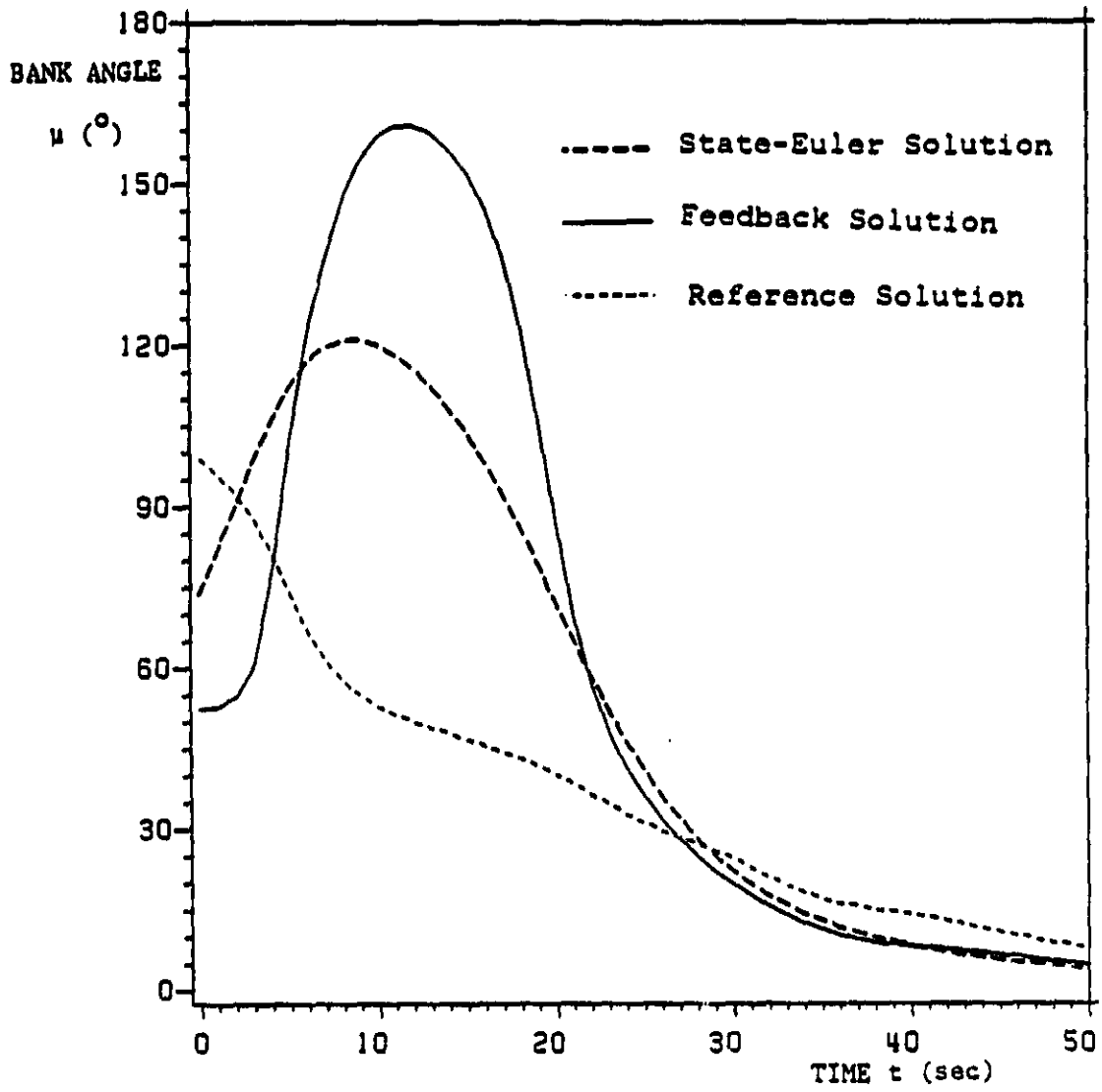


Figure 43. Bank-angle history for example 4.

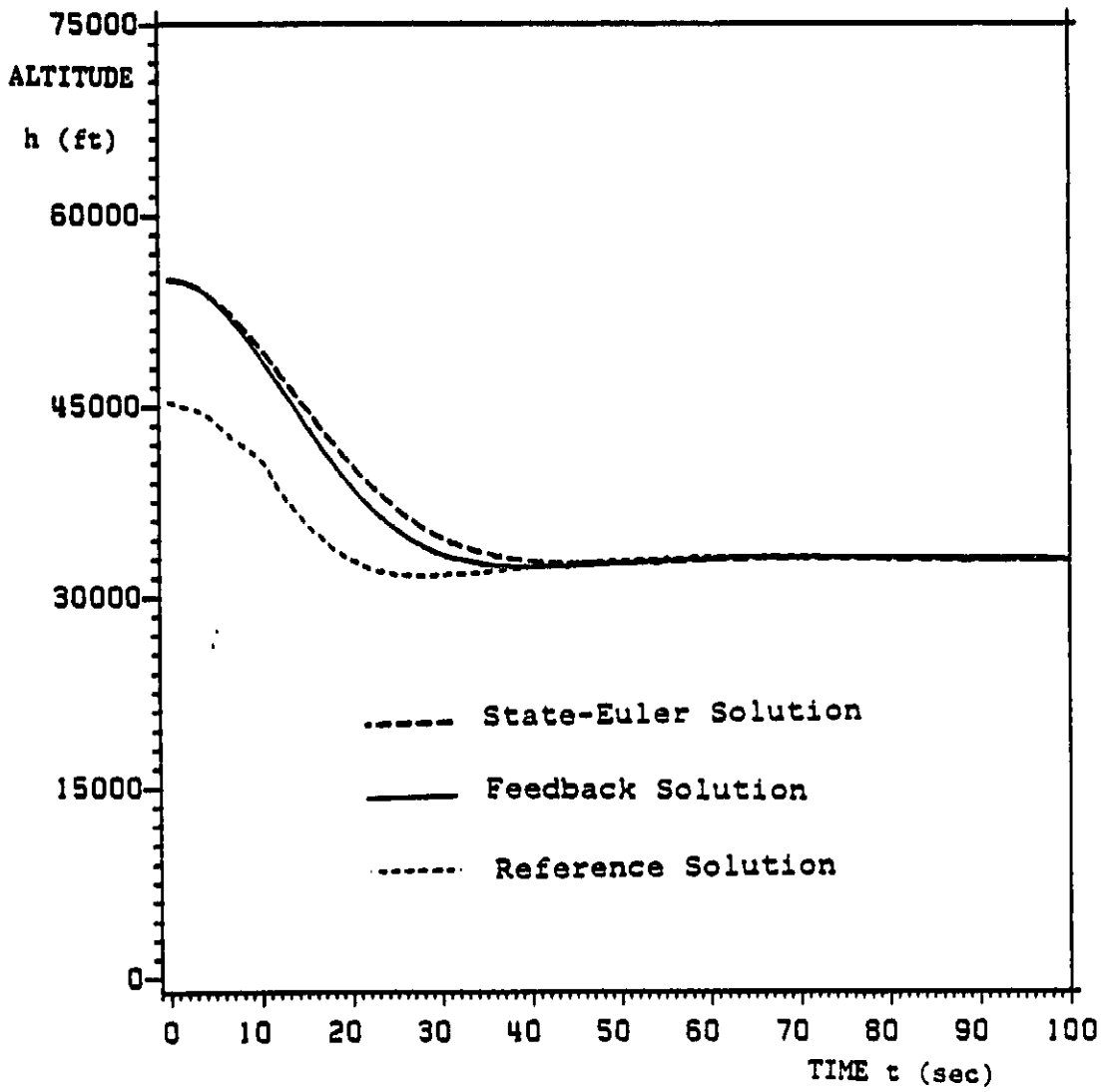


Figure 44. Altitude history for example 5.

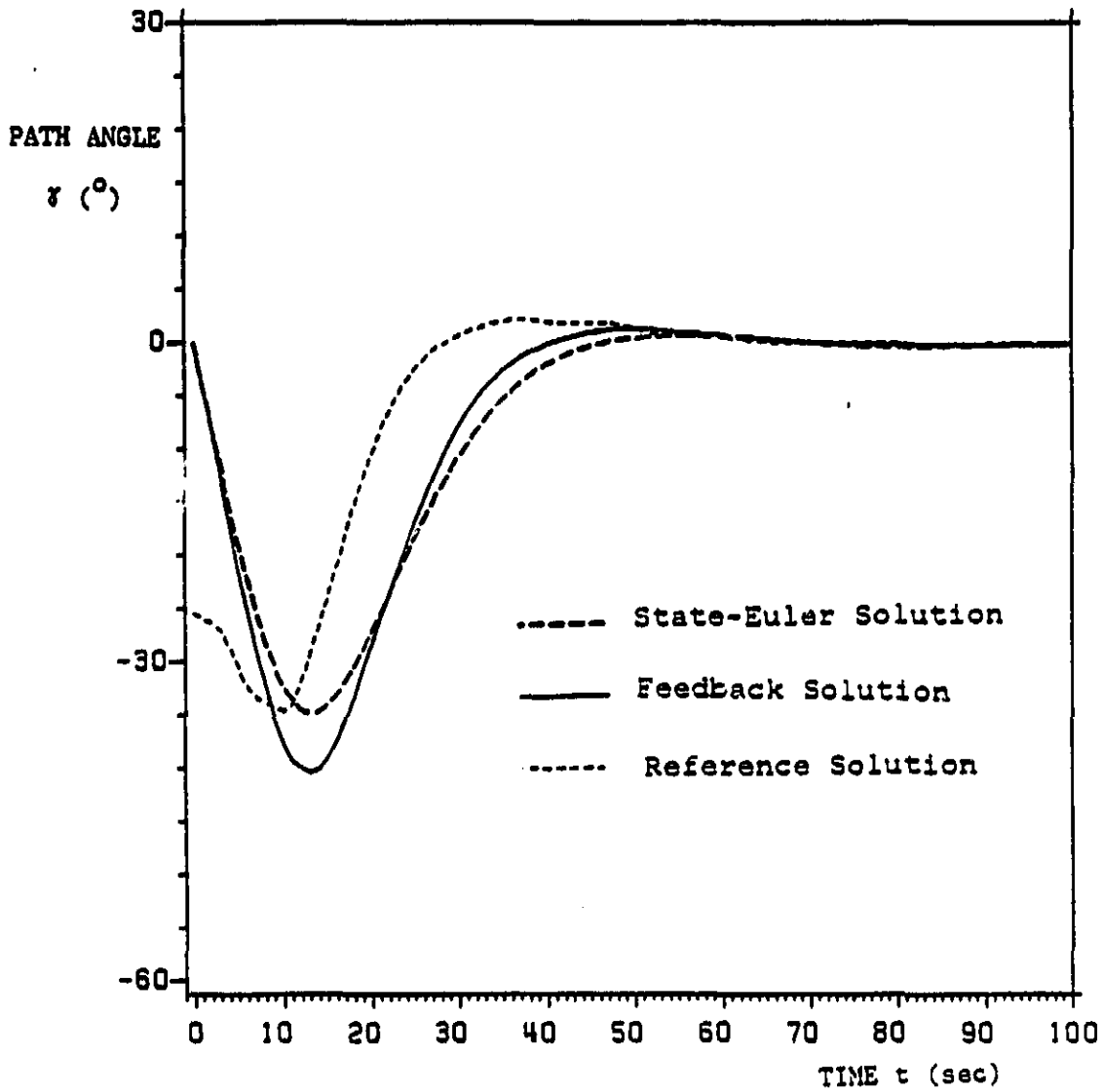


Figure 45. Path-angle history for example 5.

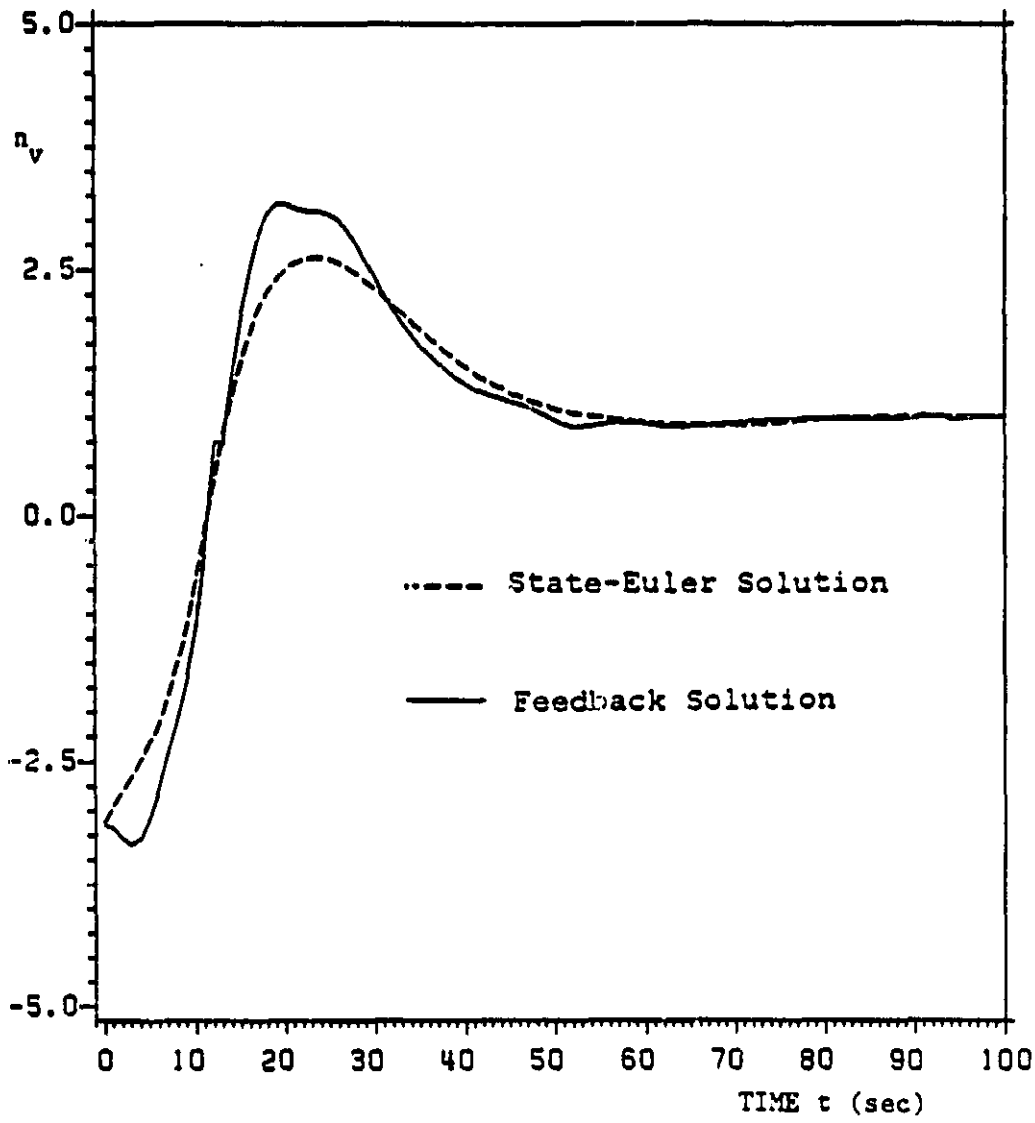


Figure 46. $n_v$ history for example 5.

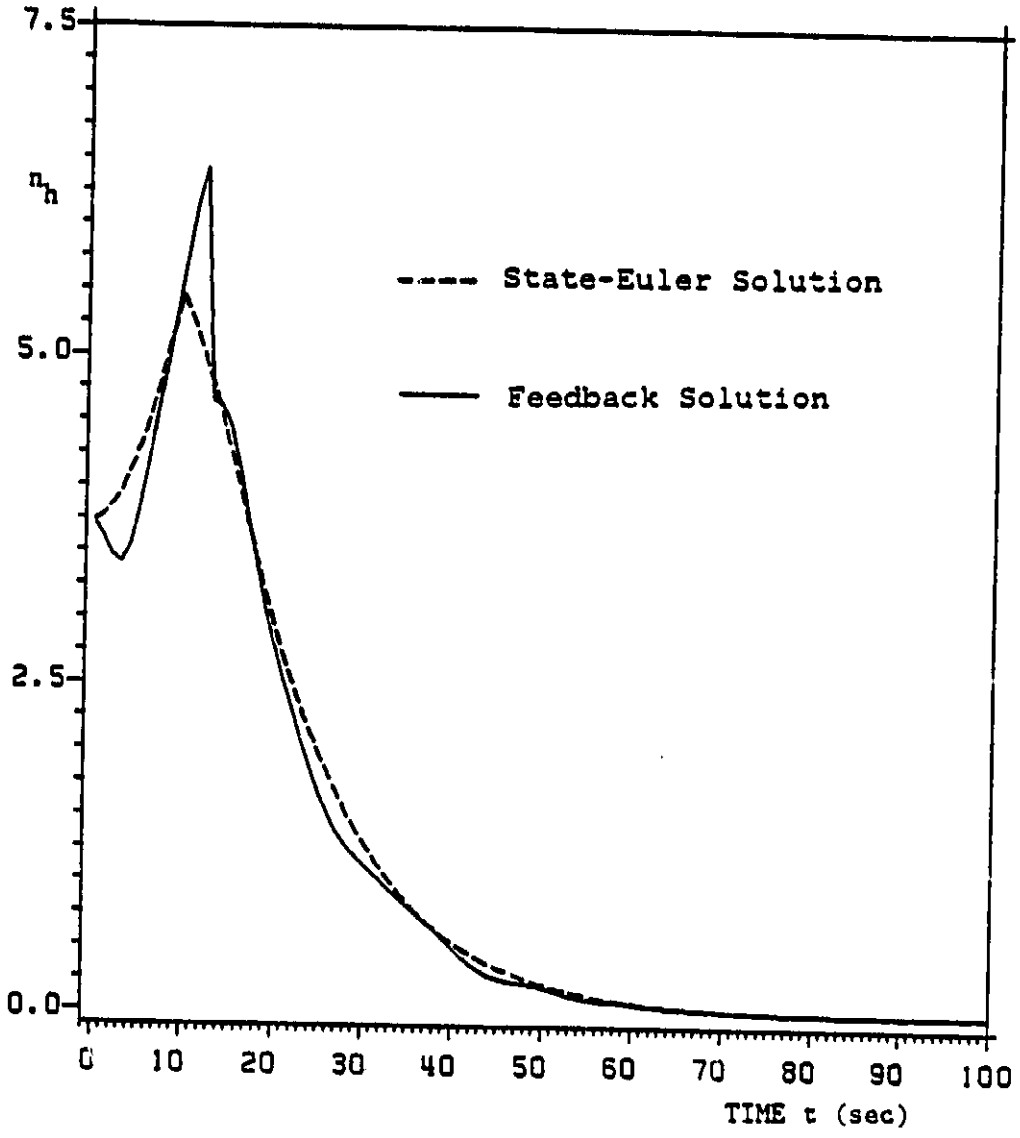


Figure 47. $n_h$ history for example 5.

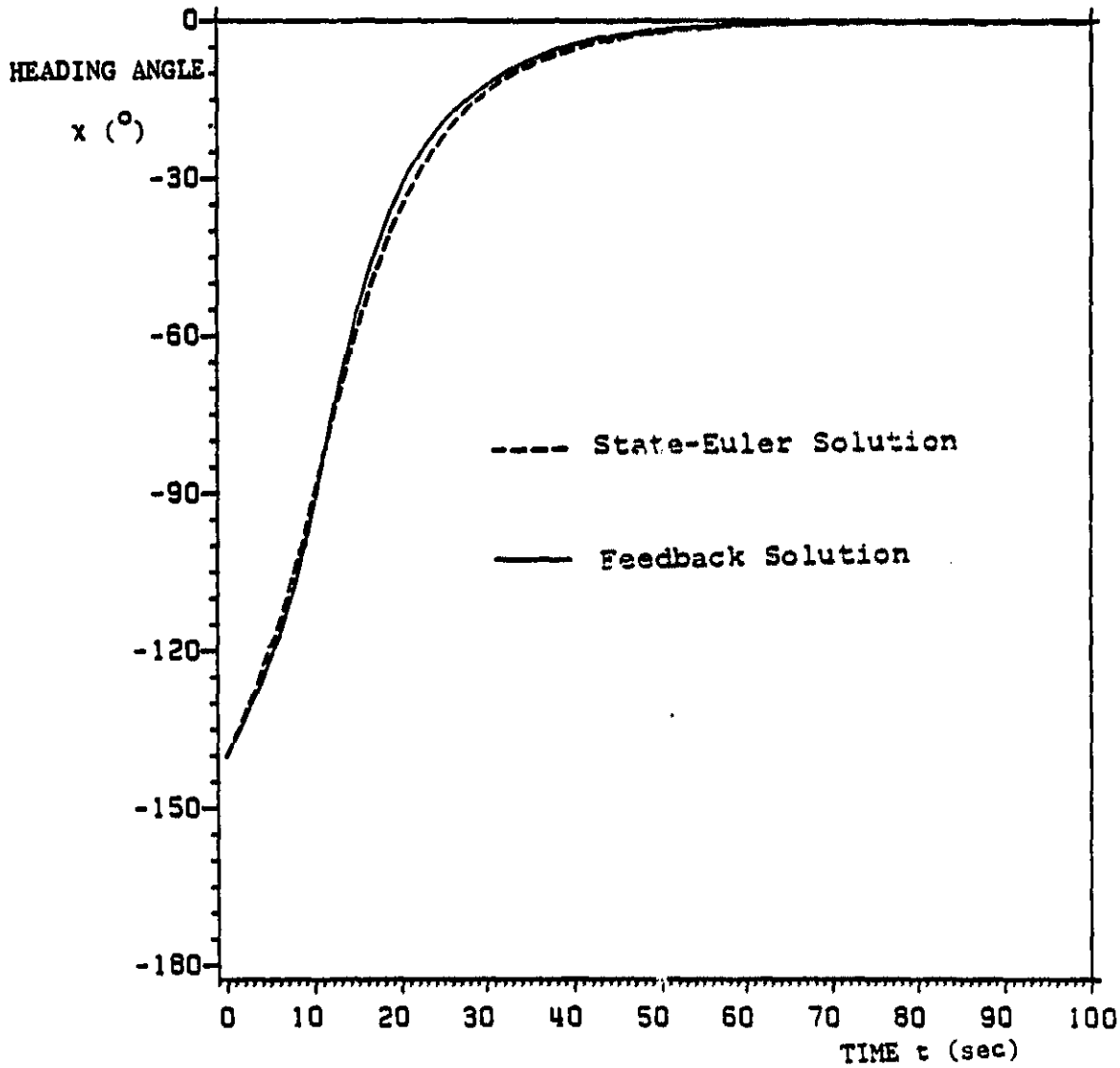


Figure 48. Heading-angle history for example 5.

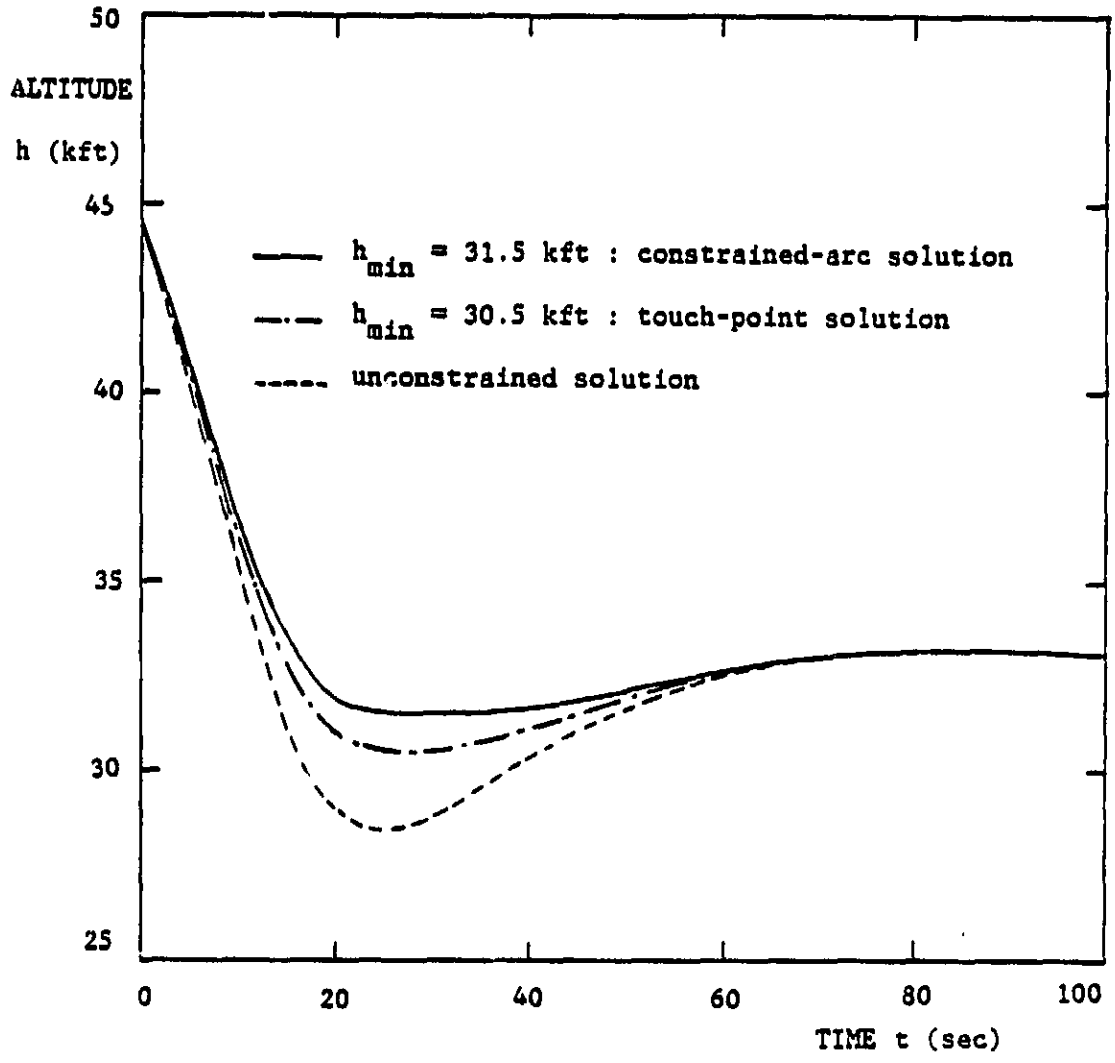


Figure 49. Example of altitude-constrained flight paths.

REFERENCES.


1. Stoer, J. and Bulirsch, R., "Introduction to Numerical Analysis", Springer, Berlin, 1980.

2. Keller, H.B., "Numerical Methods for Two-point Boundary Value Problems", Blaisdell, London, 1968.

3. Kaiser, F., "Der Steigflug mit Strahlflugzeugen - Teil I, Bahngeschwindigkeit Besten Steigens", Versuchsbericht 262-02-L44, Messerschmitt A.G., Augsburg, April 1944.

4. Merrit, S.R., Cliff, E.M. and Kelley, H.J., "Energy-Modelled Climb and Climb-Dash - The Kaiser Technique", Ninth IFAC World Congress, Budapest, Hungary, July 1984.

5. Rutowski, E.S., "Energy Approach to the General Aircraft Performance Problem", Journal of the Aeronautical Sciences, Vol.21, March 1954, pp.187-195.

6. Bryson, A.E., Desai, M.N. and Hoffman, K., "Energy-State Approximation in Performance Optimization of Supersonic Aircraft", Journal of Aircraft, Vol.6, Nov.-Dec. 1969, pp.481-488.

7. Kelley, H.J., "Reduced-Order Modeling in Aircraft Mission Analysis", AIAA Journal, Vol.9, Feb. 1971, pp.349-350.

8. Schulz, R. and Zagalsky, N. R., "Aircraft Performance Optimization", Journal of Aircraft, Vol. 9, Feb. 1972, pp.108-114.

9. Hedrick, J.K. and Bryson, A.E., "Three-Dimensional Minimum-Time Turns for a Supersonic Aircraft", Jounal of Aircraft, Vol.9, Feb. 1972, pp.115-121.

10. Kelley, H.J. and Lefton, L., "Supersonic Aircraft Energy Turns", Automatica, Vol.8, Sept. 1972, pp.575-580.

11. Wasow, W., "Asymptotic Expansions for Ordinary Differential Equations", John Wiley and Sons, New York, 1975.

12. Kelley, H.J. and Edelbaum, T.N., "Energy Climbs, Energy Turns and Asymptotic Expansions", Journal of Aircraft, Vol.7, Jan.-Feb. 1970, pp.93-95.

13. Kelley, H.J., "Flight-Path Optimization with Multiple Time Scales", Journal of Aircraft, Vol.8, April 1971, pp.238-240.

14. Kelley, H. J., "Aircraft Maneuver Optimization by Reduced-Order Approximation", Control and Dynamic Systems, Vol. 10, edited by C. T. Leondes, Academic Press, New York, 1973, pp.131-178.

15. Ardema M.D., "Solution of the Minimum-Time-To-Climb Problem by Matched Asymptotic Expansions", AIAA Journal, Vol.14, July 1976, pp.843-850.

16. Erzberger, H. and Lee, H.,"Constrained Optimum Trajectories with Specified Range", Journal of Guidance and Control, Vol.3, Jan.-Feb. 1980, pp.78-85.

17. Sorensen, J.A. and Waters, M.H., "Airborne Method to Minimize Fuel with Fixed Time-of-Arrival Constraints", Journal of Guidance and Control, Vol.4, May-June 1981, pp.348-349.

18. Burrows, J.W., "Fuel-Optimal Aircraft Trajectories with Fixed Arrival Times", Journal of Guidance and Control, Vol.6, Jan.-Feb. 1983, pp.14-19.

19. Chakravarty, A., "Four-Dimensional Fuel-Optimal Guidance in the Presence of Winds", Journal of Guidance, Control and Dynamics, Vol.8, Jan.-Feb. 1985, pp.16-22.

20. Uehara, S., Stewart, H.J. and Wood, L.J., "Minimum Time Loop Maneuvers of Jet Aircraft", Journal of Aircraft, Vol.15, Aug. 1978, pp.449-455.

21. Well, K.H, Faber, B.J. and Berger, E., "Optimimization of Tactical Aircraft Maneuvers Utilizing High Angles of Attack", Journal of Guidance and Control, Vol.5, Mar.-Apr. 1982, pp.124-130.

22. Ardema M.D., "Air-to-Air Combat Analysis: Review of Differential-Gaming Approaches", Joint Automatic Control Conference, Charlottesville, Va., June 1982.

23. Isaacs R.P., "Differential Games", Wiley, New York, 1965.

24. Ho, Y.C and Olsder, G.J., "Differential Games: Concepts and Applications", Mathematics of Conflict, edited by Martin Shubik, Elsevier, 1983, pp.127-185.

25. Olsder, G.J. and Breakwell, J.V., "Rôle Determination in Aerial Dogfights", International Journal of Game Theory, Vol.3, 1974, pp.47-66

26. Kelley, H.J. and Lefton, L., "Calculation of Differential-Turning Barrier Surfaces", Journal of Spacecraft and Rockets, Vol.14, Feb. 1977, pp.87-95.

27. Getz, W.M. and Leitmann, G., "Qualitative Differential Games with Two Targets", Journal of Mathematical Analysis and Applications, Vol.68, April 1979, pp.421-430.

28. Pachter, M. and Getz, W.M., "Two Target Pursuit-Evasion Differential Games in the Plane", Journal of Optimization Theory and Applications, Vol.34, 1981, pp.383-403.

29. Heymann, M. Ardema, M.D. and Rajan, N., "A Formulation and Analysis of Combat Games", NASA TM 85927, April 1984.

30. Kelley, H.J., "Differential-Turning Optimality Criteria", Journal of Aircraft, Vol.12, Jan. 1975, pp.41-44.

31. Kelley, H.J., "Differential-Turning Tactics", Journal of Aircraft, Vol.12, Dec. 1975, pp.930-935.

32. Kelley, H.J., Cliff, E.M. and Lefton L., "Thrust-vectored Differential Turns", Automatica, Vol.18, No.5, 1982, pp.565.

33. Merz, A.W, "The Homicidal Chauffeur", AIAA Journal, Vol.12, 1974, pp.259-260.

34. Merz, A.W, "The Game of Two Identical Cars", Journal of Optimization Theory and Applications, Vol.9, No.5, May 1972, pp.324-343.

35. Breakwell, J.V. and Merz, A.W, "Minimum Required Capture Radius in a Coplanar Model of the Aerial Combat Problem", AIAA Journal, Vol.15, Aug. 1977, pp.1089-1094.

36. Ardema, M.D., "Singular Perturbations in Flight Mechanics", NASA TM X-62, 1974 (revised 1977)

37. Calise, A. J., "Singular Perturbation Methods for Variational Problems in Aircraft Flight", IEEE Transactions on Automatic Control, Vol. AC-21, no.3, June 1976, pp.345-353.

38. Calise, A. J., "Extended Energy Management Methods for Flight Performace Optimization", AIAA Journal, Vol.15, no.3, March 1977, pp.314-321.

39. Calise, A. J., "A New Boundary Layer Matching Procedure for Singularly Perturbed Systems", IEEE Transactions on Automatic Control, Vol. Ac-23, no.3, June 1978, pp.434-438.

40. Mehra, R., Washburn, R., Sajan, S. and Carroll, J., "A Study of the Application of Singular Perturbation Theory", NASA CR-3167, 1979.

41. Visser, H.G., "An Introduction to the Technique of Singular Perturbations Applied to Performance Optimization Problems in Atmospheric Flight Mechanics", Report LR-374, Dept. of Aerospace Engineering, Delft University of Technology, Delft, The Netherlands, Dec. 1982

42. Shinar, J., "On Applications of Singular Perturbation Techniques in Nonlinear Optimal Control", Automatica, Vol.19, No.3, 1983, pp.203-211.

43. Ardema, M.D. and Rajan, N., "Separation of Time Scales in Aircraft Trajectory Optimization", Journal of Guidance, Control and Dynamics, Vol.8, Mar.-Apr. 1985, pp.275-278.

44. Calise, A. J., "A Singular Perturbation Analysis of Optimal Aerodynamic and Thrust Magnitude Control ", IEEE Transactions on Automatic Control, Vol. AC-24, no.5, Oct. 1979, pp.345-353.

45. Sridar, B. and Gupta, N.K., "Missile Guidance Laws Based on Singular-Perturbation Methodology", Journal of Guidance and Control, Vol.3, Mar.-Apr. 1980, pp.158-165.

46. Calise, A. J.,"Optimal Thrust Control with Proportional Navigation Guidance", Journal of Guidance and Control, Vol.3, July-Aug. 1980, pp.312-318.

47. Calise, A. J., "Singular Perturbation Techniques for On-Line Optimal Flight Path Control", Journal of Guidance and Control, Vol.3, July-Aug. 1981, pp.398-405.

48. Shinar, J.,Farber, N. and Negrin, M., "A Three-Dimensional Air Combat Game Analyses by Forced Singular Perturbations", AIAA Paper 82-1327,1982.

49. Shinar, J. and Negrin, M., "An Explicit Feedback Approximation for Medium Range Interception in the Vertical Plane", Optimal Control Applications and Methods, Vol.4, No.4, 1983, pp.303-323.

50. Shinar, J., "Zeroth-Order Feedback Strategies for Medium Range Interception in the Horizontal Plane", Journal of Guidance, Control and Dynamics, Vol.8, Jan.-Feb. 1985, pp.9-15.

51. Kelley H. J., "Comments on 'A New Boundary-Layer-Matching Procedure for Singularly Perturbed Systems'", IEEE Transactions on Automatic Control, Vol. AC-23, No. 3, June 1978.

52. Weston, A. R., Cliff, E. M. and Kelley, H. J., "Altitude Transitions in Energy Climbs", Automatica, Vol. 19, No. 2, 1983, pp.199-202.

53. Visser, H.G., Shinar, J. and Guelman, M., "Analyitical First-Order Corrections in Singularly Perturbed Nonlinear Control Problems", 25th Israel Annual Conference on Aviation and Astronautics, Haifa, Israel, Feb. 1983.

54. Visser, H.G. and Shinar, J., "A Highly Accurate Feedback Approximation for Variable Speed Interceptions in the Horizontal Plane", 12th Atmospheric Flight Mechanics Conference, Snowmass, Colorado, Aug. 1985.

55. Kelley, H. J., "Guidance Theory and Extremal Fields", IRE Transactions on Automatic Control, Vol.7, No.5, 1962, pp.75-82.

56. Breakwell, J. V., Speyer, J. L. and Bryson, A. E., "Optimization and Control of Nonlinear Systems using the Second Variation", Journal of SIAM Control, Vol.1, No.2, 1963, pp.193-223.

57. Kelley, H. J., "An Optimal Guidance Approximation Theory", IEEE Transactions on Automatic Control, Vol.9, No.4, 1964, pp.375-380.

58. Powers, W.F., "A Method for Comparing Optimum Linear Perturbation Guidance Schemes", AIAA Journal, Vol.6, No.12, 1968, pp.2451-2452.

59. Powers, W.F., "Techniques for Improved Convergence in Neighboring Optimum Guidance", AIAA Journal, Vol.8, No.12, 1970, pp.2235-2341.

60. Speyer, J. L. and Bryson, A. E., " A Neighboring Optimum Feedback Control Scheme Based on Estimated Time-to-Go with Application to Re-Entry Flight Paths", AIAA Journal, Vol.6, No.5, June 1968, pp.769-776.

61. Wood, L.J., "Perturbation Guidance for Minimum Time Flight Paths of Spacecraft", AIAA Paper 72-915.

62. Pesch, H.J., "Neighboring Optimum Guidance of Space Shuttle Orbiter Type Vehicle", Journal of Guidance and Control, Vol.3, No.5, 1980, pp.386-392.

63. Rajan, N. and Ardema, M.D., "Computations of Feedback Strategies for Interception in a Horizontal Plane", AIAA Paper 83-0281, 1983.

64. Rajan, N. and Ardema, M.D., "Interception in Three Dimensions: An Energy Formulation", Journal of Guidance, Control and Dynamics, Vol.8, No.1, 1985, pp.23-30.

65. Kelley, H.J. and Well. K., "An Approach to Intercept On-Board Calculations", American Control Conference, San Francisco, California, June 1983.

66. Weston, A.R., Cliff, G. and Kelley, H., "On-Board Near-Optimal Climb-Dash Energy Management", Journal of Guidance and Control, Vol.8, No.3, 1985, pp.320-324.

67. Weston, A.R., "On-Board Near-Optimal Climb-Dash Energy Management", Ph.D. dissertation, Department of Aerospace and Ocean Engineering, VPI&SU, 1982

68. Mummolo, F. and Lefton, L., "Cubic Splines and Cubic Spline Lattices for Digital Computation", Analytical Mechanical Associates Inc. Report No. 72-28, July 1972, (revised 1974)

69. Vinh, N.X., "Optimal Trajectories in Atmospheric Flight", Elsevier, Amsterdam, 1981

70. Bryson, A.E. and Ho, Y.-C., "Applied Optimal Control", Hemisphere, Washington, 1975

71. Boyd, J.R, Christie, T.P. and Gibson, J.E., "Energy Maneuverability", Armament Laboratory Report, Vols.I and II, Eglin Air Force Base, 1966

72. Kelley, H.J., Cliff, E.M., Weston, A.R., "Energy-State Revisited", AIAA Atmospheric Flight Mechanics Conference, Gatlinburg, Tenn., Aug. 1983.

73. Akima, H., "A Method of Bivariate Interpolation and Smooth Surface Fitting for Irregularly Distributed Data Points", ACM Trans. Math. Software 4, June 1978, pp.148-159.

74. Anonymous, "The IMSL Library", Volume 2, Edition 9.2 (revised Nov. 1984).

75. Sampson, R.J., "Surface II Graphics System", Series on Spatial Analysis, Kansas Geological Survey, Lawrence, Kansas.

76. De Boor, C., "A Practical Guide to Splines", Springer-Verlag, New York, 1967.

77. Well, K.H., Wever, U.A., "Aircraft Trajectory Optimization Using Quaternions - Comparison of a Nonlinear Programming and a Multiple Shooting Approach", Ninth IFAC World Congress, Budapest, Hungary, July 1984.

78. Visser, H.G., Kelley, H.J. and Cliff, E.M, "Energy Management of Three-Dimensional Minimum-Time Intercept", 12th AIAA Atmospheric Flight Mechanics Conference, Snowmass, Colorado, August, 1985.

79. Shinar, J., Fainstein, V., "Improved Feedback Algorithms for Optimal Maneuvers in a Vertical Plane", 12th AIAA Atmospheric Flight Mechanics Conference, Snowmass, Colorado, August, 1985.

80. Price, D.B., Calise, A.J., Moerder, D.D., "Piloted Simulation of an Onboard Trajectory Optimization Algorithm", Journal of Guidance and Control, Vol.7, May-June 1984, pp.355-360.